INVESTIGATION OF THE SEISMIC PERFORMANCE OF REINFORCED HIGHWAY EMBANKMENTS

by

Yasin Sait Toksoy

B.S., Civil Engineering, Yıldız Technical University, 2011

Submitted to Kandilli Observatory and Earthquake Research Institute
in partial fulfillment of the requirements for the degree of
Master of Science

Graduate Program in Earthquake Engineering

Boğaziçi University

2014

ACKNOWLEDGEMENTS

Foremost, I would like to thank my thesis supervisor Assoc. Prof. Ayşe Edinçliler who has always supported and encouraged me in any case during my graduate studies and thesis stage. I appreciate her continious guidance, patience and research experience.

I would like to thank my committee members Prof. Dr. Erdal Şafak and Prof. Dr. Ayfer Erken for their contributions and guidances.

I would like to thank experts and technicians who helped me during my experiments in KOERI Shaking Table Laboratory.

Finally, I would like to express my deepest gratitude to my friends for their support and my precious family for their endless motivation.

ABSTRACT

INVESTIGATION OF THE SEISMIC PERFORMANCE OF REINFORCED HIGHWAY EMBANKMENTS

Embankments which are quite stable under static load conditions can simply collapse during earthquakes due to the destructive seismic loading. This situation poses a high sequence thread to the structural integrity of the embankment, service quality and serviceability.

The objective of this thesis is to determine the effect of the geosynthetic reinforcement on the seismic performance of the highway embankments and evaluate the seismic performance of the geotextile reinforced embankment under different earthquake motions. A 1/50 scale highway embankment model is designed and reinforced with geosynthetics in order to increase the seismic performance of the embankment model. A series of shaking table tests were performed for the identical unreinforced and reinforced embankment models using dynamic motions with different characteristics. The experimental results were evaluated comparing the unreinforced and reinforced cases. Results revealed that reinforced embankment models perform better seismic performance especially under specificied dynamic motions used in this study. Also, the prototype embankment was numerically modelled using the software PLAXIS 2D 2012. It is seen that seismic performance trend of the numerical simulations are close to that of the experimental results.

ÖZET

DONATILI YOL DOLGULARININ SİSMİK PERFORMANSININ İNCELENMESİ

Karayolu dolgu şevleri, eğimli geometrileriyle, karayolu yapılarında stabilite problemlerinin yaygın görüldüğü bölgelerdir. Deprem etkisi veya herhangi bir mekanik dış faktör altında şev stabilitesinin bozulması, karayolunun yapı bütünlüğünü, servis kalitesini ve hizmet verebilirliğini tehdit eder.

Bu çalışmada, deprem etkisi altındaki karayolu şevleri geosentetik malzemeyle güçlendirilmiştir. Geosentetiklerin deprem etkisi altında performans arttırıcı ve sismik enerjiyi sönümleyici etkileri literatür çalışmalarıyla da desteklenmektedir. Özellikleri daha önceden laboratuvar çalışmalarıyla belirlenmiş kum kullanılarak, bir kutu içerisinde belirli eğim ve yüksekliğe sahip model karayolu dolgusu şevleri, hem güçlendirilmiş hem de güçlendirilmemiş durumlar için, sarsma masasında farklı karakteristiklerdeki deprem hareketlerine maruz bırakılmış ve sonuçlar karşılaştırılmıştır. Ayrıca sonlu elemanlar yöntemini kullanarak, PLAXIS 2D 2012 yazılımı yardımıyla nümerik analizler gerçekleştirilmiş ve elde edilen sonuçlar deneysel çalışmalardan elde edilen sonuçlarla karşılaştırılmıştır. Sonuç olarak, sarsma masası testlerinden elde edilen sonuçlar ile sonlu elemanlar yöntemi kullanılarak elde edilen sonuçlar arasında paralellik olduğu gözlemlenmiştir.

TABLE OF CONTENTS

LIST OF FIGURES

LIST OF TABLES

LIST OF SYMBOLS / ABBREVIATIONS

a	Acceleration
A	Accelerometer
AF	Amplification factor
a_{max}	Maximum horizontal acceleration
ASTM	American society for testing and materials
a_y	Yielding acceleration
CA	California
C_c	Coefficient of curvature
C_u	Coefficient of uniformity
D	Displacement sensor
Dr	Relative density
EPS	Expanded polystyrene
f	Frequency
F_h	Horizontal pseudostatic force
FOS	Factor of safety
ft	Feet
g	Acceleration of gravity
GCL	Geosynthetic clay liner
Hz	Hertz
k_h	Seismic coefficient
M	Magnitude
m	Total mass of the sliding mass
MSE	Mechanically stabilized earth
M_w	Moment magnitude
PGA	Peak ground acceleration
PIV	Particle image velocimetry
SA	Spectral acceleration
SP	Poorly graded sand
T	Natural period of vibration

TDA	Tire derived aggregate
T_{ult}	Ultimate tensile strength
USCS	Unified soil classification system
W	Total weight of the sliding mass

1. INTRODUCTION

1.1. General

The stability of highways and roads is generally involved in the static and dynamic analysis of slopes and embankments.

The research and studies on the stability of slopes and embankments focus on to maintain safety and reduce the costs of engineering applications. First step is to determine geotechnical, material, environmental and economical parameters in detail. Second step is to research the dimensions, nature and the possible reasons of the failure of the slopes which requires advanced studies from engineering geology to soil and rock mechanics. A realistic slope stability analysis must consider so many factors such as load conditions, topography, properties of materials and geologhy.

The stability of earth masses against sliding, or gravity effects, is clearly a serious problem. Stability problems must be solved in most earthwork construction. Due to the problem that the ground is not being level, which results in gravity components of the weight tending to move the soil mass from a higher to a lower elevation. Every soil mass located beneath a sloping ground surface or beneath the sloping sides naturally has the tendency to move downward and outward under the gravity forces. If this tendency is counteracted by shearing resistance or some applied reinforcements, stabilization can be provided, otherwise a slide occurs.

1.2. Problem Statement

Earthquakes pose a significant threat especially to the stability of man made engineering applications. Due to the propagating ground motions followed by its secondary effects, earthquakes are one of the most destructive natural disasters. Despite the existance of numerious studies in the literature that focus on mitigating related earthquake hazards on engineering structures, highway embankments are one of the

least studied structures amongst them. However, highway embankments and roads are clearly vulnerable to earthquake induced damage. It is very important to improve the seismic performance of highways as well as to mitigate earthquake related hazard to provide continious operation of such lifeline vulnerable structures.

1.3. Objective of the Thesis

The objective of this thesis is to determine the effect of the geosynthetic reinforcement on the seismic performance of the highway embankments and evaluate the seismic performance of the geotextile reinforced embankment under different earthquake motions. Experimental study covers detemination of the effects of the slope inclination, amplitude and predominant frequency of the motion on the seismic performance of unreinforced and reinforced embankment models. It is expected to decrease the transmitted accelerations using energy absorbent geotextile materials in order to keep the highway structure stabile under different earthquake conditions.

1.4. Organisation of the Thesis

This study investigates the seismic performance of geosynthetic reinforced highway embankments under different earthquake excitations. The scope of this thesis covers two different studies as experimental and numerical. To evaluate the seismic performance, two different modelling studies were performed. Experimental program consists of designing the unreinforced and reinforced embankment models, performing shaking table tests and the evaluation of the experimental results. The influence of the slope inclination, amplitude and predominant frequency of the motion on the seismic performance of unreinforced and reinforced embankment models are given. In addition, numerical dynamic analysis were performed in the prototype scale using the similar earthquake motions used in experimental program.

2. STABILITY PROBLEMS & FAILURES OF SLOPES AND EMBANKMENTS

Landslide or slope failure both express the situation of when a slope fails. Slope failures and slope movements may occur due to internal stability problems or as a secondary effect of earthquakes. The main reason of landslides or slope failures is the exceedance of resistance of soil by the driving forces.

There are seven velocity classes of landslides starting from extremely slow to extremely rapid. Each class represents a velocity of a movement of 100 times faster than the previous class as can be seen in Table 2.1.

Table 2.1. Velocity Classification of Slope Movements (Abramson, 2002).

Class	Description	Velocity
7	Extremely Rapid	$5x10^{3}$
6	Very Rapid	50
5	Rapid	0.5
4	Moderate	$5x10^{-3}$
3	Slow	$50x10^{-6}$
2	Very Slow	$0.5x10^{-6}$
1	Extremely Slow	-

Kinematically, there are five different types of slope movements represented as follows (Abramson, 2002):

- Falling
- Toppling
- Sliding
- Spreading
- Flowing

The terms falling and toppling are generally associated with very steep rock slopes. Sliding, spreading and flowing are common types of movements in soil slopes. Sliding can be defined as the downslope movement of a soil mass. Slides may be translational, rotational or compound depending on the soil properties. Spreading occurs when driving forces exceed only the resisting forces resulting in the large scale lateral deformation. Flows represent a continious movement of a viscous liquid over the critical failure surface of a slope. Figure 2.1 shows schematically the situations of falling, toppling, sliding, spreading and flowing with respect.

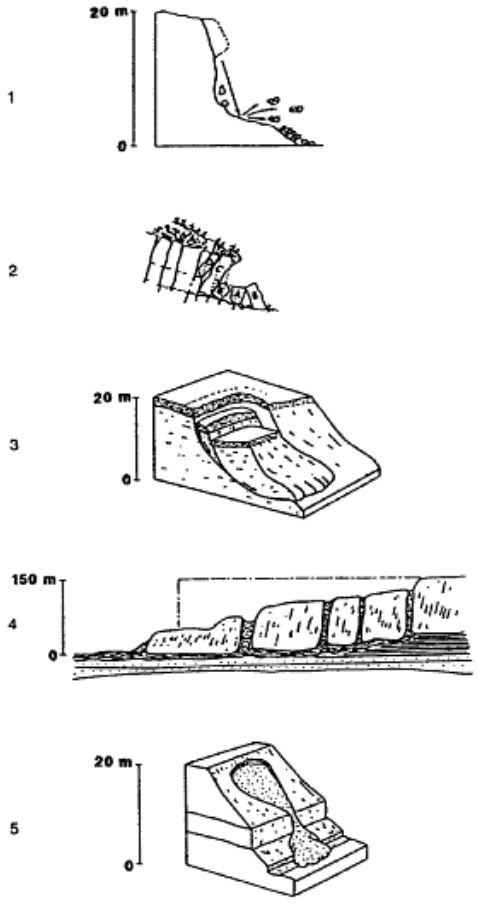

Figure 2.1. Types of Landslides (1) Falling, (2) Toppling, (3) Sliding, (4) Spreading, (5) Flowing (Abramson, 2002).

2.1. Causes of Slope Failures

The basic principle for the slope stability is satisfying equilibrium of forces. A slope or embankment will remain stable as long as the shear strength of the soil is greater than the shear stresses. However, there are many external factors to dissatisfy this equilibrium. Overall, these factors lead to a decrease or an increase in shear strength which directly influence the stability of slopes.

2.1.1. Decrease in Shear Strength

There are several processes that result in decreasing the shear strength of the slope and embankments. The most important ones are given below (Duncan, 2005) :

- *Increase of Pore Pressure*: An increase in pore water pressure as a result of a rise in groundwater level reduces the effective stress.
- *Cracking*: The development of cracks due to the tension in the soil may result in failures as the shear strength is reduced.
- *Swelling*: Swelling can be defined as the increase in the void ratio. Low confining pressures and the existance of water increase the void ratio of soil.
- *Development of Slickensides*: This situation occurs in highly plastic clays which has a very low internal friction angle.
- *Decomposition of Clayey Rock Fills*: Clayey rocks may turn into smaller pieces due to the water effect and once the pores of the rock fills are clogged by the clay particles, the shear strength of the fill is decreased significantly.
- *Creep under Sustained Loads*: Highly plastic clays tend to creep especially under sustained loads.
- *Leaching*: Salt leaching from the pore water of marine clays may lead to the development of quick clays with no strength.
- *Strain Softening*: Brittle soils experience strain softening when they are subjected to stress values higher than their shear strength.
- *Weathering*: Weathering due to physical, chemical and biological processes may decrease the shear strength of the soils and rocks.

- *Cyclic Loading*: The effect of cyclic loading on soils is the increase of pore water pressure. Loading may result in breaking the bonds of soil particles which causes an increase in pore pressures. Loose sands may even liquefy under cyclic loading and the shear strength decreases to zero.

2.1.2. Increase in Shear Strength

A stable slope or embankment may fail due to the changes of loads effecting on it. This situation causes an increase in shear strength which may lead to instability problems. Some of the cases of this situation is given below (Duncan, 2005) :

- *Loads at the Top of the Slope*: Additional loads at the top of slopes increase the required shear strength for stability.
- *Water Pressure in Cracks at the Top of the Slope*: The occurance of cracks at the top of slope and embankments is risky as the water filling those cracks may increase the shear stresses.
- *Increase in Soil Weight Due to Increased Water*: As the water content of the soil is increased, the weight of the soil increases as well which may lead to instability problems.
- *Excavation at the Bottom of the Slope*: Excavation processes on slopes and embankments increases the shear strength required for stability.
- *Drop in Water Level at the Base of a Slope*: Sudden changes in water level at the base of slopes causes instability problems due to the changes in pore pressure and external pressure.
- *Earthquake Shaking*: Seismic waves have a direct influence on the stability of slopes and the strength of soils.

2.2. Case Studies of Slope Failures

Due to the heavy precipitation of rain, The London Road in Oakland, CA experienced a serious landslide in 1970. The depth of the landslide surface was 20 meters deep, which was enough to destroy 14 houses and heavily damage the fet fuel

pipeline on the area. The reason of the deep seated failure was the extreme amount of rain recorded in the last two years. Figure 2.2 below represents the catastrophic event.

Figure 2.2. The London Road Landslide, Oakland, CA (Duncan, 2005).

In 1982, a strong storm hit San Francisco Bay area with a huge amount of rain fall in a short period of time resulting thousands of landslides from small to large scale. However, this time many of the slides were shallow (1 meter deep) because only 24h of intense rainfall triggered the failures as fully saturated upper layers of the soil lost most of its shear strength. Figure 2.3 below, shows a flow slide on Highway 24.

Figure 2.3. Flow slide on Highway 24 (Duncan, 2005).

The 1970 Great Peruvian Earthquake and the resultant landslide was one the most catastrophic natural disaster ever recorded. M 8.0 earthquake caused a huge

avalanche of ice, rock and soil with an average speed of 300km/h. As a result, the northern wall of Mount Huascarán was destabilized and the towns of Yungay and Ranrahirca were burried under avalanche (Figure 2.4).

Figure 2.4. Yungay town under mud and rocks (Day, 2002).

One of the largest earthquakes on Earth was recorded in Anchorage, Alaska in 1964. M_w 9.2 earthquake reshaped the area causing a lot of landslides and flowslides. Turnagain Heights region of the city experienced a large scale slide. Seismic waves broke the area into blocks at first and then whole area slid 610m towards the ocean destroying 75 houses located in the zone. The failure is illustrated in Figure 2.5.

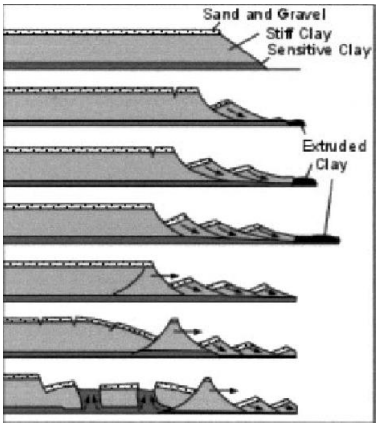

Figure 2.5. Illustration of Turnagain Heights landslide (Day, 2002).

Government Hill School area in Anchorage was also heavily damaged due to the earthquake induced slope failure. The school complex experienced both lateral and vertical displacement and ripped the building in two (Figure 2.6).

Figure 2.6. Government Hill School damage after earthquake induced slope failure (Day, 2002).

2.3. Common Earthquake Effects on Slopes

An earthquake is the vibration of Earth produced by the rapid release of accumulated energy in elastically strained rocks.The energy released radiates in all directions from its source and it propagates in the form of seismic waves which may cause extensive damage because it effects the soil layers. Common earthquake effects can be generally listed in topics of Surface Rupture, Regional Subsidence, Liquefaction, Slope Movement and their secondary effects.

2.3.1. Surface Rupture

Surface rupture occurs when movement on a fault deep within the earth breaks through to the surface. Most earthquakes will not generate ground surface rupture especially the ones with small magnitudes, earthquakes generated at great subduction zones and earthquakes generated on blind faults. On the other hand large earthquakes at transform boundaries usually generate a ground surface fault rupture on strike-slip faults.

Fault displacement is defined as the relative movement of the two sides of a fault, measured in a specific direction and it can reach up to 11 meters. Every man made structure especially highway or railway embankments are expected to experience a significant damage under surface rupture conditions. An example to this situation is represented in Figure 2.7.

Figure 2.7. Fault displacement after the 1999 Kocaeli Earthquake.

2.3.2. Liquefaction

The development of high pore water pressures due to the rapid shaking of the earth and the upward flow of water may turn the sand into a liquefied condition which is also termed as liquefaction.

Liquefaction occurs when the soil condition is loose sand,which has been newly deposited or placed with a groundwater table near ground surface. During an earthquake the propagation of shear waves causes the loose sand to contract, resulting in an increase in pore water pressure causes an upward flow of water to ground surface where it emerges in the form of mud spouts or sand boils. Earthquake induced damage on a road is shown in Figure 2.8.

Figure 2.8. Earthquake induced damage after the 1989 Loma Prieta Earthquake (Day, 2002).

Site conditions and soil type that are most susceptible to liquefaction are given as follows:

Site Conditions

- Very close to the epicenter of a major earthquake or a fault rupture
- Site which has a groundwater table close to ground surface

Soil Type

- Sand with uniform gradation and rounded particles
- Very loose or in a loose density state
- Recently deposited with no cementation between particles
- No prior preloading or seismic shaking

2.3.3. Slope Movement

Slope movement is another secondary effect of the earthquakes.There can be many different types of slope movements due to earthquakes but generally they are divided into falls and slides.Falls are distinguished by the relative free-falling of the rocks from hills or mountains.

Slides are different from falls.In slide events,there is shear displacement along a distinct failure surface. A comprehensive table related with soil movement from slopes are represented in Table 2.2.

Table 2.2. Detailed types of slope movements (Day, 2002).

Main type of slope movement	Subdivisions	Material type	Minimum slope inclination	Comments
Falls	Soil falls	Granular soils that are slightly cemented or contain clay binder.	40° (1.2 : 1)	Particularly common on stream banks, terrace faces, coastal bluffs, and artificially cut slopes.
Slides	Soil avalanches	Loose, unsaturated sands.	25° (2.1 : 1)	Occasionally reactivation of preexisting soil avalanche deposits.
	Disrupted soil slides	Loose, unsaturated sands.	15° (3.7 : 1)	Often described as *running soil* or *running ground.*
	Soil slumps	Loose, partly to completely saturated sand or silt; uncompacted or poorly compacted artificial fill composed of sand, silt, or clay, preexisting soil slump deposits.	10° (5.7 : 1)	Particularly common on embankments built on soft, saturated foundation materials, in hillside cut-and-fill areas, and on river and coastal flood plains.
	Soil block slides	Loose, partly to completely saturated sand or silt; uncompacted or slightly compacted artificial fill composed of sand or silt, bluffs containing horizontal or subhorizontal layers of loose, saturated sand or silt.	5° (11 : 1)	Particularly common in areas of preexisting landslides along river and coastal floodplains, and on embankments built of soft, saturated foundation materials.
Flow slides and lateral spreading	Slow earth flows	Stiff, partly to completely saturated clay, and preexisting earth flow deposits.	10° (5.7 : 1)	An example would be sensitive clay.
	Flow slides	Saturated, uncompacted or slightly compacted artificial fill composed of sand or sandy silt (including hydraulic fill earth dams and tailings dams); loose, saturated granular soils.	2.3° (25 : 1)	Includes debris flows that typically originate in hollows at heads of streams and adjacent hillsides; typically travel at tens of miles per hour or more and may cause damage miles from the source area.
	Subaqueous flows	Loose, saturated granular soils.	0.5° (110 : 1)	Particularly common on delta margins.
	Lateral spreading	Loose, partly or completely saturated silt or sand, uncompacted or slightly compacted artificial fill composed of sand.	0.3° (190 : 1)	Particularly common on river and coastal floodplains, embankments built on soft, saturated foundation materials, delta margins, sand spits, alluvial fans, lake shores, and beaches.

3. SEISMIC ANALYSIS

Seismic waves generated from an earthquake are capable of inducing destructive inertial forces in natural or artificial slopes. Destabilization problems may occur due to the earthquake ground motions. Sudden and intense loads generated from earthquakes may affect the shear strength of the slopes such as the generation of the excess pore water pressure. The combined effect of the earthquake loads and the differences in the shear strength may lead to an overall decrease in the stability of the slopes. On the other hand, generation of the high pore water pressure due to the cyclic loads may turn the loose, cohesionless and saturated materials (sand, silt etc.) into a liquefied condition where the shear strenght of the soil essentially decrease to zero.

In the literature, the stability of slopes under earthquake motions are evaluated using four methods of analyses (Houston *et al*. 1987):

- Pseudostatic Method
- Newmark's Displacement Method
- Post-Earthquake Stability (Weakening Slope Stability)
- Dynamic Finite Element Analysis

3.1. Pseudostatic Method

Pseudostatic Method uses the earthquake inertial forces simulated by the inclusion of a static vertical and horizontal force in a limit equilibrium analysis. This method is the most commonly used and easily understood and applied approach. The cyclic nature of the ground motions are ignored, instead earthquake loads are applied as an additional static force upon the slope.

$$F_h = ma = Wa/g = Wa_{max}/g = k_hW \quad (3.1)$$

where;

F_h : Horizontal pseudostatic force acting through the center of the sliding mass

m : total mass of the sliding mass

W : total weight of the sliding mass

a : acceleration

a_{max} : maximum horizontal acceleration

k_h : seismic coefficient

Seismic coefficient used in this method depends on the following which directly affects the desired FOS (Abramson, 2002) :

- Earthquake Intensity
- Duration of Shaking
- Frequency Content

Seismic loading is assumed to affect horizontally only perpendicular to the weight of the slope (Figure 3.1). The difficulty of this method is to choose the proper seismic coefficient among the different conditions (Table 3.1).

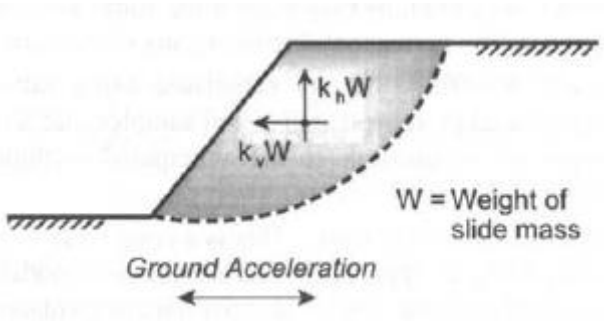

Figure 3.1. Pseudostatic Equilibrium Method Analyses under seismic loading (Abramson, 2002).

Table 3.1. Seismic coefficients used in Pseudostatic Equilibrium Method Analyses (Abramson, 2002).

Seismic Coefficient	Remarks
0.10	Major earthquake, FOS > 1.0 (Corps of Engineers, 1982)
0.15	Great earthquake, FOS > 1.0 (Corps of Engineers, 1982)
0.15–0.25	Japan, FOS > 1.0
0.05–0.15	State of California
0.15	Seed (1979), with FOS > 1.15 and a 20 percent strength reduction
$\frac{1}{3}$–$\frac{1}{2}$ PGA[a]	Marcuson and Franklin (1983), FOS > 1.0
$\frac{1}{2}$ PGA	Hynes-Griffin and Franklin (1984), FOS > 1.0 and a 20 percent strength reduction

3.2. Newmark's Displacement Method

This method is proposed by Newmark in 1965 and it is considered as an extended version of the pseudostatic method. The method is based on the comparison between the yield acceleration and a representative accelerogram of the affected slope in order to determine the permanent displacements (Figure 3.2). These displacements represent the motion of the center of gravity of the sliding mass.

This method assumes that slope deformes and moves where the FOS value is less than one. Also, slip surface is well defined in Newmark's method. Slide material is assumed as plastic and while seismic shaking occurs, the loss of shear strength is negligible. Permanent strains are expected when the dynamic stress exceeds the shear resistance.

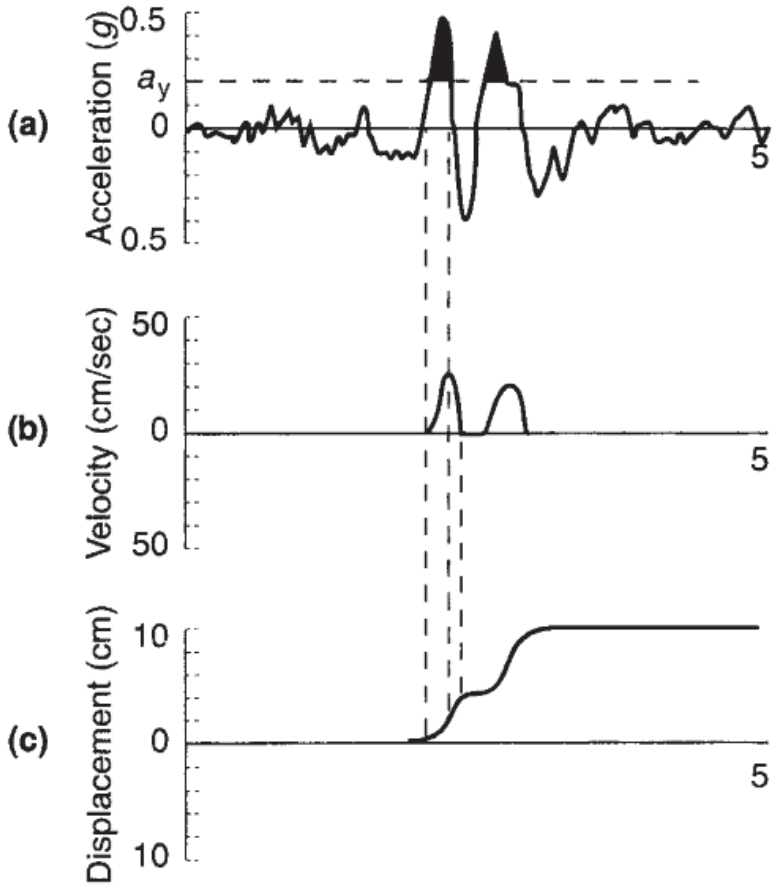

Figure 3.2. Schematic diagram of Newmark's Method (Day, 2002).

Displacement of the slopes are affected by four major parameters in this method, which are listed below (Day, 2002):

- Yielding Acceleration (a_y)
- Peak Ground Acceleration (a_{max})
- Length of Time
- Number of Acceleration Pulses

The general equation based on considering two of the listed parameters is given as follows;

$$\log d = 0.90 + \log \left[\left(1 - \frac{a_y}{a_{max}} \right)^{2.53} \cdot \left(\frac{a_y}{a_{max}} \right)^{-1.09} \right] \quad (3.2)$$

3.3. Weakening Slope Stability Analysis

This method is generally preferred where the shear strength of the materials decrease significantly as a result of the earthquake motions. Common types of this materials and situations are given as follows (Day, 2002):

- Fructable rocks that may lead to rock falls and slides during earthquakes
- Sensitive clays losing shear strengths easily under ground motions
- Organic soils and soft clays susceptible to plastic slow and slow earth flows
- Loose soil conditions below groundwater table, liquefaction, flow slide and lateral spreading conditions.

3.4. Finite Element Method

Finite element method enables engineers to evaluate the stability of complex structures. This method was first introduced to geotechnical engineering by Clough and Woodward (1967) and today it is commonly used especially for the analyses of complex earth structures such as natural slopes or earth dams. The advantage of this method is to bypass the inherent deficiencies in limit equilibrium methods (Abramson, 2002).

Finite Element Method (FEM) divides soil continuum into discrete elements which are called finite elements. Those elements are connected to each other at nodes (Figure 3.3). The FEM uses a simple approximation of unknown variables to transform partial differential equations into algebraic equations. Physical laws and numerical methods are based on the neccessary solutions and calculations are carried out using a computer (Dhatt, 2012 (Finite Element Method)).

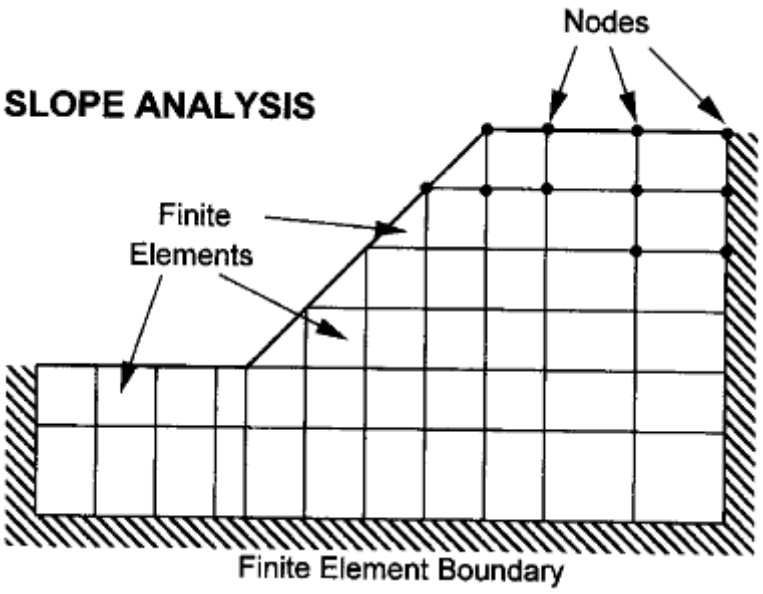

Figure 3.3. Basis of Finite Elements Method for slope analysis (Abramson, 2002).

4. GEOSYNTHETICS & SEISMIC HAZARD MITIGATION

The importance of the earthquake induced destructive effects on structures are still being underestimated. Many of the most populated and economically developed cities are located very close to dangerous and seismically active fault zones and in history. There are many devastating examples of how earthquake induced strong ground motions may cost billion of dollars to global and local economies. For this reason, mitigation of earthquake effects by means of site improvement methods are essential. In this chapter some of these methods are handled.

In order to stabilize slopes, resisting forces should be increased, driving forces should be reduced or both. In general the following applications can be applied to increase the resisting forces within a slope (Abramson, 2002):

- Drainage applications
- Elimination of weak and potential failure zones
- Building retaining structures or similar
- Conducting in-situ soil improvement methods
- Chemical treatment of the slope to increase the shear strength

In this thesis, only geosynthetic reinforcement method and various types of geosynthetics are handled in detail.

Geosynthetics is the term used to describe a range of generally polymeric products used to solve civil engineering problems. The term is generally regarded to encompass eight main product categories: geotextiles, georids, geonets, geomembranes, geosynthetic clay liner, geofam, geocells and geocomposites.

Steepened slopes have become increasingly advantageous due to the desire to increase land usage and decrease site development costs. The proven concept of tensile

reinforcement allows construction of slopes with far steeper face angles than are permitted by the soils natural angle of repose.

Slopes are common geographic features located adjacent to highways and along the periphery of building sites in many areas of the country. For construction on highway and building projects, relatively flat areas are preferred. These areas must be excavated out of the existing terrain, often leaving significant grade changes at the edges of the excavation. The economic feasibility of constructing a particular highway alignment or the development of a parcel of land may be determined by the ability to create sufficient flat, or level, land to satisfy space safety, or access requirements. Reinforced steepened slopes provide a cost-effective means to achieve more efficient grade changes than is possible with unreinforced slopes. Figure 4.1, represents the most common engineering applications of geosynthetic reinforcement.

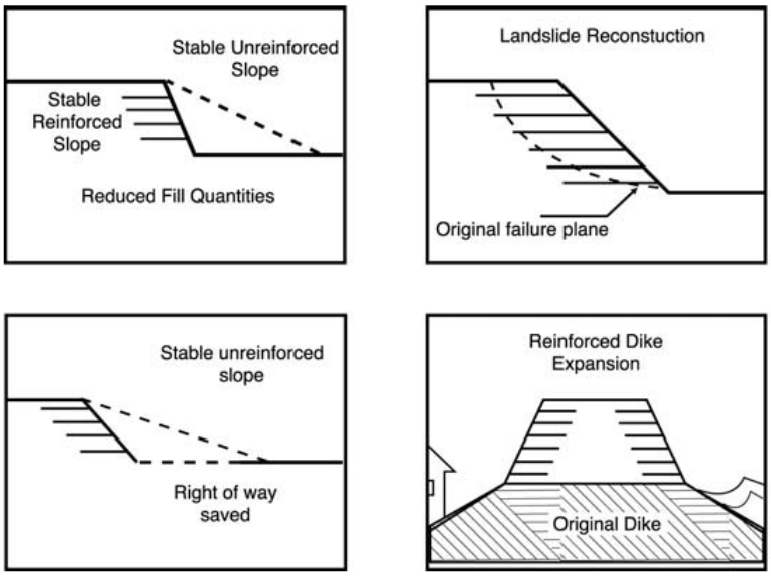

Figure 4.1. Common engineering applications of geosynthetics for reinforcement purposes.

Geosynthetic reinforced steepened slopes are soil structures constructed with slope face angles up to as high as 70 degrees from horizontal. Typical unreinforced soil slopes are limited to slope face angles of approximately 25 to 30 degrees or less, depending on the slope soil (Figure 4.2).

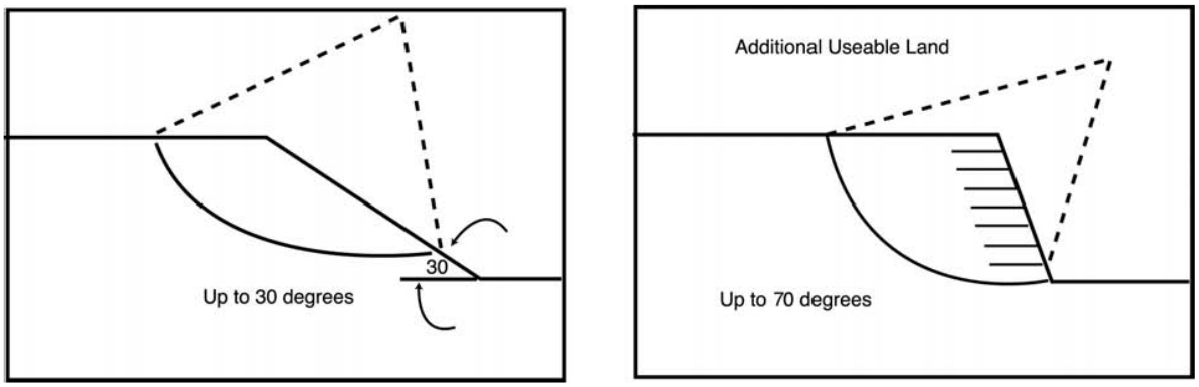

Figure 4.2. The comparison of conventional and geosynthetic reinforced slopes.

The stability of earth masses, such as slopes and embankments, against sliding or gravity effects is a serious problem. It should be permenantly solved in earthwork constructions. This is because the ground is not being level, which results in gravity components of the weight tending to move the soil mass from a higher to a lower elevation. Every mass of soil located beneath a sloping ground surface or beneath the sloping sides has the tendency to move downward and outward under the influence of gravity forces. This situation requires engineering applications of reinforcement to satisfy stability conditions.

A geosynthetic is a planar product manufactured from polymeric material used with soil, rock, earth or other geotechnical engineering related materials as an integral part of a human-made project, structure or system (Koerner, 2005).

Recently, the use of geosynthetics has grown rapidly and today, geosynthetics are commonly used in many of the engineering applications as a reason of the following advantages (Koerner, 2005) :

- Quality-Control Manufactures in Factories
- Rapid Installation
- Replacement of Raw Material Resources
- Replacement of Difficult Design of Soil and Construction Materials
- Appropriate Timing
- Required Use by Regulations in Some Cases
- Relatively Cheap
- Enables Impossible Designs and Applications
- Widely Available
- Design and Testing Criterias are Established
- Integration into the Profession

Geosynthetics have five major functions. These are seperation, reinforcement, filtration, drainage and containment. The aim of using geosynthetic for engineering purposes is to achieve better performance for less money.

There are eight types of geosynthetics today, which are geotextiles, geogrids, geonets, geomembranes, geosynthetic clay liners, geopipes, geofoams and geocomposites (Koerner, 2005).

4.1. Geotextiles

Geotextiles are thin, flexible and permeable sheets of synthetic material used to stabilize and improve the performance of soil associated with engineering applications. Correctly designed and installed, geotextiles have the ability to filter, drain, reinforce and separate soil. In many applications, geotextile may be designed and selected to perform a combination of these functions. For example, when installed at the base of a granular fill embankment constructed over soft clay, all four functions may operate together.

4.2. Geogrids

Geogrids are commonly used and preferred materials. Geogrids are made of plastic formed into a shape of grids with openings. Depending on the area of use, geogrids are produced in various ways (Koerner, 2005):

- Streched in one or two dimensions for the improved strength
- Weaved or knitted
- Made by bonding rods or straps together

4.3. Geonets

Geonets are also known as geospacers as they are formed by parallel sets of polymeric ribs. When these ribs are opened, it shapes a netlike configuration. Geonets are generally used for drainage purposes.

4.4. Geomembranes

Geomembranes are very thin impervious polymeric sheets widely used for lining and covers in construction works such as canals, landfills and reservoirs especially where leakage or contamination problems are a matter of question. The use of geomembranes increases rapidly in construction industry.

4.5. Geosynthetic Clay Liners

A geosynthetic clay liner (GCL) is a type of geocomposite that is frequently used in envrionmental containment applications and is an alternative to traditional compacted clay liners. It is primarily used for the lining of landfills. Due to the protection of environment, any seepage from landfills must be collected and properly disposed of, otherwise contamination of the surrounding ground water may cause major environmental and ecological problems.

4.6. Geopipe

Geopipes are also known as burried plastic pipes. Geopipe is being used in many aspects of geotechnical, transportation and environmental engineering. It sees uses in water and gas distribution, sewer and wastewater, oil and gas production, industrial and mining uses, power and communications, duct and irrigation systems.

4.7. Geofoam

Geofoams are produced by polymeric expansion process which makes them extremely light. Geofoam has been used as a geotechnical material since the 1960s. As a lightweight fill, geofoam reduces the loads imposed on adjacent and underlying soils and structures. They can also be used for seperation and drainage purposes.

4.8. Geocomposites

The term geocomposite defines the combination of two or more types of geosynthetics. There are a great number of applications available for the use of geocomposites and a wide range of functions.

5. EMBANKMENT FAILURE MODES AND CASE STUDIES

Road and highway embankments have been affected significantly and damaged by major earthquakes in the past. Earth embankments are easier to repair than other concrete like structures but the important point is to restrict the level of damage in the allowable limit. There are five main failure mode of embankments which are; shallow surface sliding, development of slip surface within the body of embankment, development of slip surface reaching the soft foundation soil, slumping and densification (Towhata, 2008).

5.1. Shallow Surface Sliding

Shallow surface sliding is a common failure mode of embankments triggered by many different factors such as earthquakes, ground water or load conditions. Shallow surface sliding is illustrated in Figure 5.1 below.

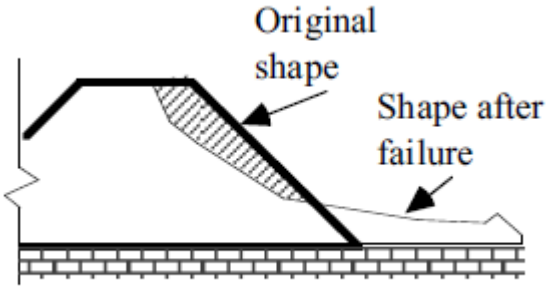

Figure 5.1. Illustration of shallow surface sliding (Towhata, 2008).

The 2004 Niigata-Chuetsu Earthquake caused a sliding failure of a road embankment. Due to the strong ground motions, the road embankment experienced a great displacement destroying the burried pipelines within the structure as can be seen in Figure 5.2. Another example of a failed road embankment due to the same earthquake is shown in Figure 5.3.

Figure 5.2. A sliding failure of a road embankment and destroyed pipelines after 2004 Niigata-Chuetsu Earthquake (Towhata, 2008).

Figure 5.3. A failed road embankment due to sliding failure (Towhata, 2008).

5.2. Development of the Slip Surface within the Body of Embankment

The failure mechanism of this type is quite similar to sliding failure mode but a deeper slip plane generates more damage. The illustration of development of the slip surface within the body of embankment is represented in Figure 5.4, below.

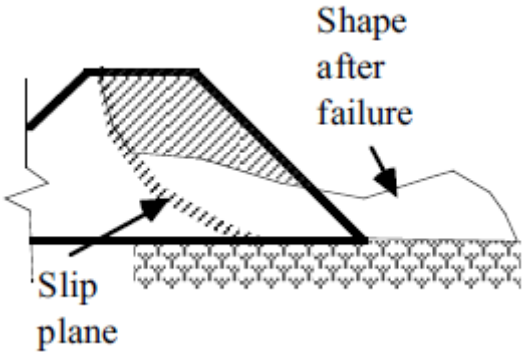

Figure 5.4. Illustration of development of the slip surface within the body of embankment (Towhata, 2008).

In 1993, the Kushiro-Oki Earthquake motions damaged a residential site after the failure of an embankment fill affected by the ground water level. Embankment fill was located between the stiff soil and peat (Figure 5.5) and when the earthquake occured the peat level was unable to sustain the embankment fill. The residential area located on the failed embankment is shown in Figure 5.6.

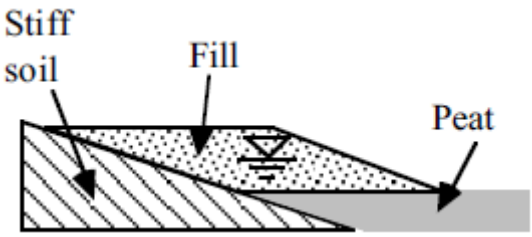

Figure 5.5. Illustration of the location of the residential site located at the failed embankment (Towhata, 2008).

Figure 5.6. The residential area located on the failed embankment (Towhata, 2008).

5.3. Development of Slip Surface Reaching the Soft Foundation Soil

This kind of failure occurs when the slip surface reaches to the soft foundation soil due to the rising ground water level and dynamic loading (Figure 5.7). That was the case in the M 6.4 Sumatra Earthquake in 2007 and the M 6.3 Adana Earthquake in 1998 where river side embankments were failured due to the earthquake excitations. Figure 5.8, represents the collapsed river bank located on the failured embankment in Adana and Figure 5.9, represents the damaged neighbourhood of Sumatra experienced the failure of a slip surface embankment failure.

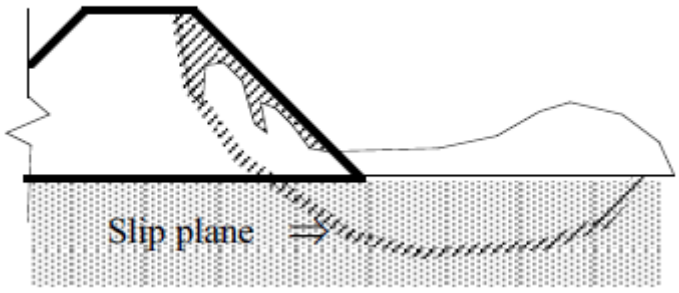

Figure 5.7. Illustration of development of the slip surface reaching the soft foundation soil (Towhata, 2008).

Figure 5.8. Collapsed river bank located on the failed embankment (Japan Society of Civil Engineering Reports, 1998).

Figure 5.9. Collapsed neighbourhood of Sumatra located on the failed embankment (Japan Society of Civil Engineering Reports, 1998).

5.4. Slumping Damage of Embankments

This kind of damage on embankments are usually triggered by the liquefaction or lateral spreading of the soft soil deposits beneath the embakments during an earthquake and this type of failure may cause notable damage in the area. The illustration of the slumping damage is shown in Figure 5.10, below.

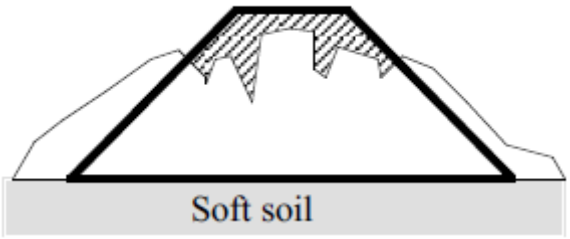

Figure 5.10. Illustration of slumping damage on embankments (Towhata, 2008).

The 1983 Nihonkai-Chubu Earthquake caused the failure of road embankment which experienced slumping due to the seismic shaking. The road embankment was located at the edge of a Hachiro-gata Lake and was connecting to a bridge crossing the lake. However the area suffered liquefaction of the subsoil and the road embankment slumped as given in Figure 5.11.

Figure 5.11. Slumping of a road embankment (Towhata, 2008).

5.5. Densification Damage of Embankments

Densification damage occurs where earthquake related subsidence is present. When subsidence is observed along highway and road embankments or near the abutments of a bridge, transportation stops and the road can not be in operation for a

certain period of time. The illustration of the densification damage is shown in Figure 5.12, below.

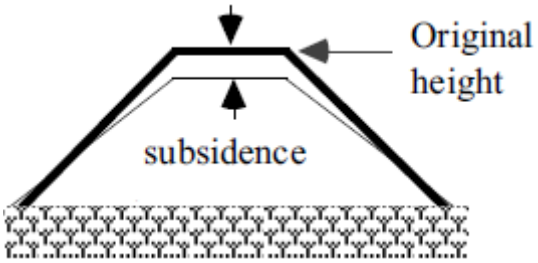

Figure 5.12. Illustration of densification damage on embankments (Towhata, 2008).

The 2004 Niigata-Chuetsu Earthquake led to many different kinds of geotechnical problems in the area including subsidence. A heavily damaged road embankment suffering densification damage located on a subsided zone is represented in Figure 5.13, below.

Figure 5.13. Densification damage of a road embankment due to subsidence (Towhata, 2008).

6. PREVIOUS STUDIES

This part of the study consists of detailed literature review about reinforced embankments. Firstly, studies about the failure mechanisms of embankments are given. Next, geosynthetic reinforced embankments are reviewed. Studies of reinforced embankments using tire derived aggregates and EPS beads are summarised later on.

6.1. Studies on Failure Mechanisms of Embankments

A study by Wartman *et al*. (2005) focuses on seismically induced deformations in slopes performing shaking table tests with the aim of determining the failure mechanisms of slopes under dynamic loading and to investigate the applicability and the accuracy of the Newmark sliding block procedure. A number of four slopes with different geometric parameters designed and instrumented in a plexiglas box and shaking table tested under 1g of acceleration. Results of the study showed that all slope models deformed under dynamic loading with the deformation type of deep rotational and translational sliding displacement. In addition, the accuracy of the Newmark method was found to be moderate for dynamic analysis.

Slope instability was modelled and centrifuge tested by Ling *et al*. (2009). Using sand with fines as material, slopes with different angles and heights were designed in a rigid aluminium box with the relative density (Dr) of 89%. With the help of a system with nozzles which mimics the natural rain fall, slopes were also tested during rain fall (Figure 6.1). Results of the experiment indicate the efficiency of the centrifuge tests in simulating slope instability and it was noted that rainfall induced instability problems in slopes might be interpreted as a reduction in apparent cohesion.

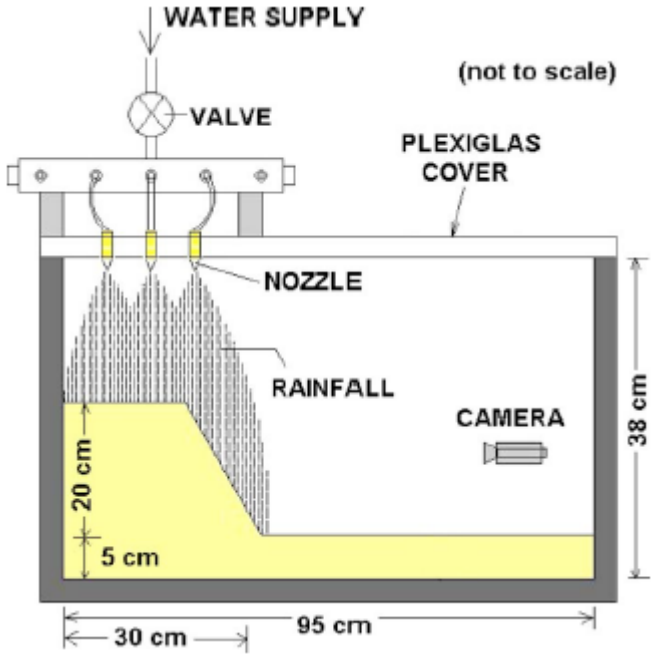

Figure 6.1. Centrifuge modelling of the tests (Ling *et al*., 2009).

A similar study by Tamate *et al*. (2012) represents the effect of heavy precipitation on the dynamic response of the slopes performing centrifuge tests. Using silica sand material, a slope model with the angle of 30° was designed in a rigid box with dimensions of 50x20x40cm. Test set-up can be seen in Figure 6.2. The study mainly focused on the failure mode of the slope in the shallow section under undrained conditions caused by the heavy precipitation.

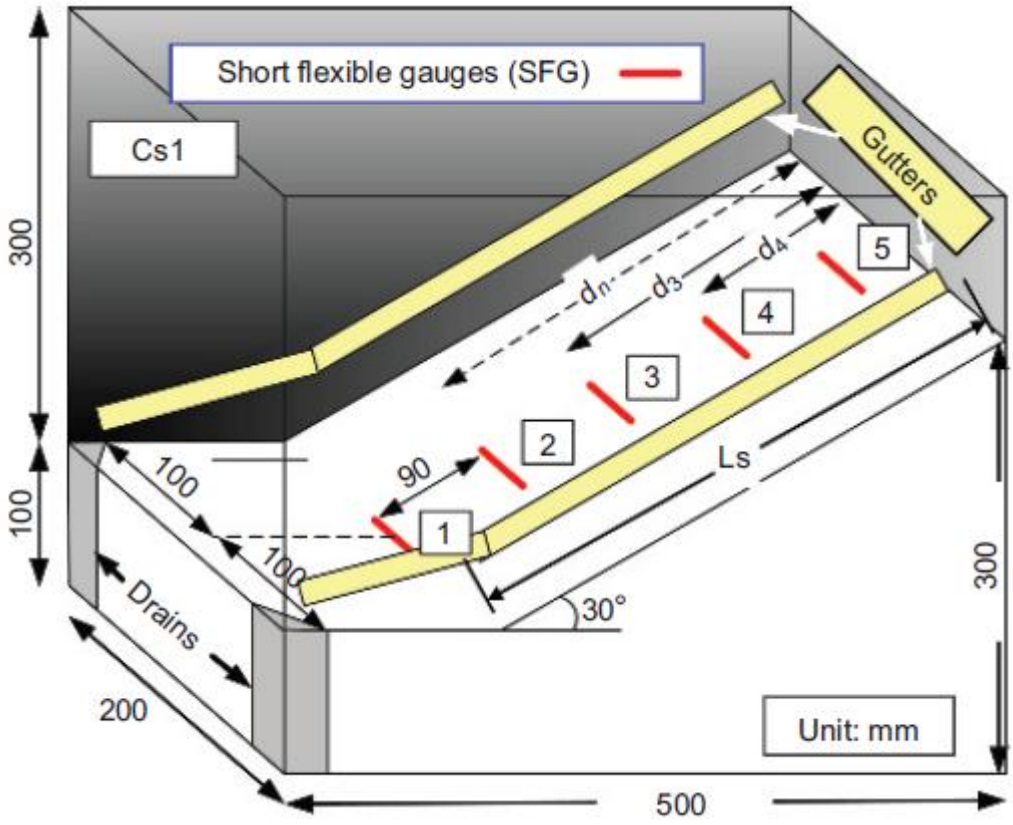

Figure 6.2. Test set-up (Tamate *et al*., 2012).

Seismic slope behavior was studied in a large-scale shaking table model test by Lin and Wang, 2006. Using a uniform medium sand, a model slope with dimensions of 0.5x1.3m and slope angle of 30° was created in order to determine the seismic behavior of the slope model. To do so, shaking table tests were performed with a large 4.4x1.3x1.2m plexiglas sided box. Scaling factor used during the experiments was 1/20. The model to be tested can be seen in Figure 6.3.

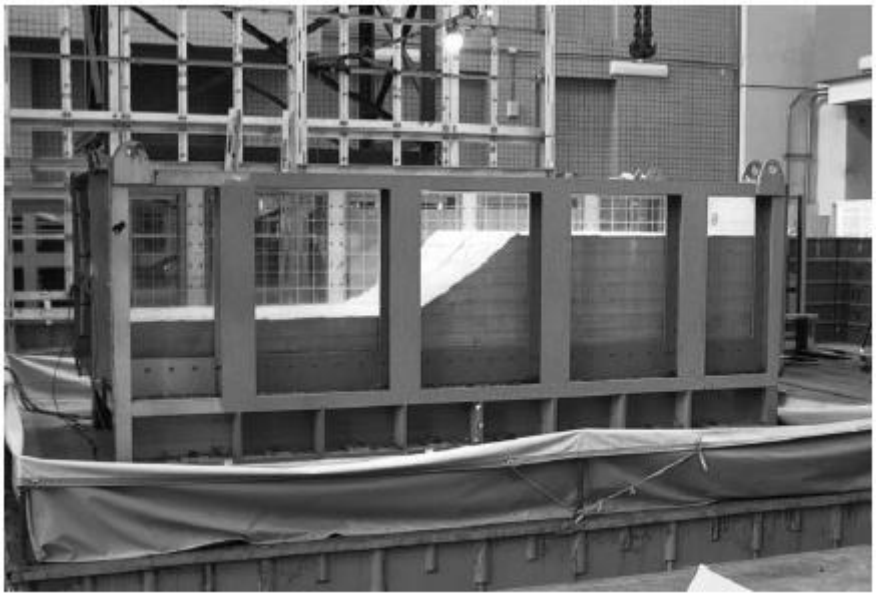

Figure 6.3. The slope model before the test (Lin and Wang, 2006).

The results of the experiment were given as follows:

- The slope model behaved elastically under accelerations up to 0.4g.
- Boundary effects were not significant according to the numerical modelling with FLAC.
- Significant soil amplification was observed especially when non-linear behavior takes place that may influence the failure of the slope.
- The failure surface was circular and close to the slope surface (Figure 6.4).

Figure 6.4. Failed slope model after seismic loading (Lin and Wang, 2006).

6.2. Geosynthetic Reinforcement on Embankments

It has been no more than 30 years since the term “geosynthetic” appeared in the literature but today geosynthetics are widely used for engineering applications especially in the fields of transportation, geotechnics, hydraulics and environment.

A study by Srilatha *et al*. (2012) investigates the effect of frequency on seismic response of slopes. As material, clayey soil was used for the experiments. Both reinforced and unreinforced slopes were shaking table tested using a laminar box (Figure 6.5). Biaxial geogrids were used for reinforcement of slopes. Properties of geogrids are listed in Table 6.1.

Figure 6.5. Laminar box used for the experiments (Srilatha *et al*., 2012).

Table 6.1. Properties of geogrids (Srilatha *et al*., 2012).

Property	Value
Ultimate tensile strength	26 kN/m
Initial modulus	183 kN/m
Secant modulus at 5% strain	125 kN/m
Mass per unit area	0.22 kg/m^2
Aperture size	35 mm × 35 mm
Aperture shape	Square

Creating two different angles of 45° and 60° , slope models were excited dynamically under 0.3g of acceleration with different frequency values of 2, 5 and 7 Hz. It was concluded that the increase in frequency values leads to an increase in measured displacement values.

Six steep geosynthetic reinforced slopes were shaking table tested in the study of Perez *et al*. (2004). Slopes were designed to have an angle of 63° with 4 ft of height and silica sand was used throughout the study. 5 Hz of frequency was chosen in order to determine the seismic behavior of slopes with different variables of L/H ratio and geosynthetic spacing. Test results show that both L/H ratio and geosynthetic spacing are essential parameters for geosynthetic reinforced slopes and embankments and as it was observed during the tests, increase in L/H ratio and decrease in geosynthetic spacing

leads to more stabilized models. Figure 6.6, schematically represents the effect of reinforcement spacing by means of yield acceleration.

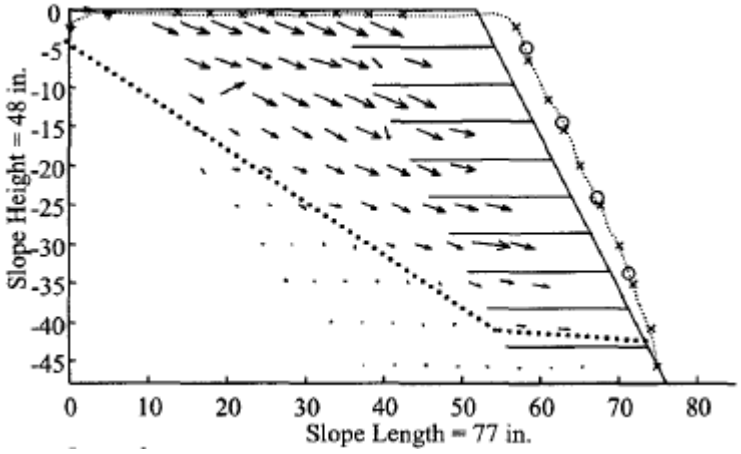

(a)

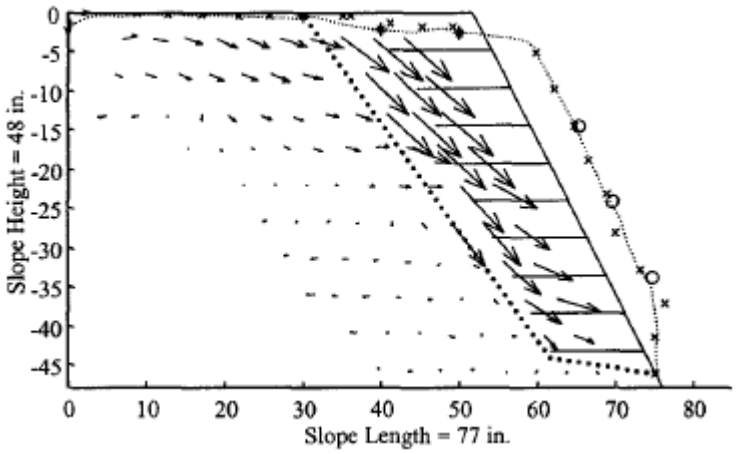

(b)

Figure 6.6. The effect of geosynthetic spacing by means of yield acceleration (Perez *et al*., 2004).

Another study related with the seismic behavior of slopes was performed by Grasso *et al*. (2005). Conducting a series of shaking table tests, both reinforced and unreinforced slopes were subjected to dynamic loading up to 0.5g of acceleration. As

represented in Figure 6.7, experiments were performed in a plexiglas box, using typical silica sand material and bi-directional polypropylene geogrid as reinforcement.

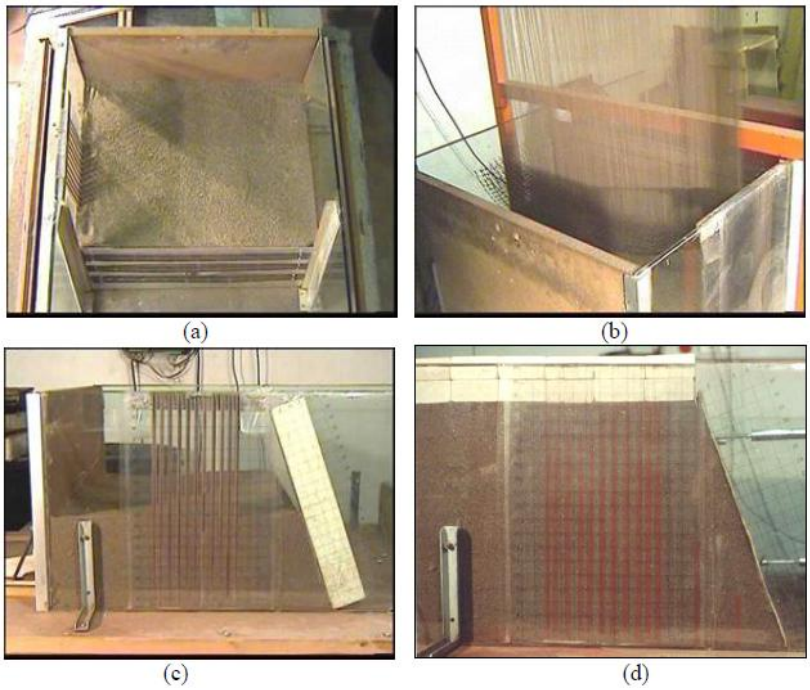

Figure 6.7. The test set-up procedure. (a) Upper view, (b) Sand pluviation method, (c) Sand markers, (d) Final model prior to tests (Grasso *et al*., 2005).

Results of the experiments were listed as follows:

- Vertical reinforcement does affect the stability of the system.
- Dense reinforcement near the top of the slope is effective for the stability.
- The presence of surcharge weight at top of the embankment influences the stability.
- Circular surface failure is observed when a surcharge load is present, hence a typical two-wedge failure mechanism applies on the contrary.
- Spacing of reinforcement should be reduced near the top of the slope.
- Surcharge loads increases the interface resistance between soil and reinforcement layers which results in a decrement of the lateral facing deformation.

A study by Rajabian *et al*. (2013), represents a centrifuge model testing of a slope which was reinforced by anchored geosynthetics. The slope model with a 2V:1H design with clayey sand material was subjected up to 50g of acceleration under steady seepage conditions which was provided by a seepage tank until the slope failures (Figure 6.8). Different parameters, such as anchor stiffness, length and pretensioning were taken into consideration as shown in Table 6.2. Results of the experiment satisfies the limit equilibrium stability analyses.

Table 6.2. Test Programme (Rajabian *et al*., 2013).

Test no.	Test legend[c]	AE_a/l_f (kN/m)	l_a [l_f+l_b] (mm)	AGS stress, (kN/m^2)[d]	Anchor load (kN)	Pretensioning (mm)	No. of anchors	S_V (mm)	S_H (mm)
1	RRS 4[c,e]	16.125	160 [100+60]	5.33	0.032	2	9	60[a]	60
2	RRS 5[c,e]	16.125	160 [100+60]	7.11	0.032	2	12	60[b]	60
3	RRS 6[c]	16.125	160 [100+60]	0	0	0	12	60[b]	60
4	RRS 7[c]	16.125	200 [100+100]	5.33	0.032	2	9	60[a]	60
5	RRS 8[c]	24	160 [100+60]	1.67	0.01	1	9	60[a]	60

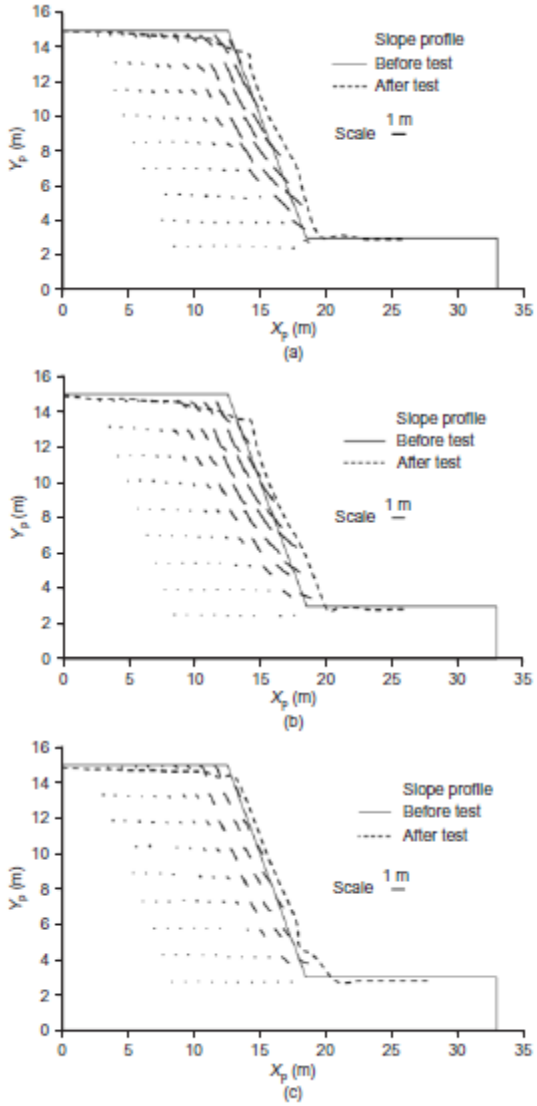

Figure 6.8. Deformation output of the cases RRS6 (a), RRS7 (b) and RRS8 (c) (Rajabian *et al*., 2013).

A numerical and experimental study was conducted by Yang *et al*. (2012) on geosynthetic reinforced soil slopes. A series of centrifuge tests were performed using a non-woven interfacing fabric reinforcement which has strength parameter of T_{ult}:0.03kN where Monterey No. 30 sand was used as backfill. Experimental test setup can be seen on Figure 6.9 below.

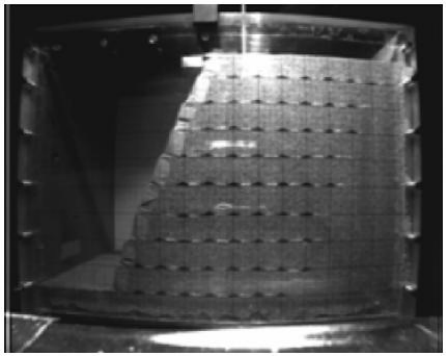

Figure 6.9. Experimental centrifuge test set-up (Yang *et al*., 2012).

Centrifuge tests were performed at 50g acceleration and after the failure surface and type is determined, finite element model of the same model was created using the program ANLOG. The FEM centrifuge model was performed analysis at 45g. It was determined that both numerical and eperimental results verifies each other as can be seen on Figure 6.10.

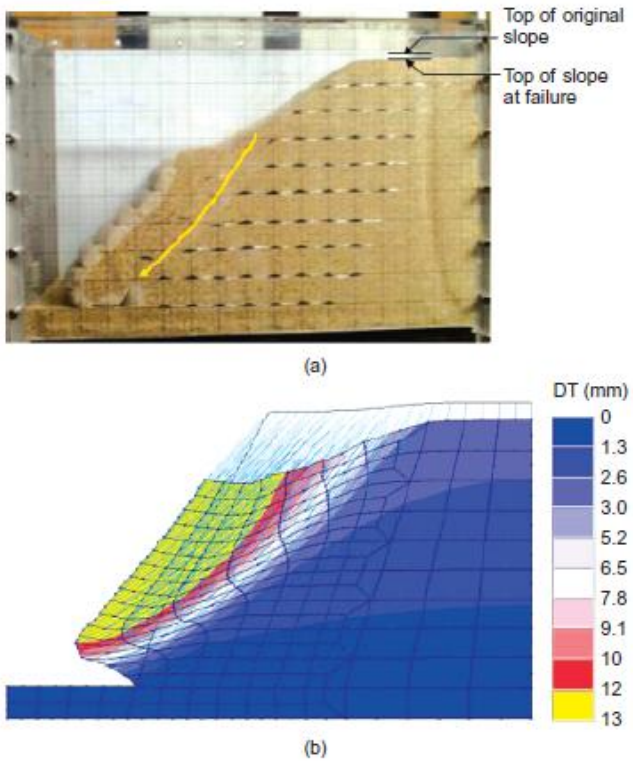

Figure 6.10. Comparison of the failure surface results (a) Experimental centrifuge test at 50g; (b) The ANLOG model at 45g.

Aklik and Wu performed centrifuge tests on geosynthetic reinforced slopes. 440x400x155mm size rigid box was used for the experiments. Uniform coarse sand with internal friction angle of 34° was used as the material. Three different slope inclinations of 65°, 75°, 85° was reinforced with six, seven and eight layers of geotextile with respect and subjected to centrifuge test. According to Viswanadham and König, 2009 a 1/N reduced geometric model must be subjected to N times higher gravitional acceleration in order to simulate the gravitional stress occurance on a prototype. With the help of a high resolution camera, Particle Image Velocimetry (PIV) method was evaluated to observe the deformations. It was seen that minor breakage deformations was observed.

An experimental study by Akay *et al*. (2013), investigates the EPS-block geofoam remediated slopes under seepage flow. Installing lysimeters, a total of 36 lysimeter experiments were performed under three different constant water pressure values and the efficiency of the geofoam blocks were investigated. Plexiglas box with the dimensions of 200x20x60cm was preferred to mimic field conditions and to be able to see the instant and permanent deformations. Laboratory setup can be seen in Figure 6.11. Results of the study suggests geofoam block system especially where shallow-seated failures are expected due to seepage flows.

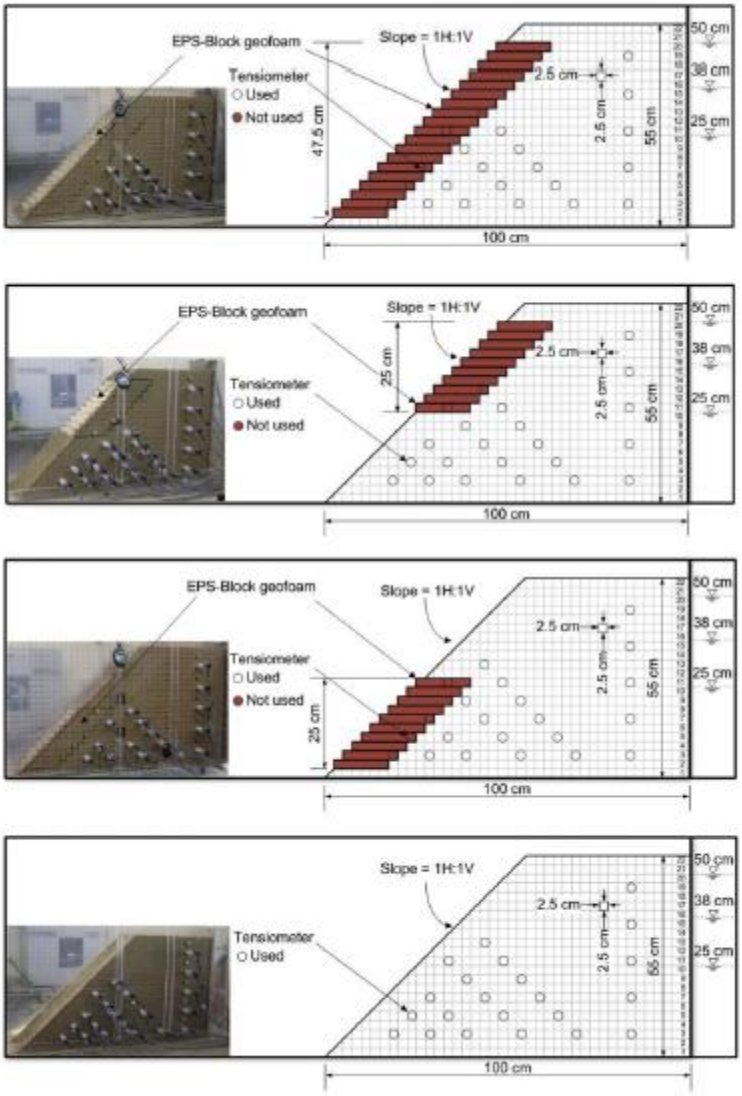

Figure 6.11. Laboratory set-up and configurations (Akay *et al*., 2013).

In order to invesitgate amplification and de-amplification responses of geosynthetic reinforced slopes, Yang *et al*. (2013) performed a series of dynamic centrifuge tests up to 50g. The size of the testing embankment models was 160x367mm with slope angles of 45° and 63.5°. During the experiments, a variety of input ground motions were used that are given in Table 6.3, below.

Table 6.3. Centrifuge test setup (Yang *et al*., 2013).

Test	Vertical Spacing s_v (m)	Tensile Strength T_{ult} (kN/m)	Facing slope β (degree)	Input motion frequency f (Hz)	Input Ground Acceleration a_g (g)
GREE-4	0.8	112	45	1	0.07, 0.13, 0.22
GREE-5	0.8	112	63.5	1	0.05, 0.11, 0.20
				4.8	0.02, 0.04, 0.07
GREE-6	0.8	62.5	63.5	1	0.07, 0.13, 0.23
				4.8	0.02, 0.05, 0.10
GREE-8	0.5	112	45	1	0.04, 0.09, 0.17
				4.8	0.01, 0.03, 0.07
GREE-9	0.5	112	63.5	1	0.06, 0.11, 0.21
				4.8	0.02, 0.04, 0.10

The objective of the study is also to demonstrate the effect of input ground acceleration, a_g, location, z, and input motion frequency, f, on the amplification and de-amplification responses of slopes. It was concluded that A_m, which is the acceleration amplification factor, is clearly affected by the changes in a_g. Also it was determined that A_m is distributed non-uniform along the height of the GRS slope and amplification and de-amplification responses increase with height. In addition to that, it was also noted that acceleration responses are very dependent on the seismic frequency. In other words, A_m increases as motion frequency f increases.

6.3. Embankment Reinforcement by the Inclusion of Scrap Tire-Sand Mixtures

Hartman *et al*. (2013) investigated the effect of tire derived aggregates (TDA) used as a backfill of MSE wall on the dynamic means of response. A rigid box with the dimension of 1.5m x 1.87m x 1.8m was used for the experiments. MSE wall was designed to have geogrid reinforcement and it is 1/3 scaled with respect to the similitude laws. Dynamic tests under the Lima Prieta Earthquake excitations indicate that TDA backfill satisfies the seismic performance of the reinforced MSE wall.

The use of recycled geomaterials such as tire chips and tire shreds are becoming more demanding each day as such materials are low-cost with high damping properties which are good at improving the seismic performance. That’s why recycled tire like

materials were described as smart geomaterials by Hazarika *et al*. (2007). The properties of such geomaterials are given below:

- Lightweight
- Elastic
- Compressible
- Highly Permeable
- Earthquake Resistant
- Thermally Insulated
- Durable

The objective of the experimental study by Hazarika *et al*. (2008) is to develop a cost effective seismic hazard mitigation technique using recycled tires. A 1/10 scaled caisson type quay wall model was tested using an underwater shaking table under 1g of acceleration. Created outline of the model can be seen in Figure 6.12.

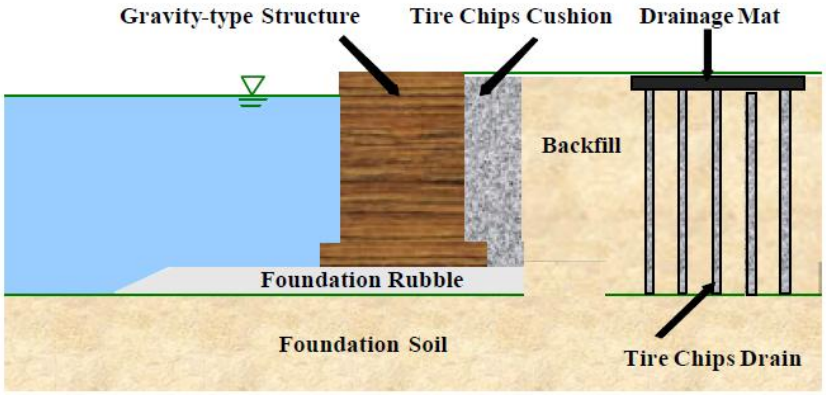

Figure 6.12. Outline of the underwater model (Hazarika *et al*., 2008).

Sohma sand No.5 was used as backfill with a relative density of 50% and Hyogo-ken Nanbu Earthquake (M 7.2) record was used for the experiments. Instrumentation was set to obtain the seismic incremental pressure difference between the conventional and tire derived backfills. Results of this study proves that the proposed method is successful at reducing the seismic load, reducing the permanent

displacements and increasing the seismic performance in a low-cost and eco-friendly manner. Results are represented below in Figure 6.13.

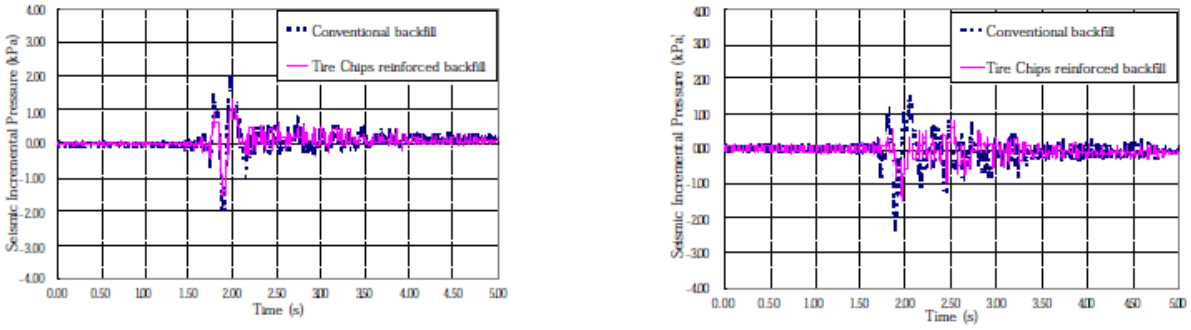

(a) (b)

Figure 6.13. Difference of seismic incremental pressure between conventional and tire derived backfill (a) At lower part of the quay wall (b) At upper part of the quay wall.

A study by Yoon *et al*. (2005) evaluates the feasibility of using tire shred-sand mixtures on road embankments, investigates the combustibility properties of the mixture and also determines the groundwater quality for a possible contamination due to the use of synthetic materials. For that purpose, a test embankment was constructed using tire shred-sand mixture (50/50 by volume). Instrumentation was planned to be able to monitor the vertical settlements and the generation of heat inside the mixture. The embankment and the instrumentation can be seen in Figure 6.14.

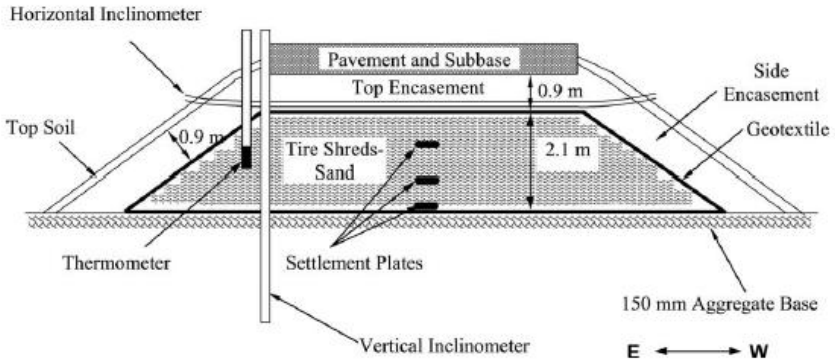

Figure 6.14. The test embankment and the instrumentation (Yoon *et al*., 2005).

It is noted that scrap tire is both lightweight and not biodegradable which makes it sustainable and durable. When scrap tire and sand is mixed together, compressibility properties of the mixture becomes limited which is an advantage for embankments. The test embankment was opened to traffic and the settlements were monitored periodically for more than one year and no crack or damage was observed on the embankment. Settlement values with respect to the traffic days is given in Figure 6.15.

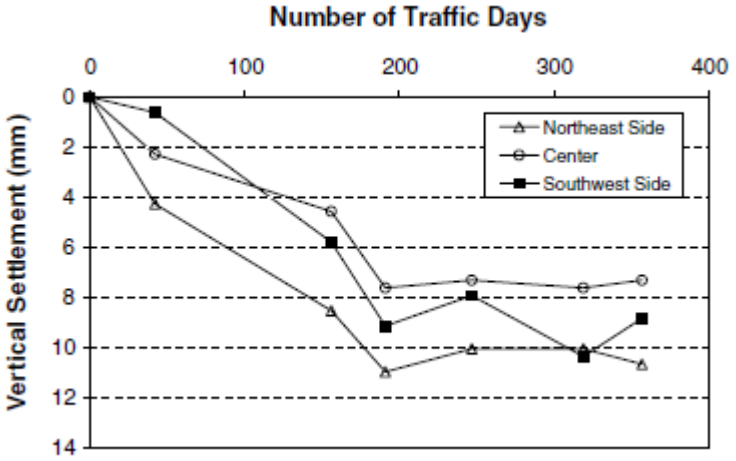

Figure 6.15. Vertical displacement values and number of traffic days (Yoon *et al*., 2005).

Self heating is an important issue when granular or scrap tire material is used for embankment construction as this situation was observed with embankments made of pure rubber material in Washington and Colorado (Humphrey, 1996). There is no self heating induced fire occurance report for embankments containing rubber-soil mixtures in the literature. Previously located thermometers monitored the temperature inside the embankment and the temperature didn't exceed 20°C during a year (Figure 6.16) which gives no evidence of self heating.

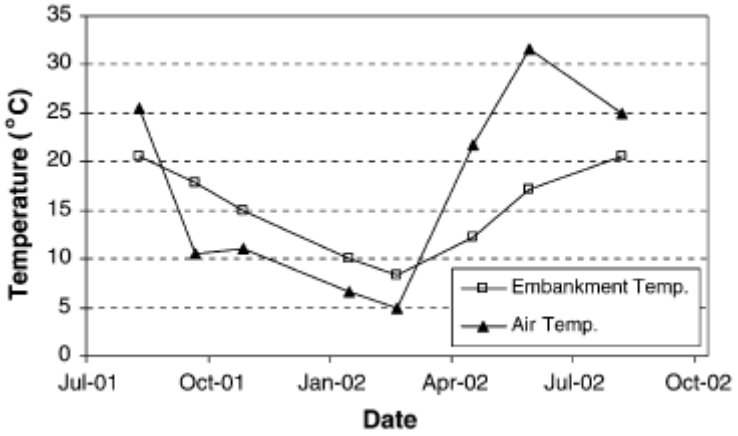

Figure 6.16. Comparison of the temperatures inside and outside of the embankment (Yoon *et al*., 2005).

In addition, a monitoring well was installed to investigate the probable contamination of the groundwater. The well was located on the same direction of the groundwater flow and extends to a a depth of 13.7m. Results of the analysis indicates that all metals except the manganese are below the standards set for secondary drinking water (EPA, 2002). By the way it is noted that manganese poses no threat for human health (US EPA, 2002).

6.4. Embankment Reinforcement by the Inclusion of EPS Beads-Sand Mixtures

A study by Liu and Chu reveals the advantages of using polystyrene pre-puff beads-soil mixtures as a backfill. In the laboratory studies, different ratios of pre-puff beads-soil mixtures are tested and the following remarks are concluded:

- Inclusion of 2-6% of pre-puff beads with soil by weight, can reduce the density of the backfill down to 700kg/m^3
- When compared to EPS geofoam blocks, the density of the soil mixture using pre-puff beads is higher. Stiffness and shear strength parameters are also found to be higher than geofoam blocks.
- The use of EPS beads-soil mixtures is an alternative lightweight backfill material especially for irregular volumes.

In order to observe the stress-strain relationship of EPS-sand mixtures, Deng and Xiao conducted CD triaxial compression tests on mixtures including different ratios of EPS beads of 0.5, 1.5, and 2.5 by weight. During the laboratory tests four different confining pressure values are used which are 100, 200, 300, and 400kPa. Summary of the testing programme is given in Table 6.4, below.

Table 6.4. Testing programme of EPS-sand mixtures (Deng and Xiao, 2010).

Series	EPS content η (by weight %)	EPS volumeratio χ (%)	Bulk unitweight (kN/m^3)	Consolidation pressure (kPa)
1	0	0	17.0	100, 200, 300, and 400
2	0.5	30	12.6	100, 200, 300, and 400
3	1.5	57	8.2	100, 200, 300, and 400
4	2.5	69	6.3	100, 200, 300, and 400

Resultant deviatoric stress-strain behavior and volumetric strain behavior for three different mixing ratios are given below. Figure 6.17, represents the 0.5% EPS beads content condition by weight, Figure 6.18, represents the 1.5% content and finally Figure 6.19, shows the 2.5% content case.

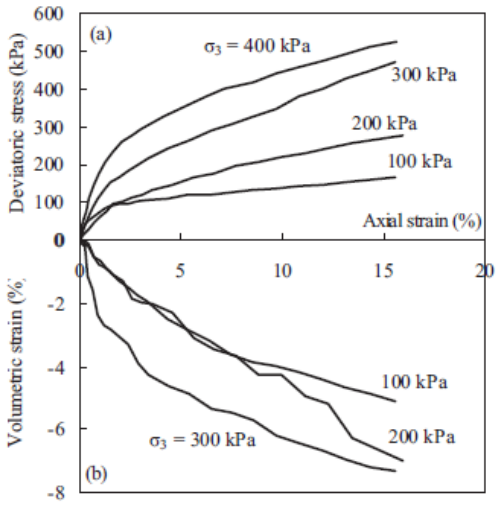

Figure 6.17. Triaxial test results of mixtures containing 0.5% EPS beads, a) deviatoric stress-strain behavior, b) volumetric stress behavior (Deng and Xiao, 2010).

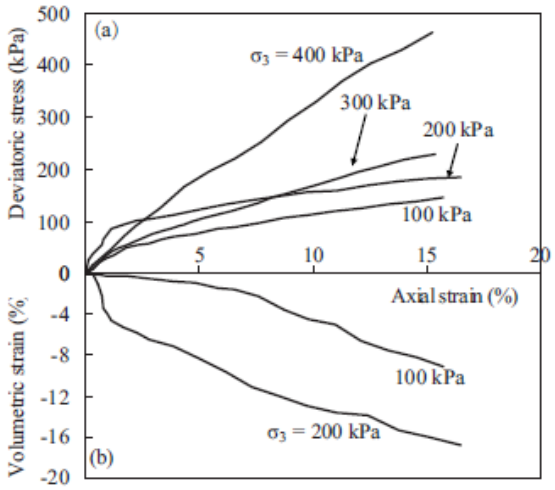

Figure 6.18. Triaxial test results of mixtures containing 1.5% EPS beads, a) deviatoric stress-strain behavior, b) volumetric stress behavior (Deng and Xiao, 2010).

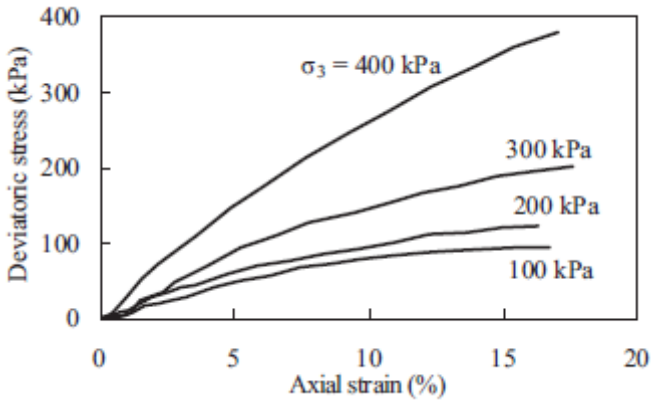

Figure 6.19. Triaxial test results of mixtures containing 2.5% EPS beads (Deng and Xiao, 2010).

The results express a hyperbolic stress-strain behavior which differs from the behavior of pure sand samples. The shear strength of the mixture decreases as the ratio of EPS beads increases. As a result, the optimum EPS beads content was suggested as 0.5% by weight due to the reasonable unit weight and shear strength parameters of the mixture.

7. EXPERIMENTAL STUDY

7.1. General

Experimental study consists of a series of shaking table tests to determine the effect of geotextile reinforcement on the seismic behavour of highway embankments under different dynamic motions. The influence of slope inclination, amplitude and predominant frequency of the earthquake motions on the dynamic behavior of 1/50 scaled, instrumented unreinforced and reinforced highway embankments are evaluated. Shaking table tests were performed with using a designed plexiglas soil box. Unreinforced and reinforced embankment models of both inclinations (45° and 30°) were prepared inside the soil box. Input dynamic motions consist of sinusoidal harmonic motions of two amplitudes (0.3g and 0.5g) with four predominant frequencies (2Hz, 5Hz, 7Hz and 14Hz) and a time scaled earthquake record of the 1999 Düzce Earthquake (M=7.2). The seismic performance of the embankment models were evaluated comparing the amount of settlements, displacements, transmitted PGA values, spectral accelerations with corresponding period values. In addition, Amplification Factors (AF) are calculated and presented. AF values are calculated as the ratio of transmitted acceleration to input acceleration value. Shaking table tests were carried out at Boğaziçi University Kandilli Observatory and Earthquake Research Institute. The shaking table used for this experiment is a uniaxial horizontal vibration shake table which is capable of carrying a maximum 10 ton payload on the 3m x 3m table with a maximum of 2g acceleration.

7.2. Materials

Preparation of the test setup consists of a few stages and disciplines. These stages are to decide the proper embankment prototype, modelling of the prototype embankment, design and production of the plexiglas soil box to accommodate the embankment model inside. It is determined that a 1/50 scaled highway embankment model is optimal for the present conditions.

7.2.1. Sand

The sand used during the experiments is named as “Silivri Sand” which is locally found around Istanbul region and it is widely used for highway embankments. The grain-size distribution of the sand according to the ASTM Standart of D422 is given in Figure 7.1, below. According to the USCS system, the sand material is classified as poorly graded sand (SP) with C_u: 2.29 and C_c : 1.1.

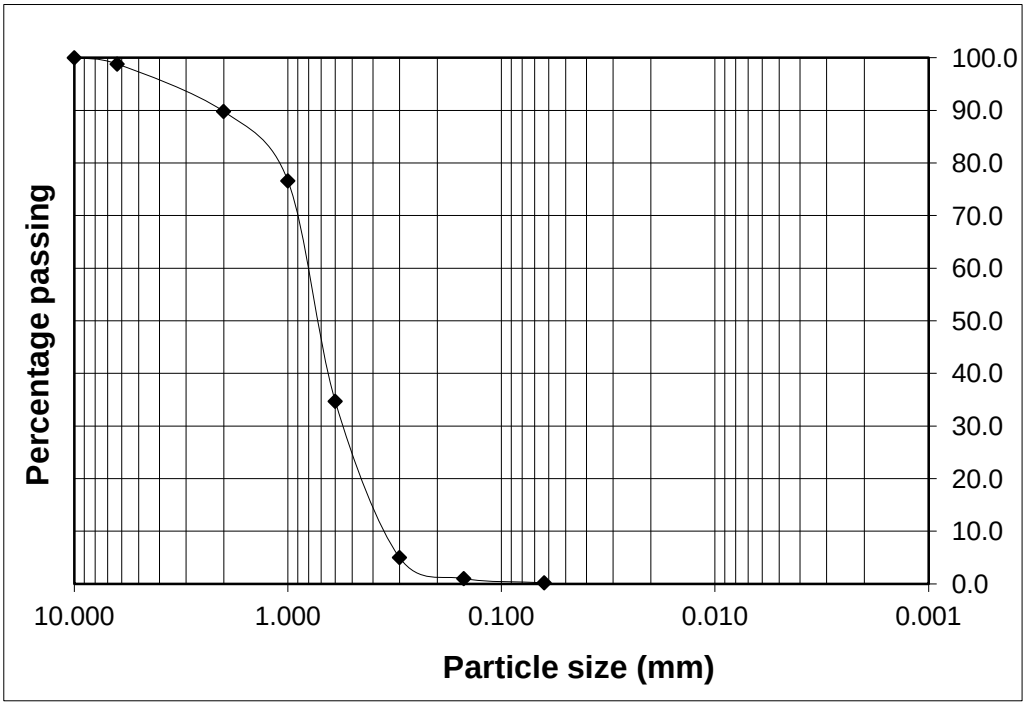

Figure 7.1. The grain-size distribution of the sand.

7.2.2. Geotextile

The geotextile used for this study is a woven type geosynthetic material. The geotextile used in the experiments is 1/50 times scaled with respect to the scaling laws of Iai (1989). Due to the scaling law, the relationship between prototype and reduced scale model reinforcement stiffness can be explained as follows:

$$J_p = J_m \lambda^2 \qquad (7.1)$$

where;

J_p : Prototype scale reinforcement stiffness

J_m: Reduced scale model reinforcement stiffness

λ: Scaling factor

7.2.3. Soil Box

A soil box with dimensions of 90x40x50cm was designed and used for shaking table experiments. The box is made of plexiglas with 15mm thickness. Plexiglas is usually preferred for shaking table experiments because the material itself is high resistant to dynamic and static loads, transparent and moreover mimics the field conditions for shaking table experiments. The soil box used for this study is represented in Figure 7.2, below.

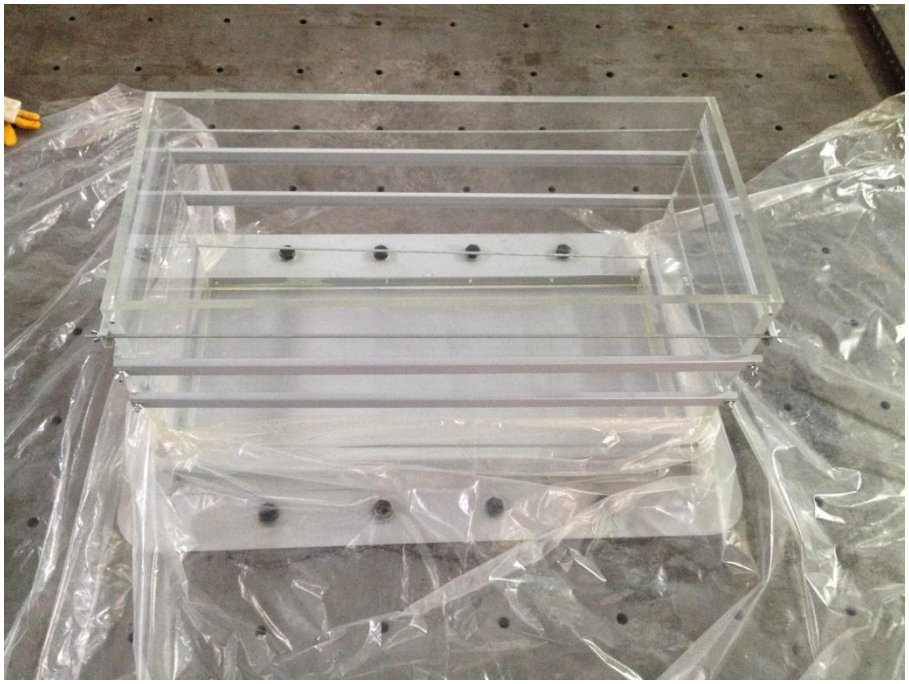

Figure 7.2. The plexiglas soil box.

7.3. Methods

This section covers the preperation of the experiemental setups, instrumentation and the verification of the soil box performance check.

7.3.1. Soil Box Performance Check

Performing shaking table experiments, it is essential to use a soil box which provides idealized soil layer boundary conditions (Taylor and Crewe, 1996). In order to check the performance of the developed soil box under dynamic loading, the sides of the soil box is gres oiled to minimize the friction in the first place (Figure 7.3). After the box is half filled with sand material and instrumented with five accelerometers which are all placed at the same elevation. The sand is compacted to the desired relative density of 70%. The soil box is expected to show similar responses on the center and each corner at the same level. The instrumentation of soil box performance check is represented in Figure 7.4.

Figure 7.3. Gres oil application on the sides of the soil box.

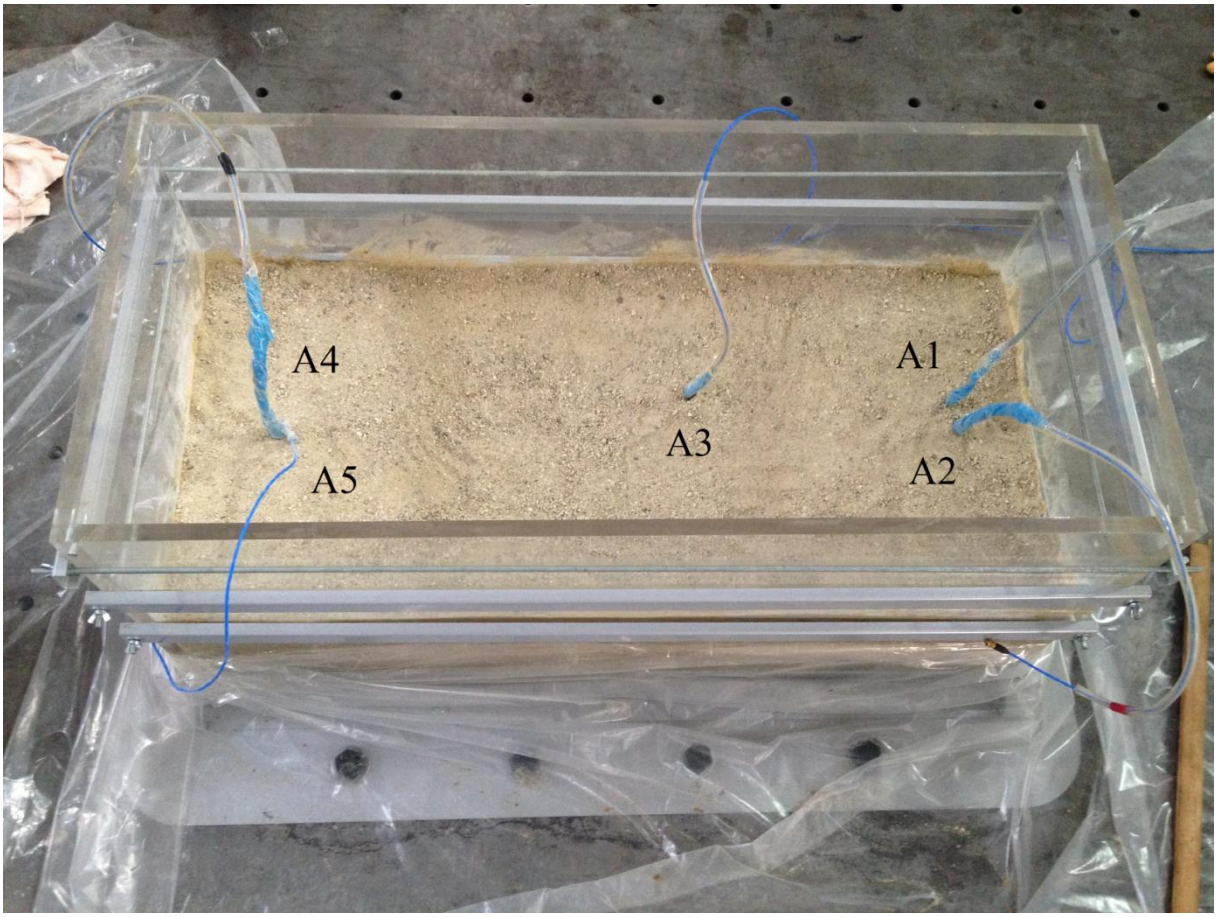

Figure 7.4. Instrumentation of the soil box performance check.

Shaking table tests were performed under El Centro Earthquake, Kobe Earthquake and Kocaeli Earthquake ground motions and a progressively increased sine wave up to 0.5g (KOERI). During the tests, acceleration responses were recorded and analysed. Acceleration-Time histories of the related ground motions are represented in figures between Figure 7.5 and Figure 7.8.

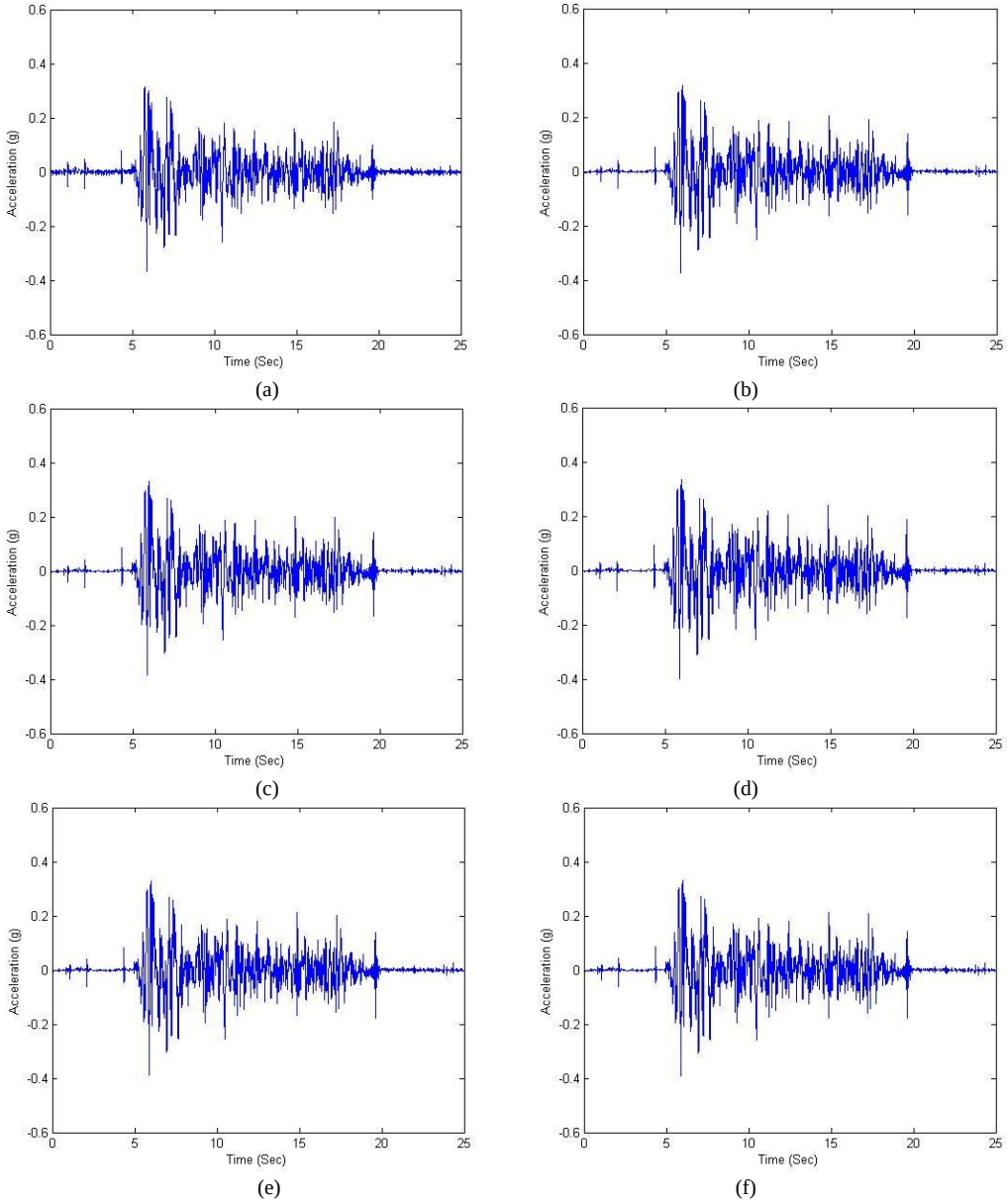

Figure 7.5. El Centro Earthquake excitations recorded by a) A1, b) A2, c) A3, d) A4, e) A5, f) A6.

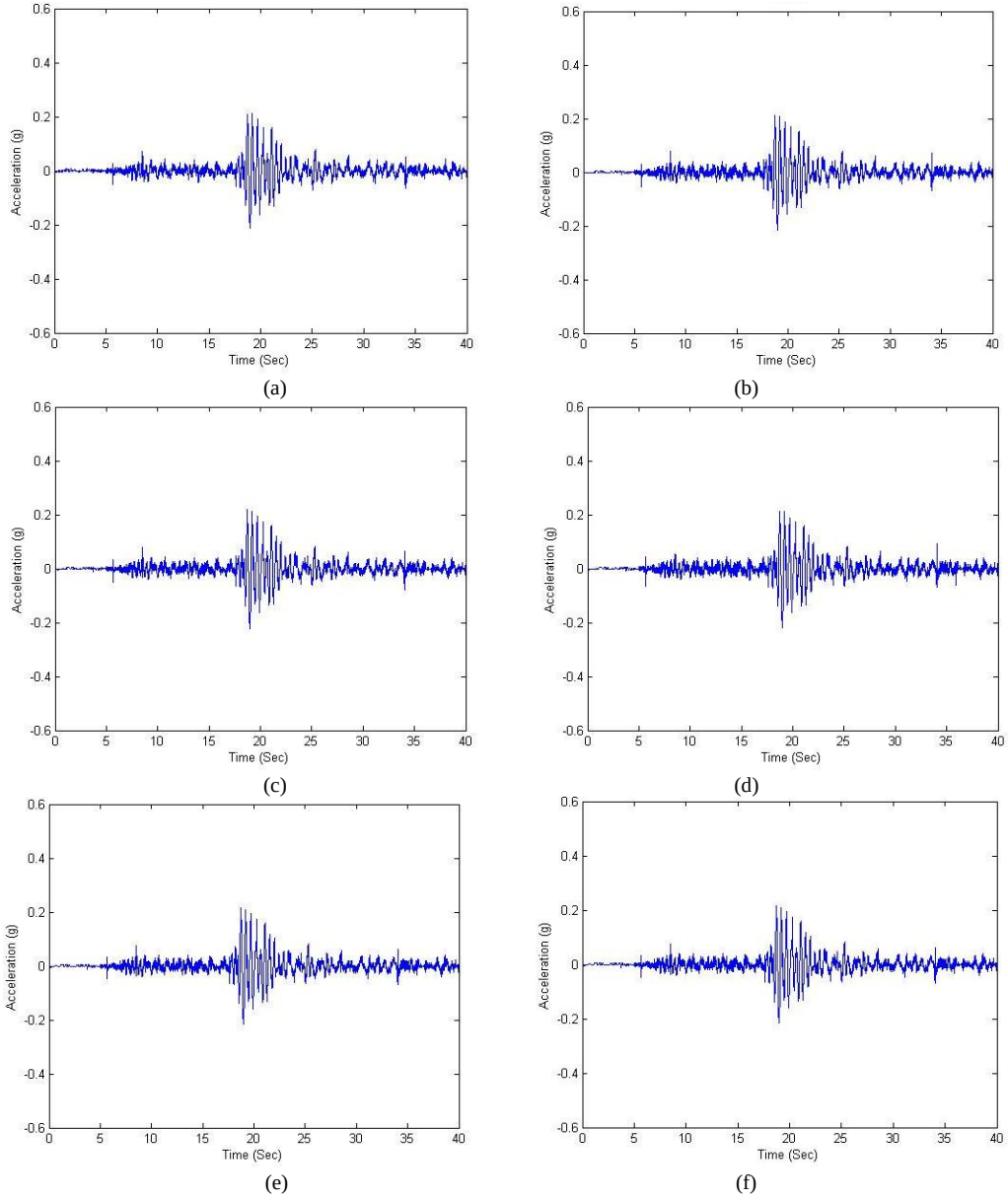

Figure 7.6. Kobe Earthquake excitations recorded by a) A1, b) A2, c) A3, d) A4, e) A5, f) A6.

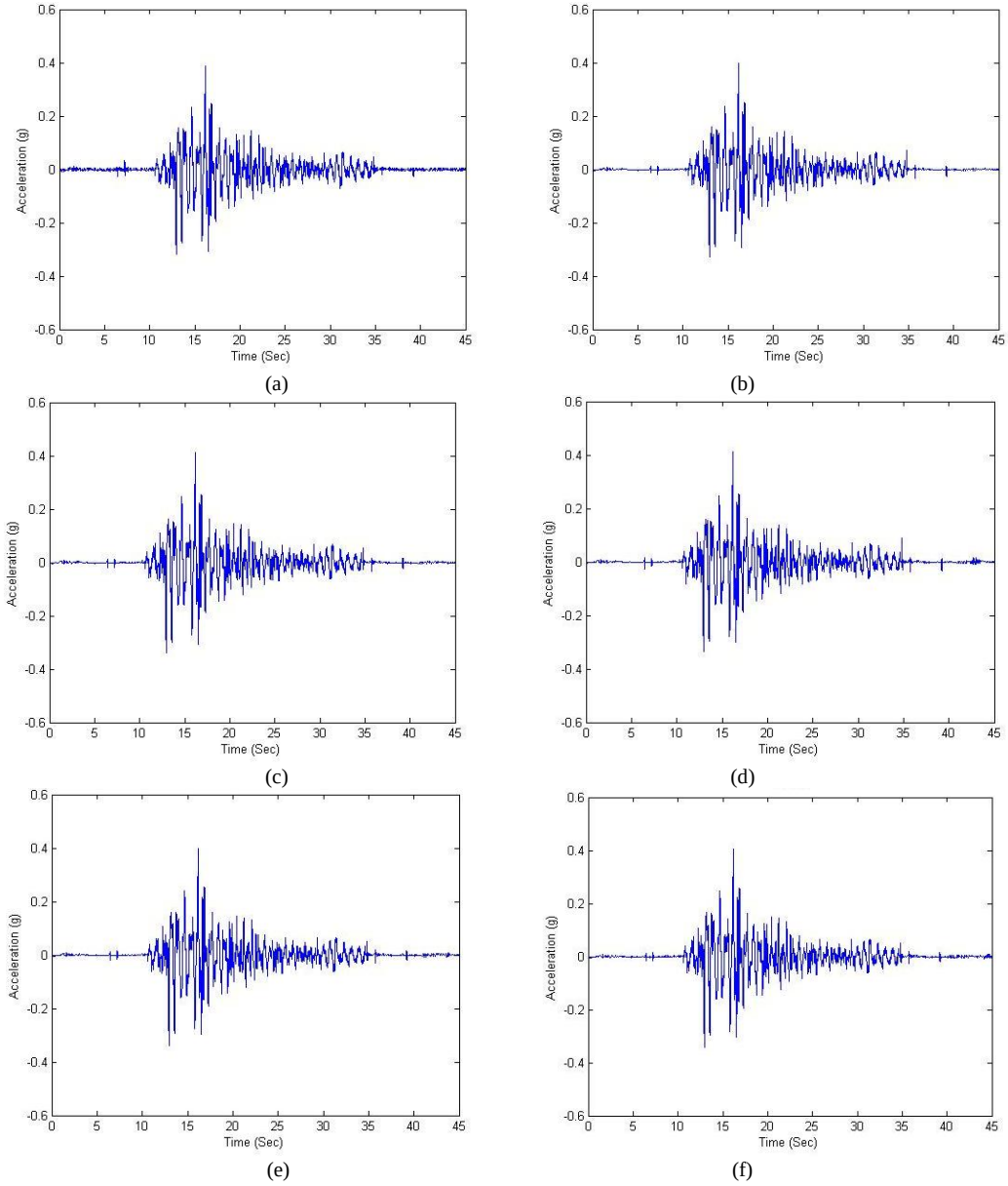

Figure 7.7. Kocaeli Earthquake excitations recorded by a) A1, b) A2, c) A3, d) A4, e) A5, f) A6.

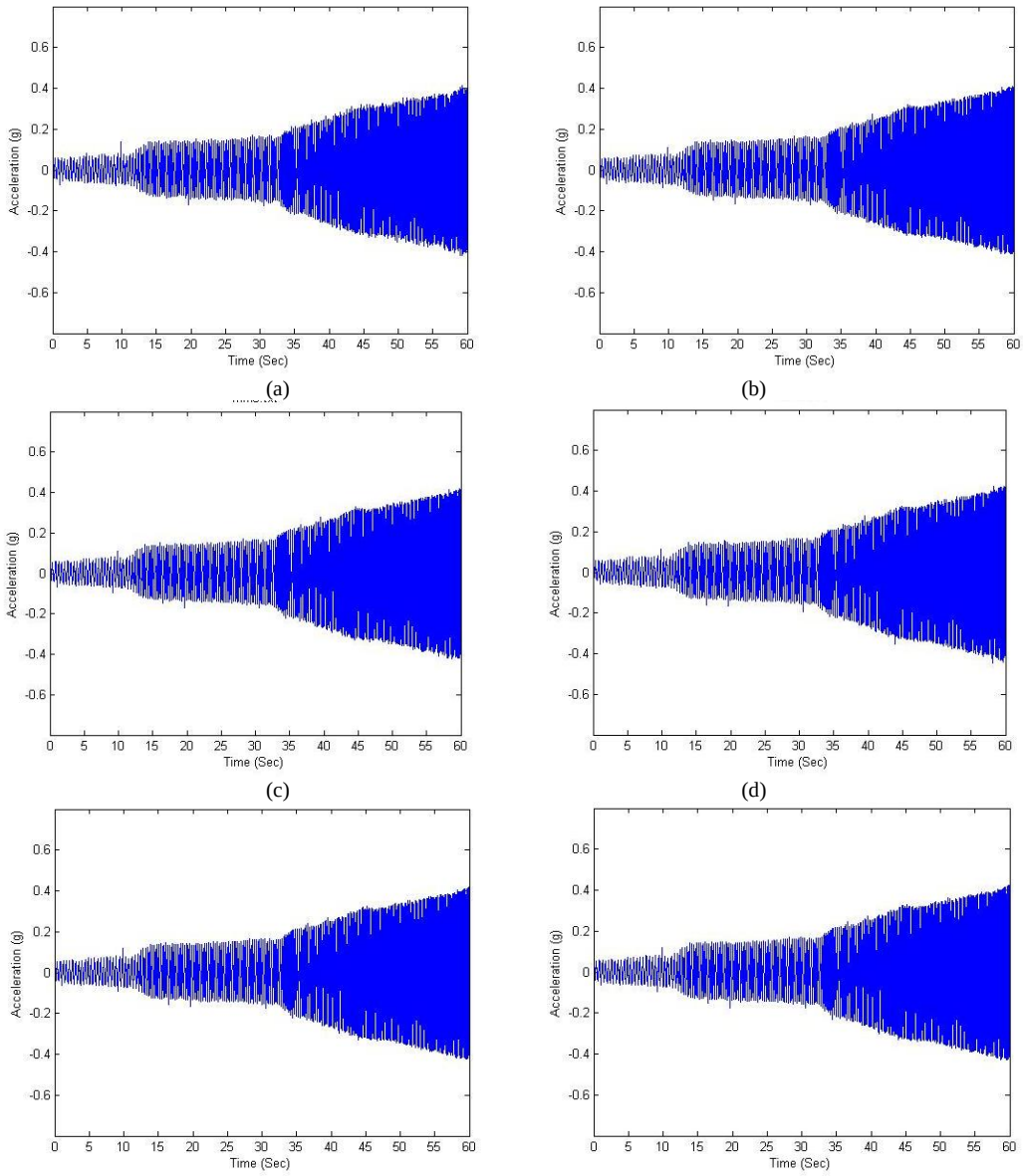

Figure 7.8. Sinusoidal motion recorded by a) A1, b) A2, c) A3, d) A4, e) A5, f) A6.

As can be inferred from the acceleration-time histories for all cases, responses are almost identical under four different dynamic loads. It is understood that the developed soil box is capable of providing idealized boundary conditions.

7.3.2. Preperation of the Test Embankments

Unreinforced and reinforced embankment models were prepared and shaking table tests were conducted under different dynamic motions. All models are designed with respect to the regulations and the recommendations of FHWA-NHI-09-083.

The prototype highway embankment is considered as a wide, four lane structure and the model embankment is designed as a 1:50 scale of the prototype. All models are placed over the same foundation soil layer with density of 16.5kN/m^3 and the relative density of Dr: 60%.

All embankment models have the same dimensions of H:20cm, L:20cm with two different inclinations of 30° and 45°. An example embankment model can be seen in Figure 7.9.

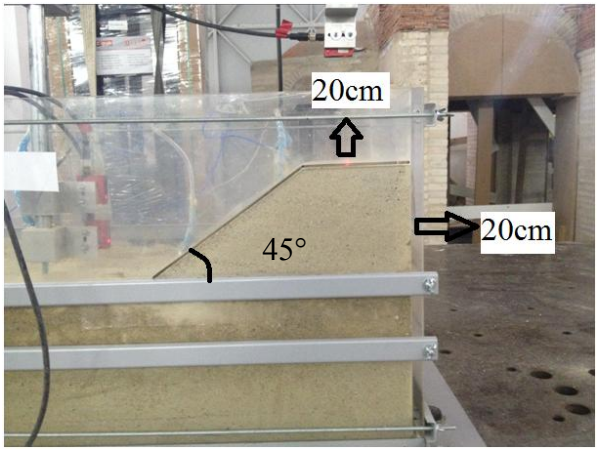

Figure 7.9. Physical appearance of the models.

Preliminary numerical studies were performed to analyze the seismic stability of embankments. Studies showed that two layers of geosynthetic reinforcement can be sufficient for obtaining the required factor of safety. Reinforced embankment models include two layers of reinforcement material, one layer is placed between the bottom of the embankment and the foundation soil and the second layer is placed right in the middle between the crest and the bottom of the embankment. The reinforcement materials are expected to increase the seismic performance of the models.

7.3.3. Instrumentation

A total of nine accelerometers and four displacement sensors are used for the experiments. Accelerometers and displacement sensors are notated with letters of “A” and “D” respectively. A1 is located on the shaking table and measures the input ground motion. A2 is located on the soil box, A3, A4, A5 and A6 are placed inside the sand foundation and are located linearly at the same level. A7 is placed under the first reinforcement layer. A8 is placed between two reinforcement layers inside the embankment and A9 is located above the second reinforcement layer at the top of the embankment. D1 is a displacement sensor and measures the input displacements. D2, D3 and D4 are laser displacement sensors. D2 measures the displacement at the bottom of the embankment models while D3 measures the displacement at the top of the models. D4 is located to measure the settlement at the top of the embankment models. Instrumentation for all models is represented in Figure 7.10.

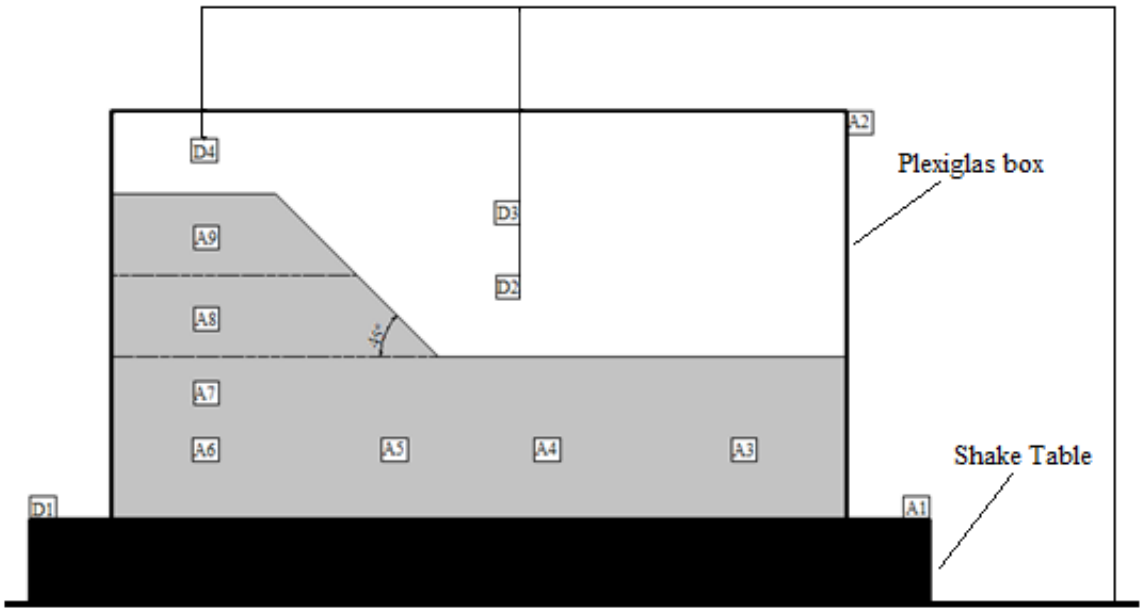

Figure 7.10. Instrumentation for all embankment models.

7.4. Shaking Table Experiments

Shaking table experiments were performed at the Boğaziçi University Kandilli Observatory and Earthquake Research Institute's Shaking Table Laboratory. Both unreinforced and reinforced embankment models are subjected to nine dynamic motions with different characteristics. Dynamic motions can be grouped in two as sinusoidal and real earthquake record. The amplitudes of the sinusoidal ground motions vary as 0.3g and 0.5g, and the predominant frequency of vibration differs as 2Hz, 5Hz, 7Hz and 14Hz. In addition to harmonic motions, time scaled real record of Düzce Earthquake was used (0.35g). Harmonic motions were applied in 40 cycles. It is pointed out that 14Hz of vibration frequency correspondes to an average earthquake frequency value of approximately 2Hz for the 1/50 scaled embankment model with regards to scale laws of Iai (1989). The rest of the frequency ranges were used to evaluate the seismic behaviour patterns of the existing embankment models. Input ground motions used during this study are given in Figures between 7.11-7.19.

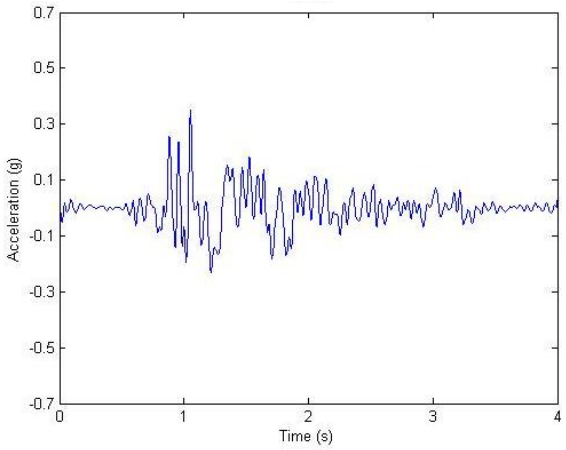

Figure 7.11. Input Düzce Earthquake motion (KOERI).

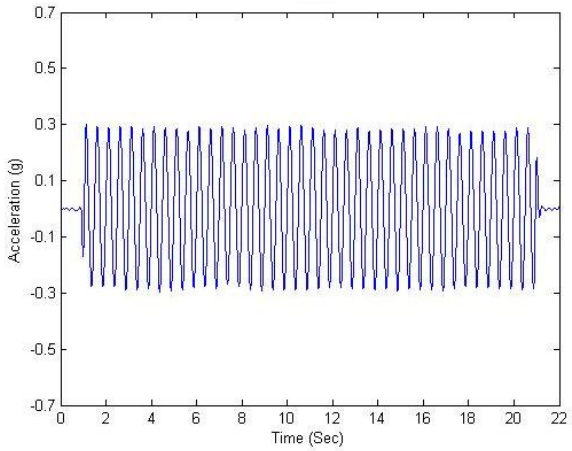

Figure 7.12. Input acceleration of 0.3g with 2Hz of frequency.

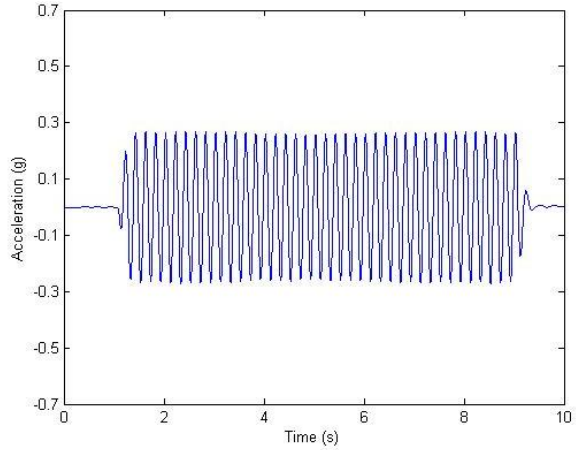

Figure 7.13. Input acceleration of 0.3g with 5Hz of frequency.

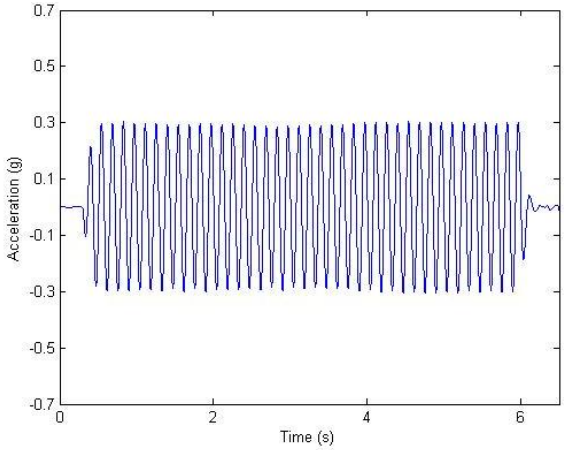

Figure 7.14. Input acceleration of 0.3g with 7Hz of frequency.

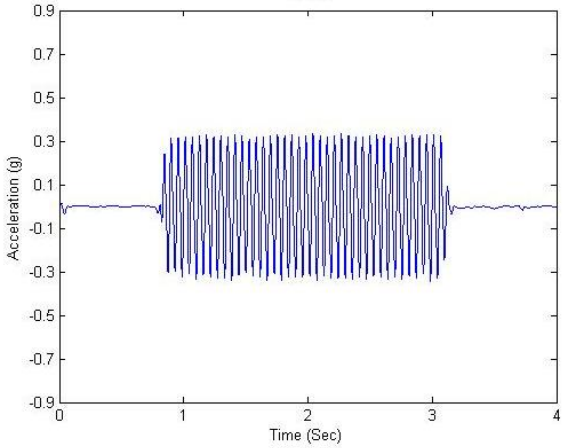

Figure 7.15. Input acceleration of 0.3g with 14Hz of frequency.

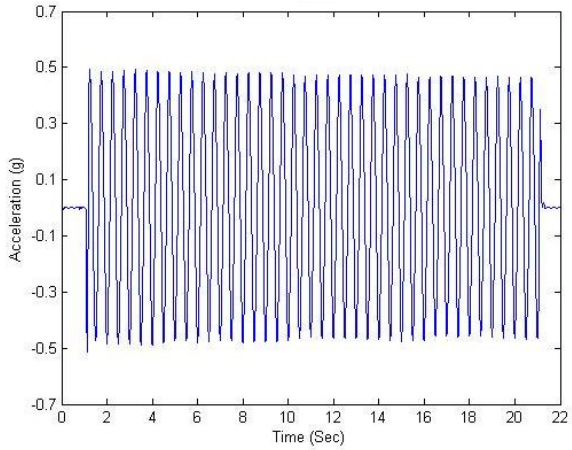

Figure 7.16. Input acceleration of 0.5g with 2Hz of frequency.

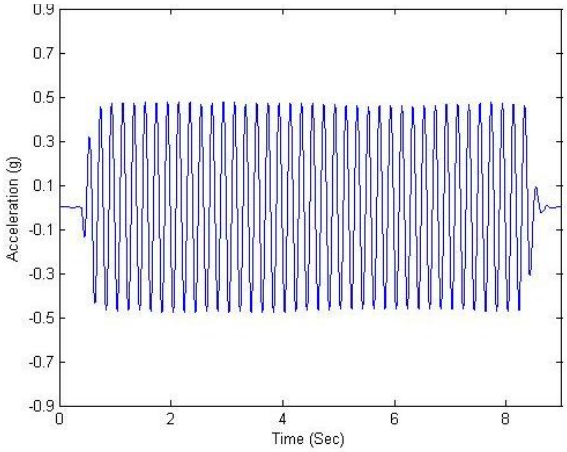

Figure 7.17. Input acceleration of 0.5g with 5Hz of frequency.

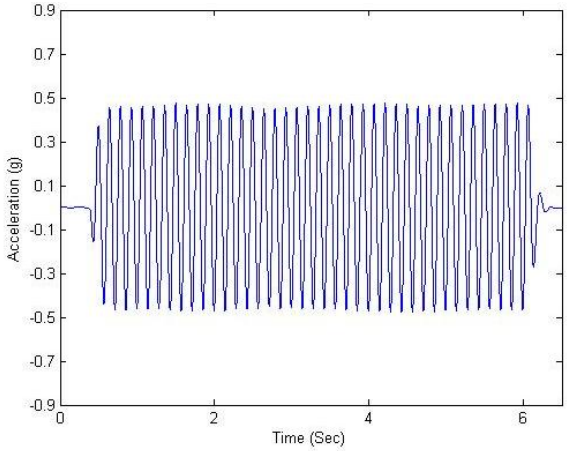

Figure 7.18. Input acceleration of 0.5g with 7Hz of frequency.

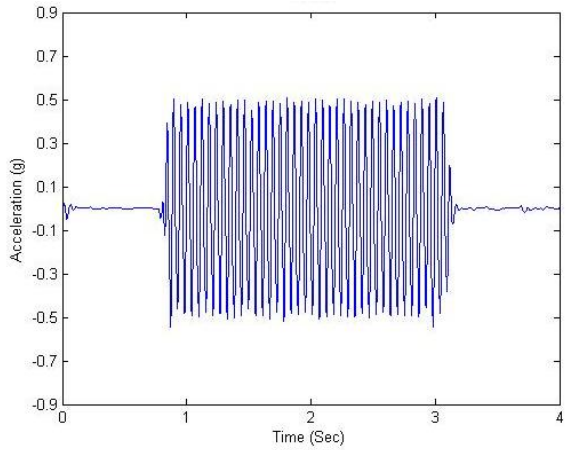

Figure 7.19. Input acceleration of 0.5g with 14Hz of frequency.

Table 7.1 represents the experimental program in detail.

Table 7.1. Experimental program.

Test No:	PGA	Frequency	Reinforcement Type	Number of Cycles	Slope Inclination
1	0.30	2	Unreinforced	40	45°
2	0.30	5	Unreinforced	40	45°
3	0.30	7	Unreinforced	40	45°
4	0.30	14	Unreinforced	40	45°
5	0.30	2	Geotextile	40	45°
6	0.30	5	Geotextile	40	45°
7	0.30	7	Geotextile	40	45°
8	0.30	14	Geotextile	40	45°
9	0.50	2	Unreinforced	40	45°
10	0.50	5	Unreinforced	40	45°
11	0.50	7	Unreinforced	40	45°
12	0.50	14	Unreinforced	40	45°
13	0.50	2	Geotextile	40	45°
14	0.50	5	Geotextile	40	45°
15	0.50	7	Geotextile	40	45°
16	0.50	14	Geotextile	40	45°
17	0.35	-	Unreinforced	-	45°
18	0.35	-	Geotextile	-	45°
19	0.30	2	Unreinforced	40	30°
20	0.30	5	Unreinforced	40	30°
21	0.30	7	Unreinforced	40	30°
22	0.30	14	Unreinforced	40	30°
23	0.30	2	Geotextile	40	30°
24	0.30	5	Geotextile	40	30°
25	0.30	7	Geotextile	40	30°
26	0.30	14	Geotextile	40	30°
27	0.50	2	Unreinforced	40	30°
28	0.50	5	Unreinforced	40	30°
29	0.50	7	Unreinforced	40	30°
30	0.50	14	Unreinforced	40	30°
31	0.50	2	Geotextile	40	30°
32	0.50	5	Geotextile	40	30°
33	0.50	7	Geotextile	40	30°
34	0.50	14	Geotextile	40	30°
35	0.35	-	Unreinforced	-	30°
36	0.35	-	Geotextile	-	30°

7.5. Shaking Table Test Results

In this part of the study, acceleration-time histories, response spectrums and displacement-time histories of embankment models for selected locations are represented in Figures from 7.21 to Figure 7.58. For the acceleration-time histories and response spectrums, transmitted acceleration measurements of A9, and for the

displacement-time histories, transmitted displacement measurements of D2 and D3 are selected and represented. Shaking table tests were performed by using the inputs defined in Section 7.4. Sensors are located in the most critical locations of the embankment model. Test setup of the embankment models is given in Figure 7.20.

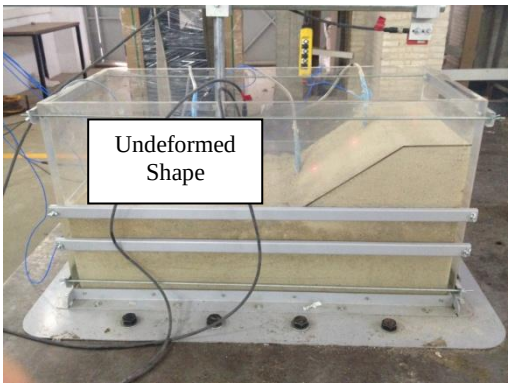

Figure 7.20. Test set-up of the embakment models.

7.5.1. Test Results for Unreinforced Embankment Model of 45° Inclination

Test results of the unreinforced embankment model with the slope inclination of 45° are represented in Figures between 7.21 and 7.29. Results of the study are given in terms of Acceleration-Time histories, Response spectrums and Displacement-Time histories for the selected sensors which are A9, D2 and D3. Test results of A9 is very important because it is located near the top of the embankment where the effectiveness of the reinforcement is best observed. Similarly, D2 and D3 measures the horizontal and vertical displacement values that are capable of revealing the reinforcement effect. Embankment model subjected to input dynamic loads of Düzce Earthquake, 0.3g with 2Hz of motion, 0.3g with 5Hz of motion, 0.3g with 7Hz of motion, 0.3g with 14Hz of motion, 0.5g with 2Hz of motion, 0.5g with 5Hz of motion, 0.5g with 7Hz of motion and 0.5g with 14Hz of motion. Selected measurements of A9, D2 and D3 are used.

7.5.1.1. Test Results for Düzce Earthquake Motion. Figure 7.21 represents the test results of the unreinforced embankment model subjected to time scaled Düzce Earthquake excitations. Real earthquake record is time scaled according to the scaling laws of Iai (1989) and with respect to the scaling ratio of the model.

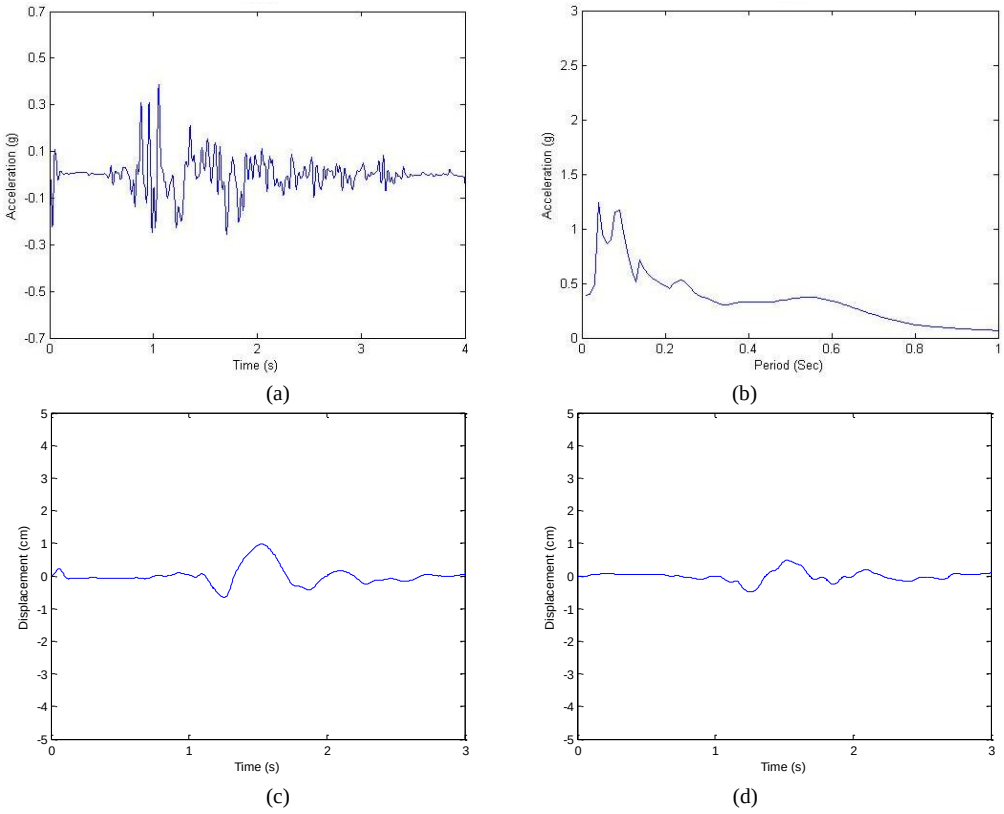

Figure 7.21. Test results for Düzce eqe. a) Acc.-Time History of A9, b) Response Spec. of A9, c) Disp.-Time History of D2, d) Disp.-Time History of D3.

7.5.1.2. Test Results under 0.3g Acceleration with 2Hz of Frequency. Figure 7.22, represents the test results of the unreinforced embankment model subjected to 0.3g 2Hz of motion for the selected measurements of A9, D2 and D3 are used.

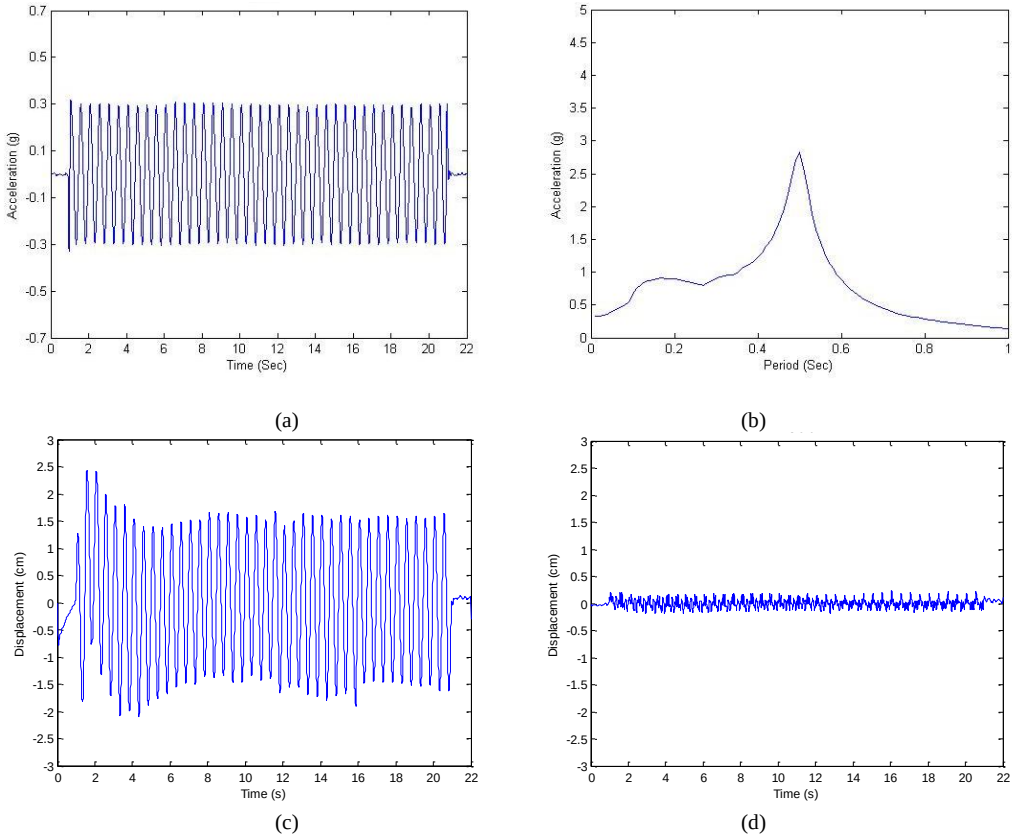

Figure 7.22. Test results for 0.3g 2Hz of motion. a) Acc.-Time History of A9, b) Response Spec. of A9, c) Disp.-Time History of D2, d) Disp.-Time History of D3.

Figure 7.23, represents the deformed shape (red dashed lines) of the unreinforced highway embankment model under 0.3g of acceleration and 2Hz of frequency motion.

Figure 7.23. Deformed shape of the unreinforced model under 0.3g of acceleration with 5Hz of frequency.

Under current dynamic loading the displacement value at the toe of the embankment was measured as 2.99cm. Crest of the embankment deformed 2.63cm while settlement at the top of the embankment model was 0.73cm.

7.5.1.3. Test Results under 0.3g Acceleration with 5Hz of Frequency. Figure 7.24, represents the test results of the unreinforced embankment model subjected to 0.3g 5Hz of motion for the selected measurements of A9, D2 and D3 are used.

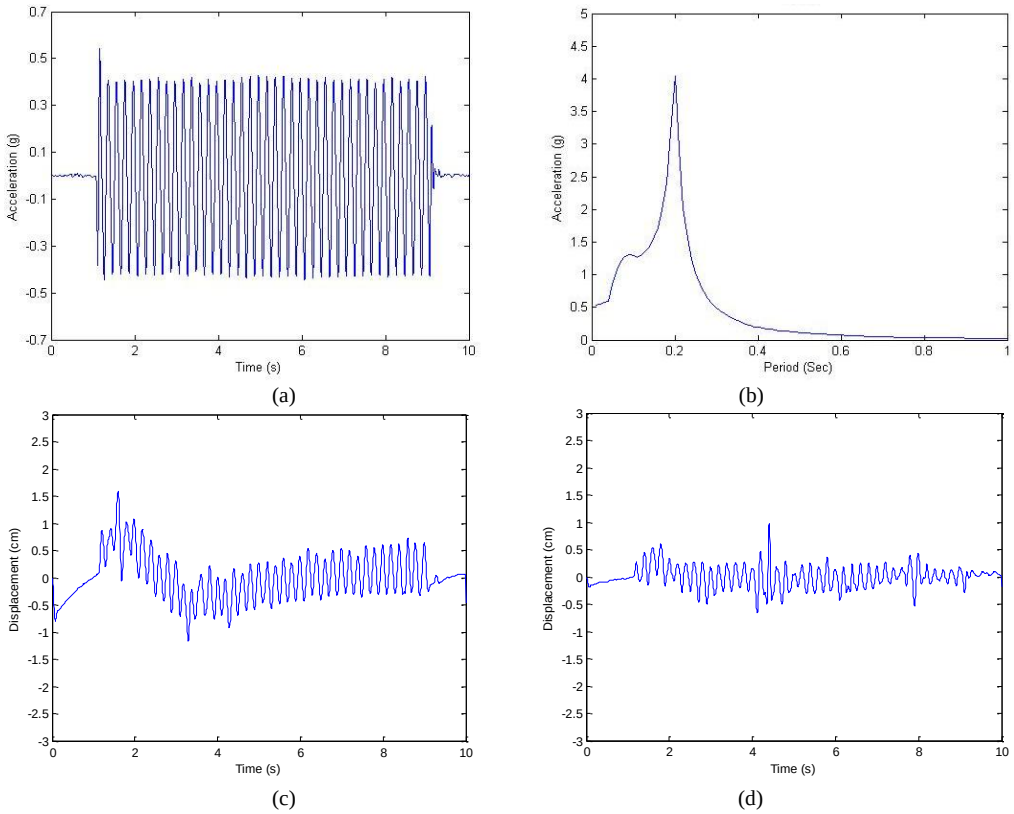

Figure 7.24. Test results for 0.3g 5Hz of motion. a) Acc.-Time History of A9, b) Response Spec. of A9, c) Disp.-Time History of D2, d) Disp.-Time History of D3.

7.5.1.4. Test Results under 0.3g Acceleration with 7Hz of Frequency

Figure 7.25, represents the test results of the unreinforced embankment model subjected to 0.3g with 7Hz of motion for the selected measurements of A9, D2 and D3 are used.

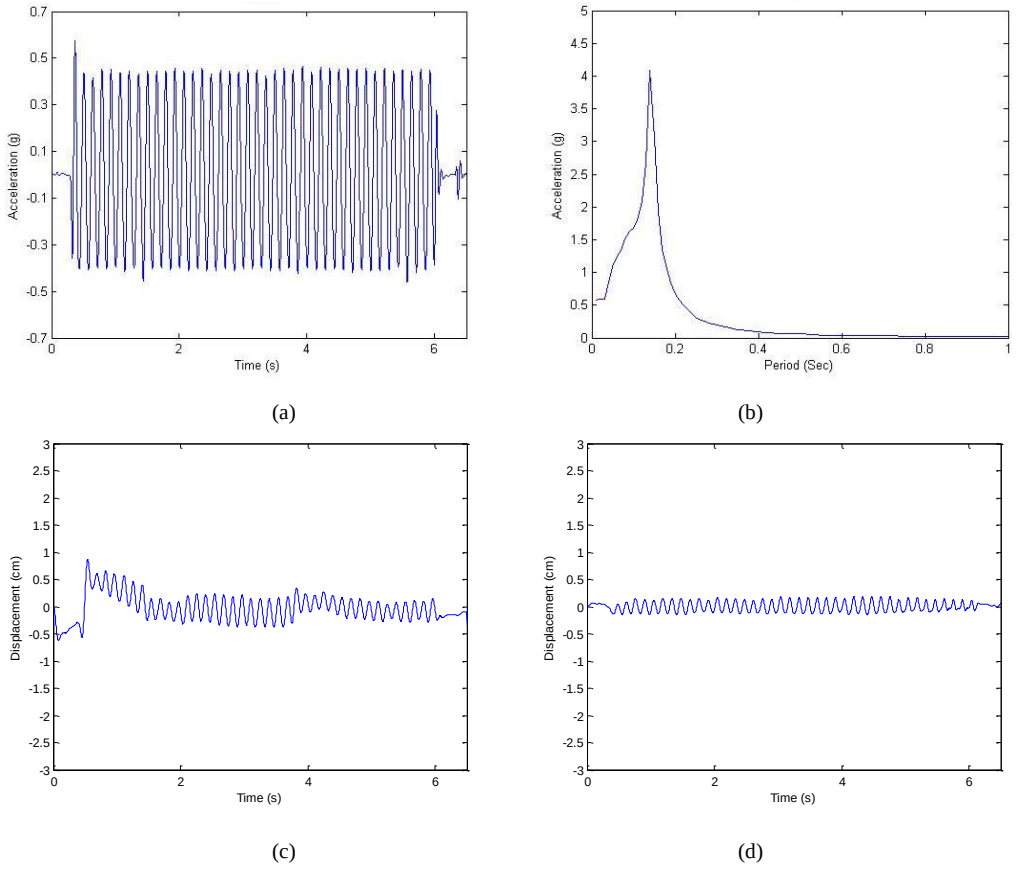

Figure 7.25. Test results for 0.3g 7Hz of motion. a) Acc.-Time History of A9, b) Response Spec. of A9, c) Disp.-Time History of D2, d) Disp.-Time History of D3.

7.5.1.5. Test Results under 0.3g Acceleration with 14Hz of Frequency. Figure 7.26, represents the test results of the unreinforced embankment model subjected to 0.3g with 14Hz of motion for the selected measurements of A9, D2 and D3.

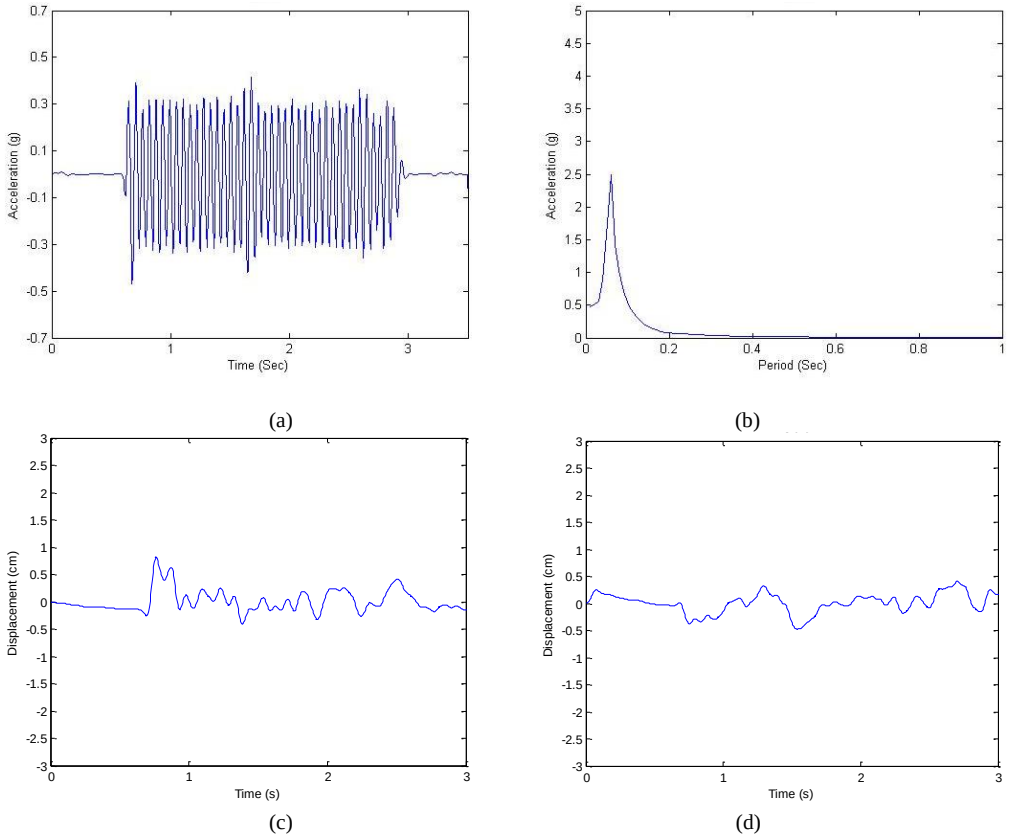

Figure 7.26. Test results for 0.3g 14Hz of motion. a) Acc.-Time History of A9, b) Response Spec. of A9, c) Disp.-Time History of D2, d) Disp.-Time History of D3.

Figure 7.27, represents the deformed shape of the unreinforced embankement model under the dynamic motion of 0.3g of acceleration and 14Hz of predominant frequency.

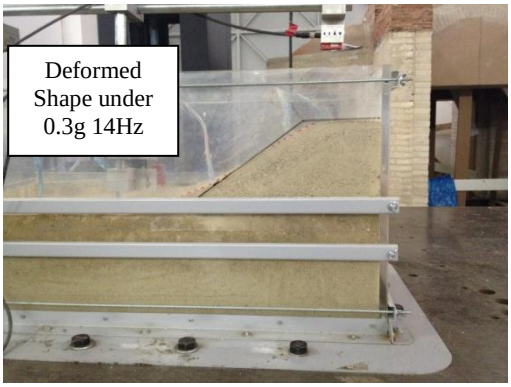

Figure 7.27. Deformed shape of the model under 0.3g acceleration with 14Hz of frequency.

Displacement measurements reveal that under current motion, toe of the model displaced 0.59cm while crest of the embankment deformed 0.26cm. Vertical displacement measurement was 0.37cm at the top of the model.

7.5.1.6. Test Results under 0.5g Acceleration with 2Hz of Frequency. Figure 7.28, represents the test results of the unreinforced embankment model subjected to 0.5g 2Hz of motion for the selected measurements of A9, D2 and D3 are used.

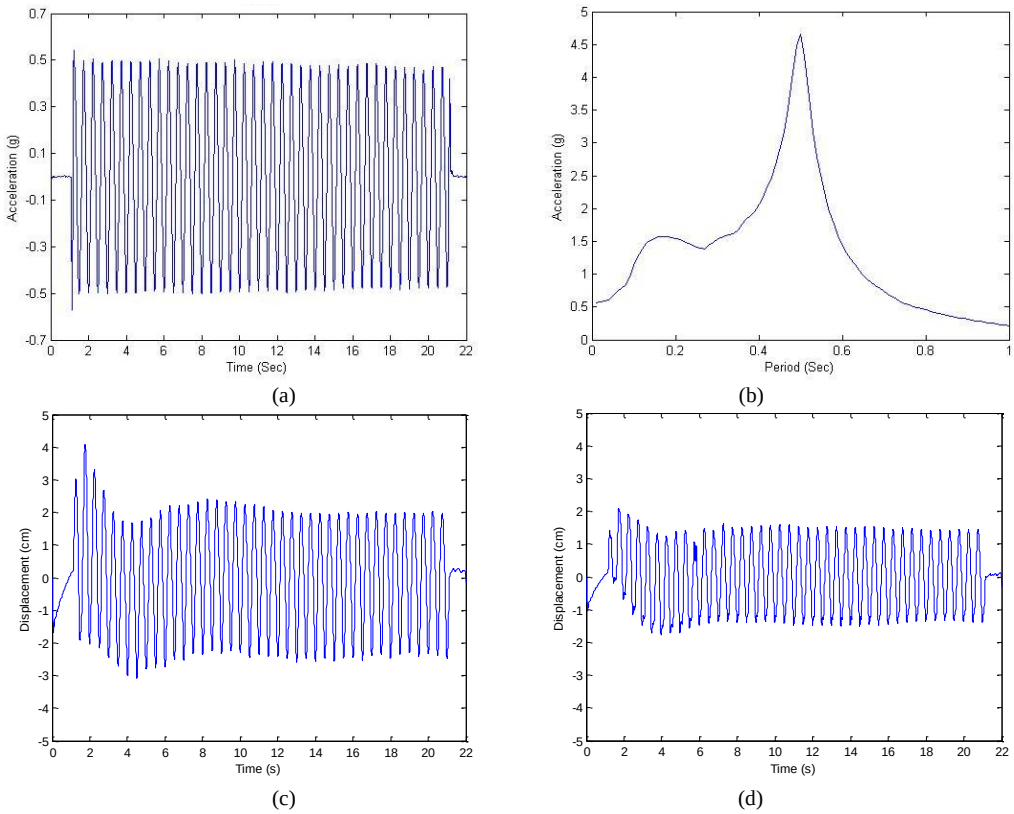

Figure 7.28. Test results for 0.5g with 2Hz of motion. a) Acc.-Time History of A9, b) Response Spec. of A9, c) Disp.-Time History of D2, d) Disp.-Time History of D3.

7.5.1.7. Test Results under 0.5g Acceleration with 5Hz of Frequency. Figure 7.29, represents the test results of the unreinforced embankment model subjected to 0.5g 5Hz of motion for the selected measurements of A9, D2 and D3 are used.

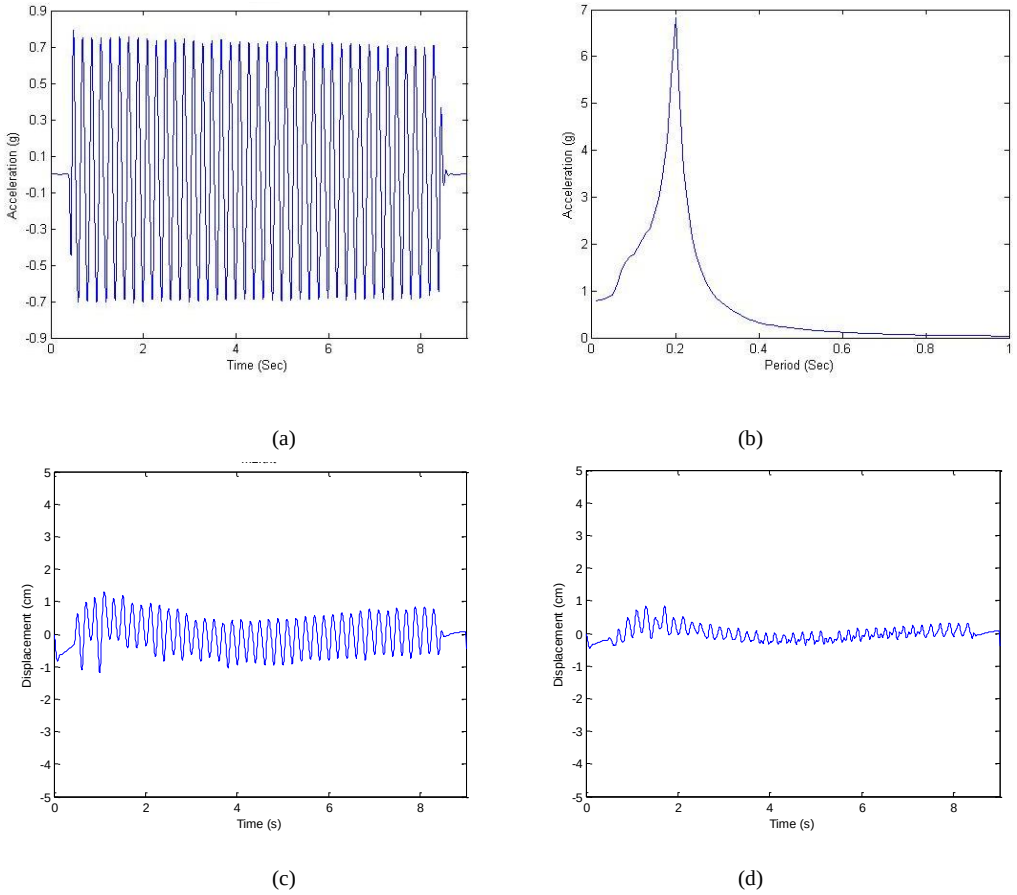

Figure 7.29. Test results for 0.5g with 5Hz of motion. a) Acc.-Time History of A9, b) Response Spec. of A9, c) Disp.-Time History of D2, d) Disp.-Time History of D3.

7.5.1.8. Test Results under 0.5g Acceleration with 7Hz of Frequency. Figure 7.30 below, represents the test results of the unreinforced embankment model subjected to 0.5g with 7Hz of motion for the selected measurements of A9, D2 and D3 are used.

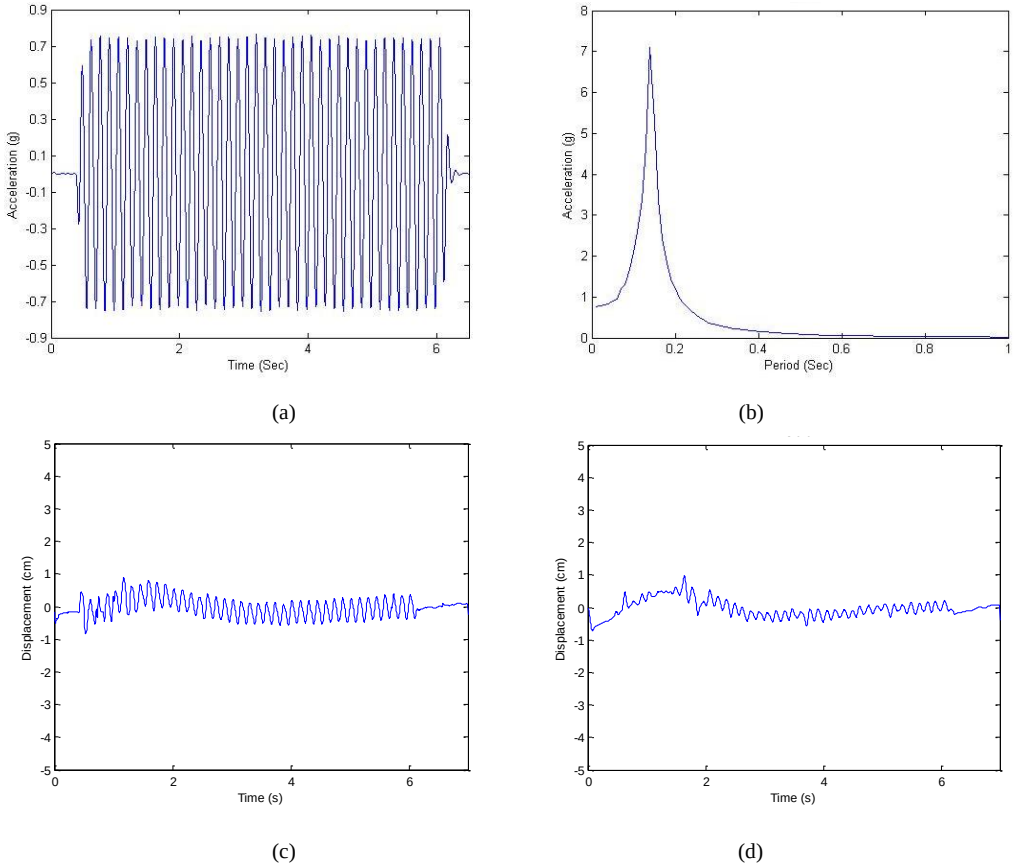

Figure 7.30. Test results for 0.5g with 7Hz of motion. a) Acc.-Time History of A9, b) Response Spec. of A9, c) Disp.-Time History of D2, d) Disp.-Time History of D3.

7.5.1.9. Test Results under 0.5g Acceleration with 14Hz of Frequency. Figure 7.31 below, represents the test results of the unreinforced embankment model subjected to 0.5g with 14Hz of motion for the selected measurements of A9, D2 and D3.

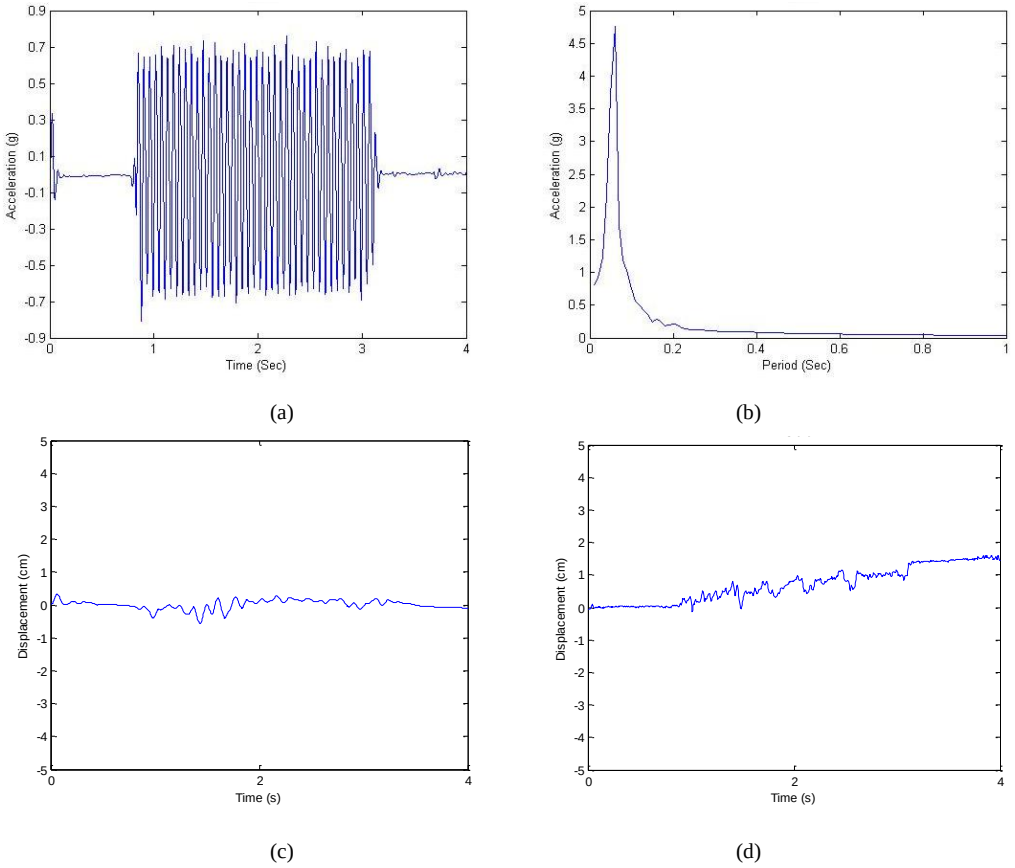

Figure 7.31. Test results for 0.5g with 14Hz of motion. a) Acc.-Time History of A9, b) Response Spec. of A9, c) Disp.-Time History of D2, d) Disp.-Time History of D3.

7.5.2. Test Results for Reinforced Embankment Model of 45° Inclination

Test results of the unreinforced embankment model with the slope inclination of 45° are represented in Figures between 7.32 to 7.40.

7.5.2.1. Test Results under Düzce Earthquake Motion. Figure 7.32, represents the test results of the reinforced embankment model subjected to time scaled Düzce Earthquake excitations. Real earthquake record is time scaled due to the scaling laws of Iai (1989) and with respect to the scaling ratio of the model. Selected measurements of A9, D2 and D3 are used.

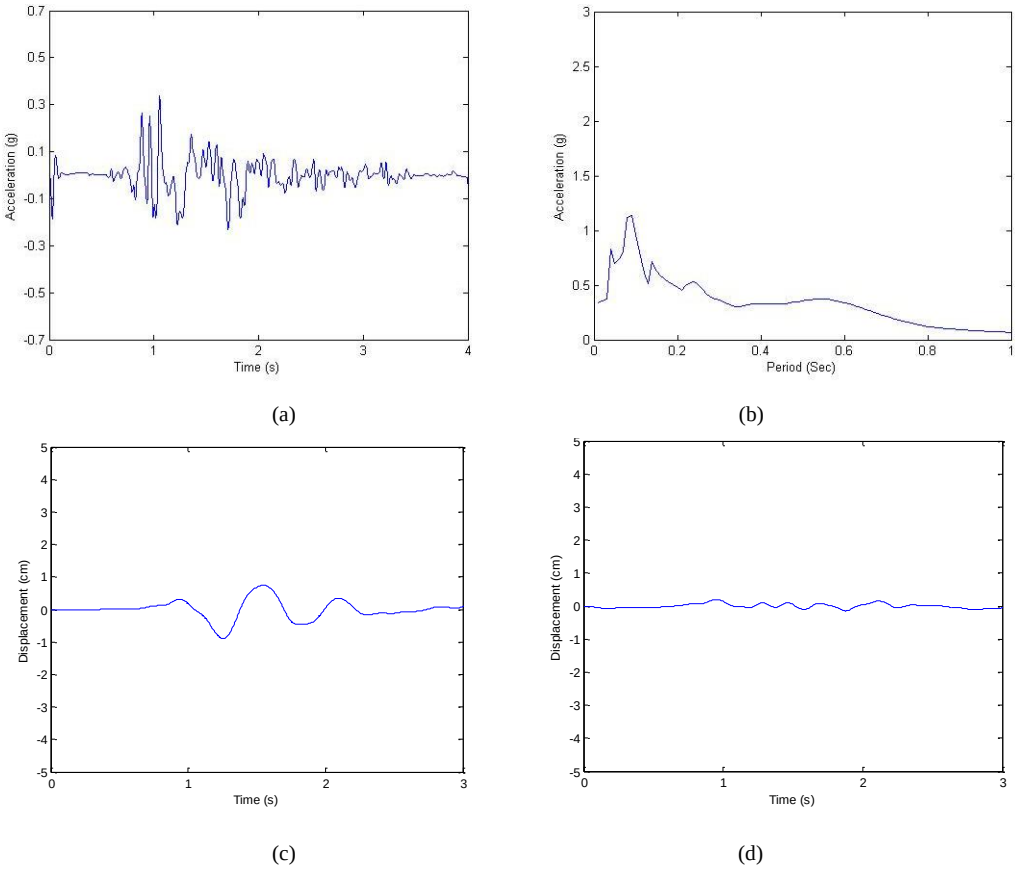

Figure 7.32. Test results for Düzce eqe. a) Acc.-Time History of A9, b) Response Spec. of A9, c) Disp.-Time History of D2, d) Disp.-Time History of D3.

7.5.2.2. Test Results under 0.3g Acceleration with 2Hz of Frequency. Figure 7.33, represents the test results of the reinforced embankment model subjected to 0.3g with 2Hz of motion for the selected measurements of A9, D2 and D3.

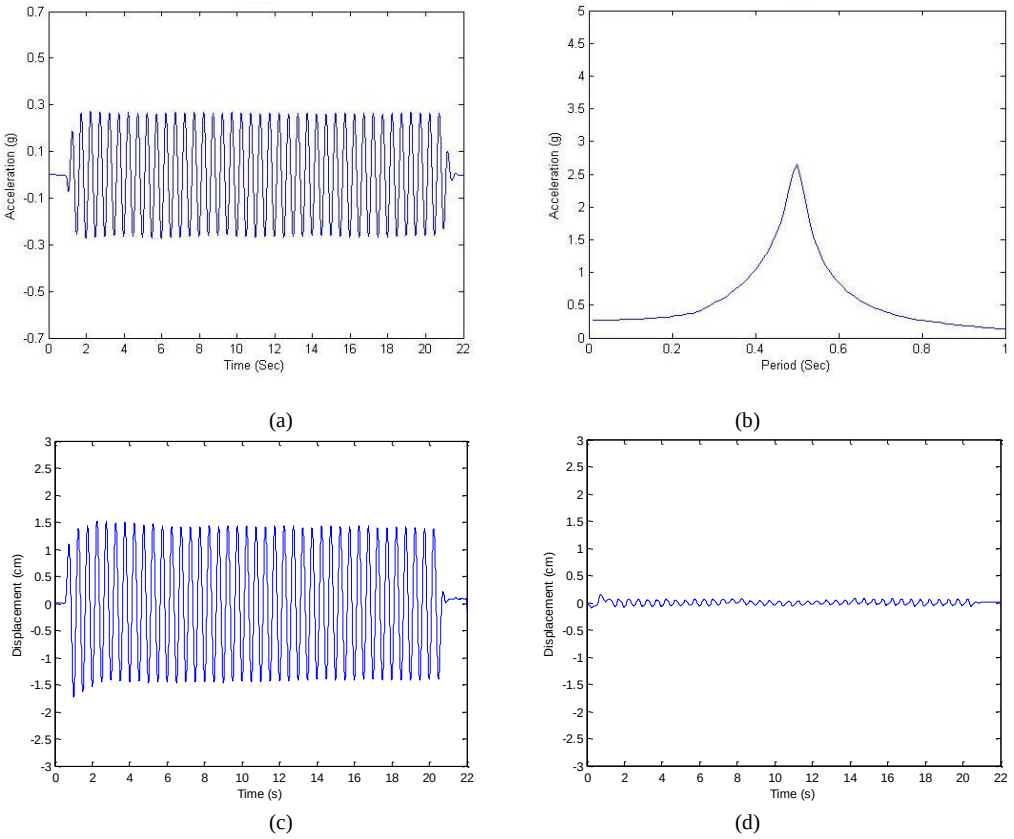

Figure 7.33. Test results for 0.3g wth 2Hz of motion. a) Acc.-Time History of A9, b) Response Spec. of A9, c) Disp.-Time History of D2, d) Disp.-Time History of D3.

7.5.2.3. Test Results under 0.3g Acceleration with 5Hz of Frequency. Figure 7.34, represents the test results of the reinforced embankment model subjected to 0.3g 5Hz of motion for the selected measurements of A9, D2 and D3.

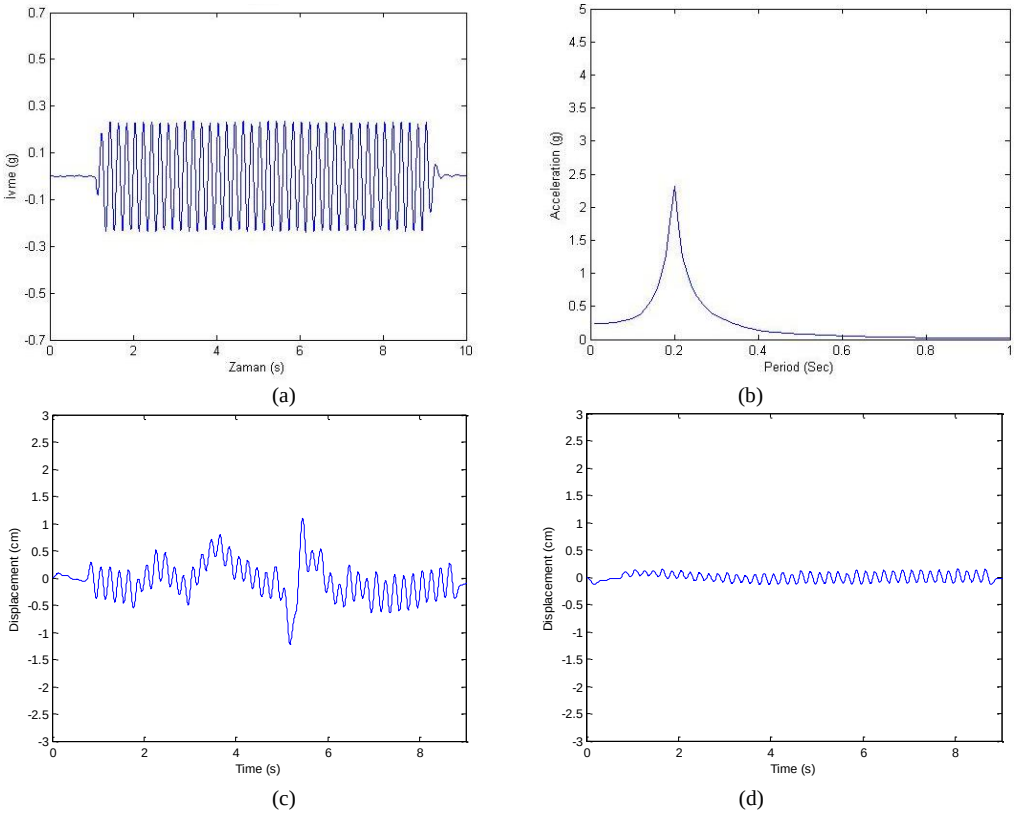

Figure 7.34. Test results for 0.3g with 5Hz of motion. a) Acc.-Time History of A9, b) Response Spec. of A9, c) Disp.-Time History of D2, d) Disp.-Time History of D3.

7.5.2.4. Test Results under 0.3g Acceleration with 7Hz of Frequency. Figure 7.35, represents the test results of the reinforced embankment model subjected to 0.3g with 7Hz of motion for the selected measurements of A9, D2 and D3.

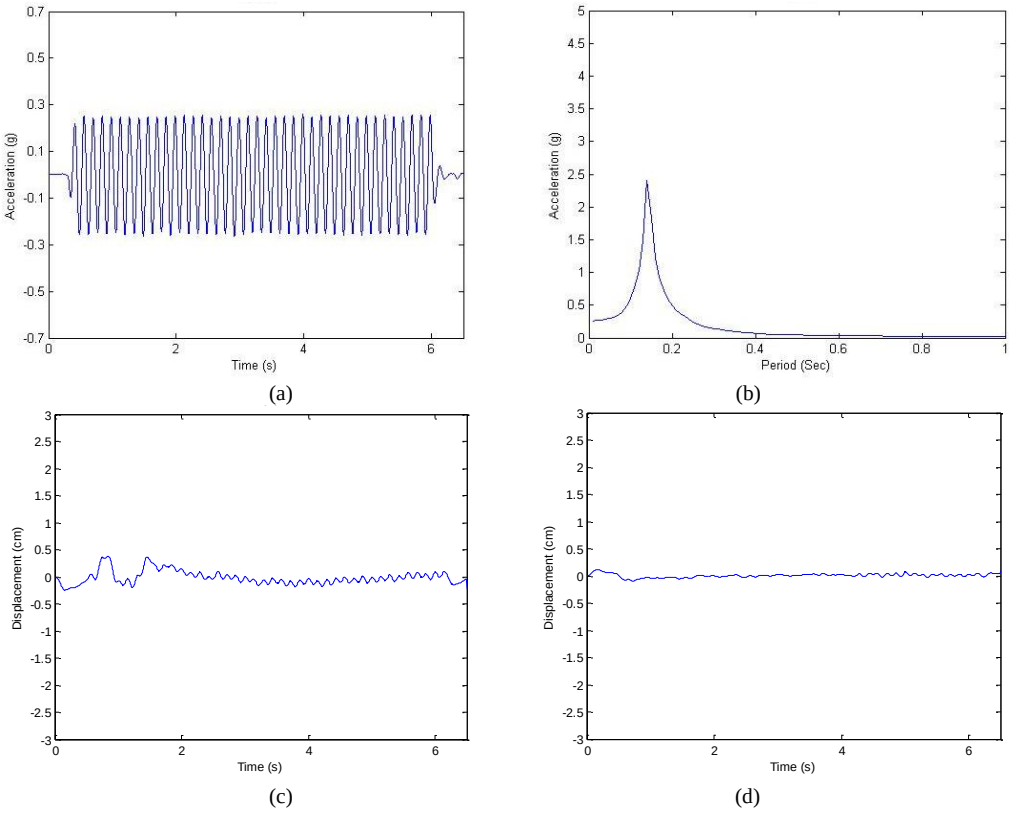

Figure 7.35. Test results for 0.3g with 7Hz of motion. a) Acc.-Time History of A9, b) Response Spec. of A9, c) Disp.-Time History of D2, d) Disp.-Time History of D3.

7.5.2.5. Test Results under 0.3g Acceleration with 14Hz of Frequency. Figure 7.36, represents the test results of the reinforced embankment model subjected to 0.3g with 14Hz of motion for the selected measurements of A9, D2 and D3.

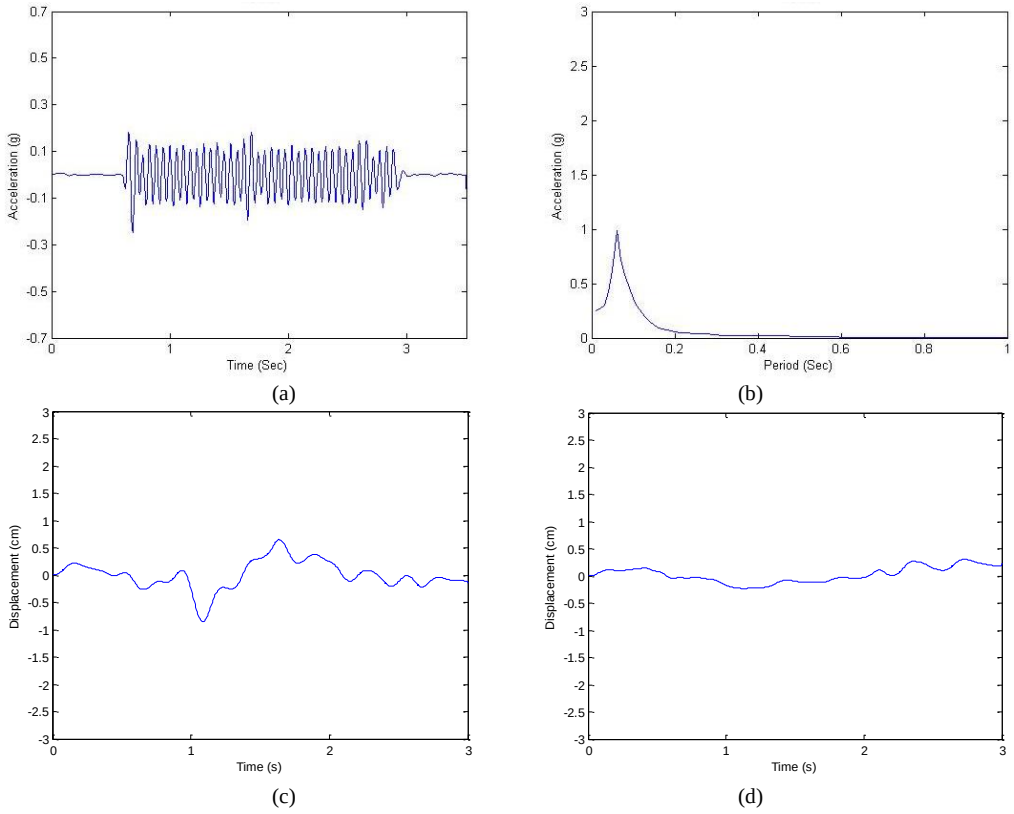

Figure 7.36. Test results for 0.3g with 14Hz of motion. a) Acc.-Time History of A9, b) Response Spec. of A9, c) Disp.-Time History of D2, d) Disp.-Time History of D3.

7.5.2.6. Test Results under 0.5g Acceleration with 2Hz of Frequency. Figure 7.37, represents the test results of the reinforced embankment model subjected to 0.5g with 2Hz of motion for the selected measurements of A9, D2 and D3.

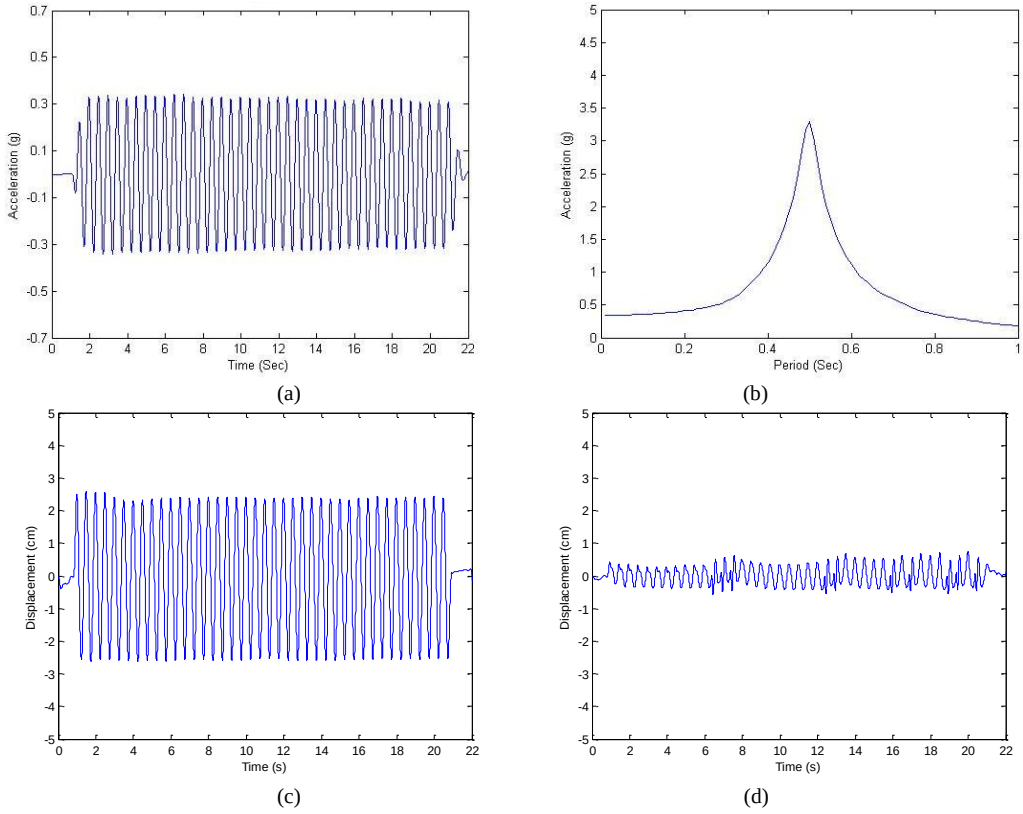

Figure 7.37. Test results for 0.5g with 2Hz of motion. a) Acc.-Time History of A9, b) Response Spec. of A9, c) Disp.-Time History of D2, d) Disp.-Time History of D3.

7.5.2.7. Test Results under 0.5g Acceleration with 5Hz of Frequency. Figure 7.38, represents the test results of the reinforced embankment model subjected to 0.5g with 5Hz of motion for the selected measurements of A9, D2 and D3.

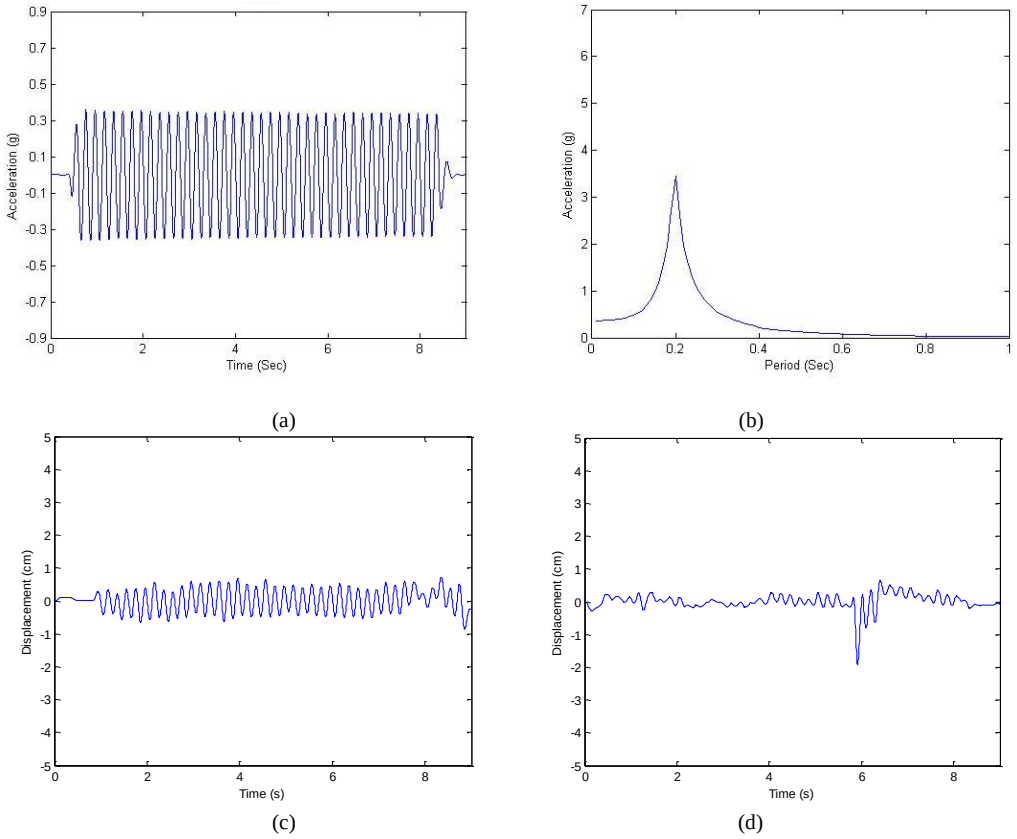

Figure 7.38. Test results for 0.5g with 5Hz of motion. a) Acc.-Time History of A9, b) Response Spec. of A9, c) Disp.-Time History of D2, d) Disp.-Time History of D3.

7.5.2.8. Test Results under 0.5g Acceleration with 7Hz of Frequency. Figure 7.39, represents the test results of the reinforced embankment model subjected to 0.5g with 7Hz of motion for the selected measurements of A9, D2 and D3.

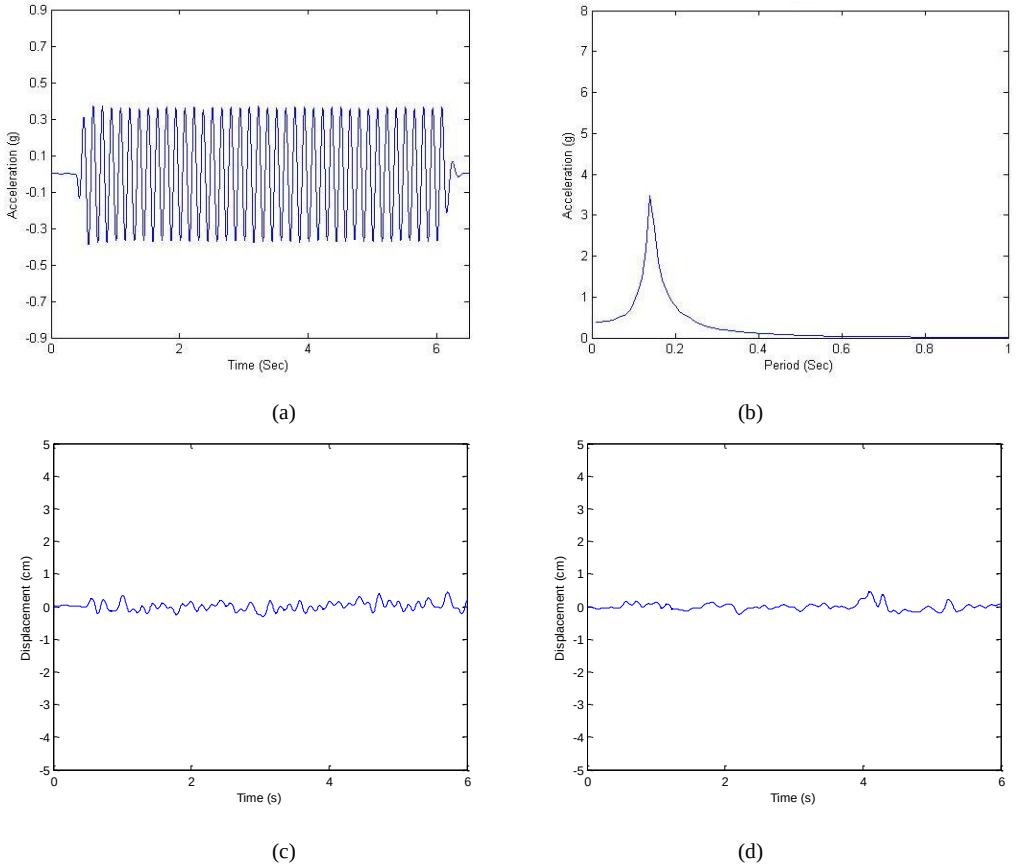

Figure 7.39. Test results for 0.5g with 7Hz of motion. a) Acc.-Time History of A9, b) Response Spec. of A9, c) Disp.-Time History of D2, d) Disp.-Time History of D3.

7.5.2.9. Test Results under 0.5g Acceleration with 14Hz of Frequency. Figure 7.40, represents the test results of the reinforced embankment model subjected to 0.5g with 14Hz of motion for the selected measurements of A9, D2 and D3.

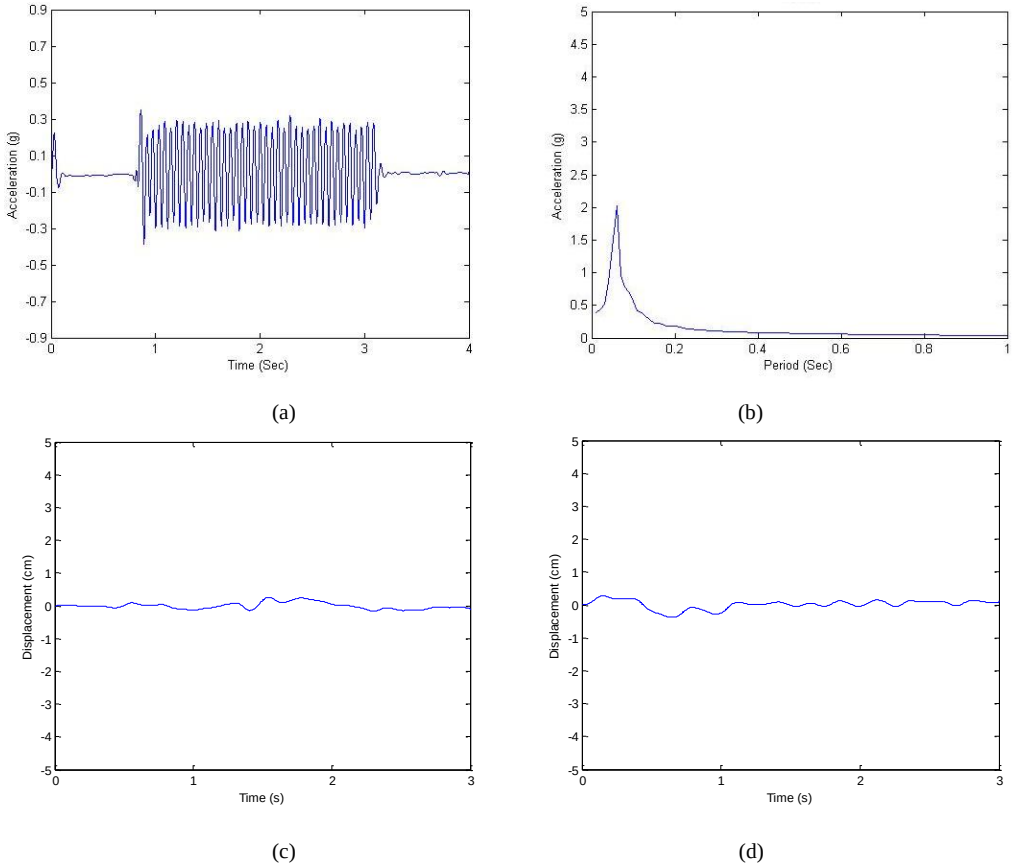

Figure 7.40. Test results for 0.5g with 14Hz of motion. a) Acc.-Time History of A9, b) Response Spec. of A9, c) Disp.-Time History of D2, d) Disp.-Time History of D3.

7.5.3. Test Results for Unreinforced Embankment Model of 30° Inclination

Test results of the unreinforced embankment model with the slope inclination of 30° are represented in Figures between 7.41 and 7.49.

7.5.3.1. Test Results for Düzce Earthquake Motions. Figure 7.41, represents the test results of the unreinforced embankment model subjected to time scaled Düzce Earthquake excitations. Real earthquake record is time scaled due to the scaling laws of Iai (1989) and with respect to the scaling ratio of the model. Selected measurements of A9, D2 and D3 are used.

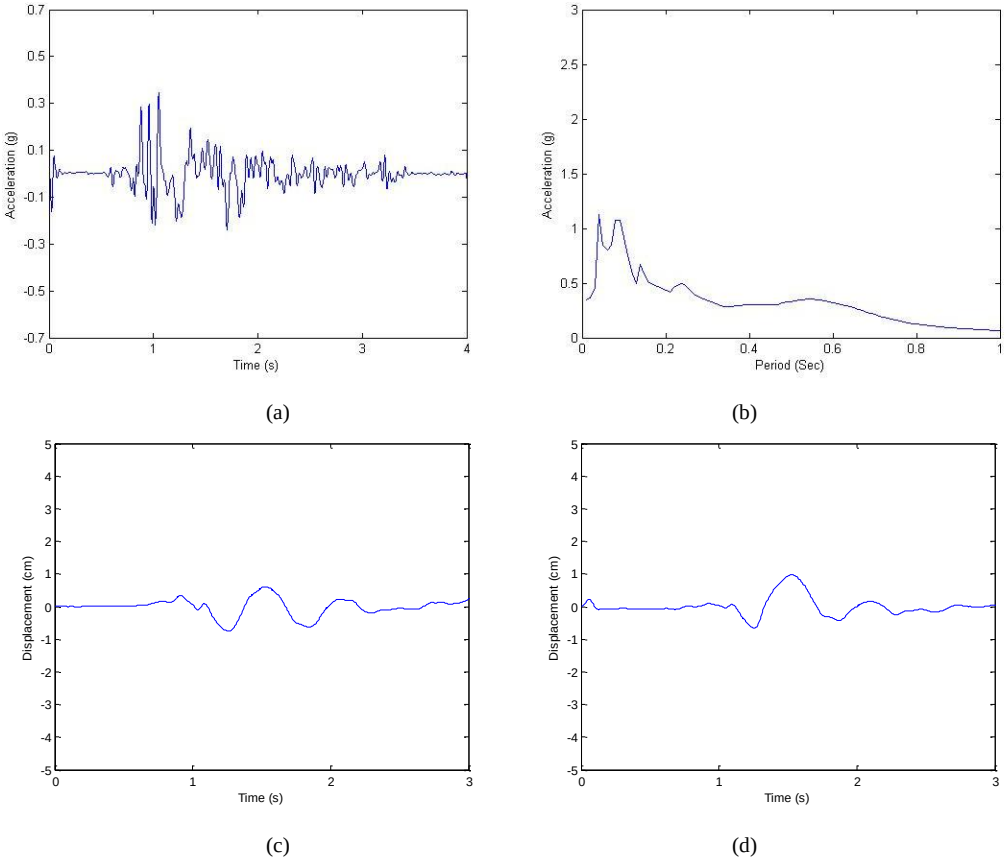

Figure 7.41. Test results for Düzce Eqe. a) Acc.-Time History of A9, b) Response Spec. of A9, c) Disp.-Time History of D2, d) Disp.-Time History of D3.

7.5.3.2. Test Results under 0.3g Acceleration with 2Hz of Frequency. Figure 7.42, represents the test results of the unreinforced embankment model subjected to 0.3g with 2Hz of motion for the selected measurements of A9, D2 and D3.

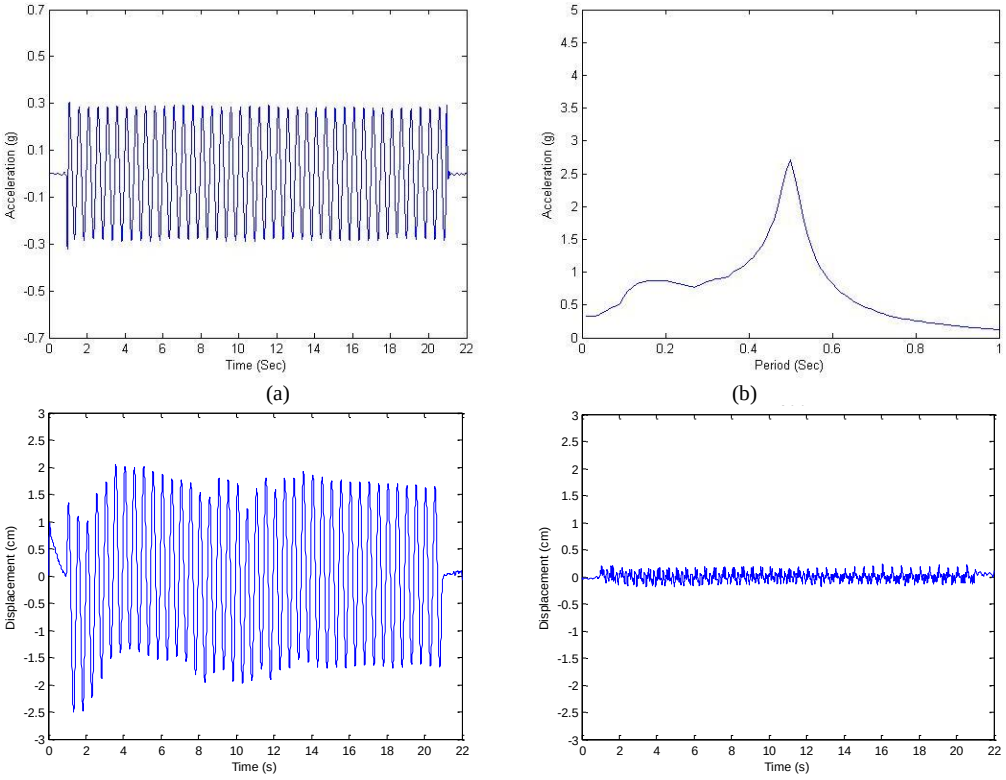

Figure 7.42. Test results for 0.3g with 2Hz of motion. a) Acc.-Time History of A9, b) Response Spec. of A9, c) Disp.-Time History of D2, d) Disp.-Time History of D3.

7.5.3.3. Test Results under 0.3g Acceleration with 5Hz of Frequency. Figure 7.43, represents the test results of the unreinforced embankment model subjected to 0.3g with 5Hz of motion for the selected measurements of A9, D2 and D3.

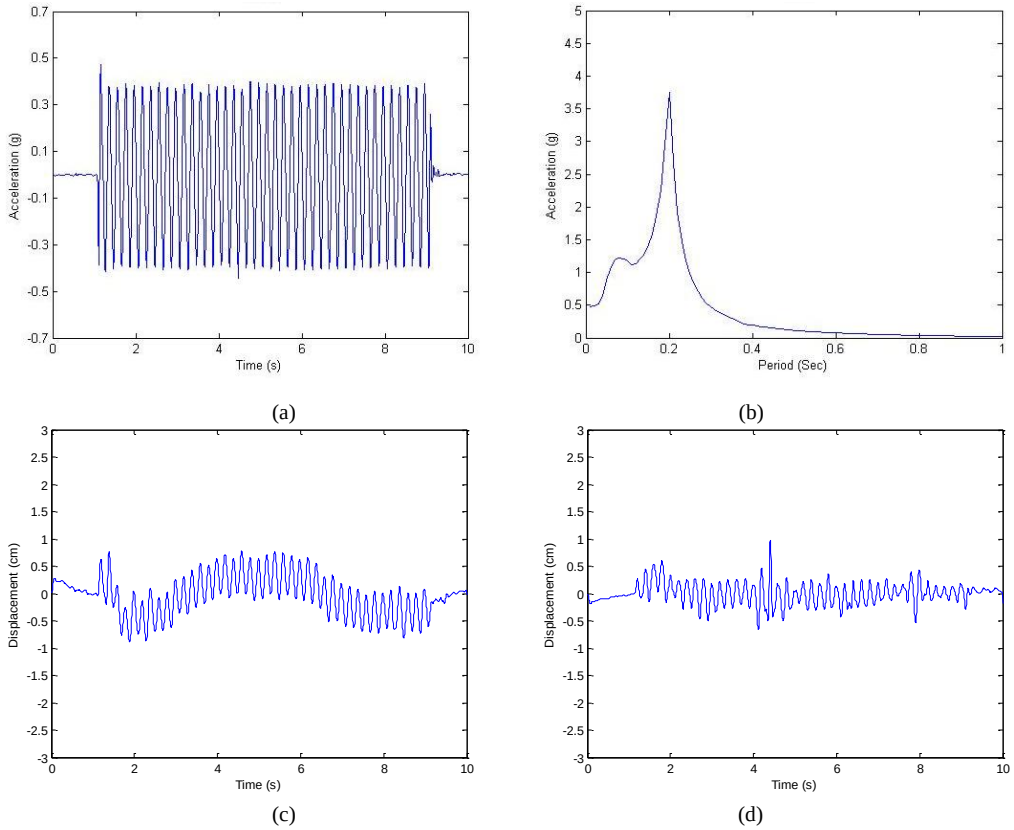

Figure 7.43. Test results for 0.3g with 5Hz of motion. a) Acc.-Time History of A9, b) Response Spec. of A9, c) Disp.-Time History of D2, d) Disp.-Time History of D3.

7.5.3.4. Test Results under 0.3g Acceleration with 7Hz of Frequency. Figure 7.44, represents the test results of the unreinforced embankment model subjected to 0.3g with 7Hz of motion for the selected measurements of A9, D2 and D3.

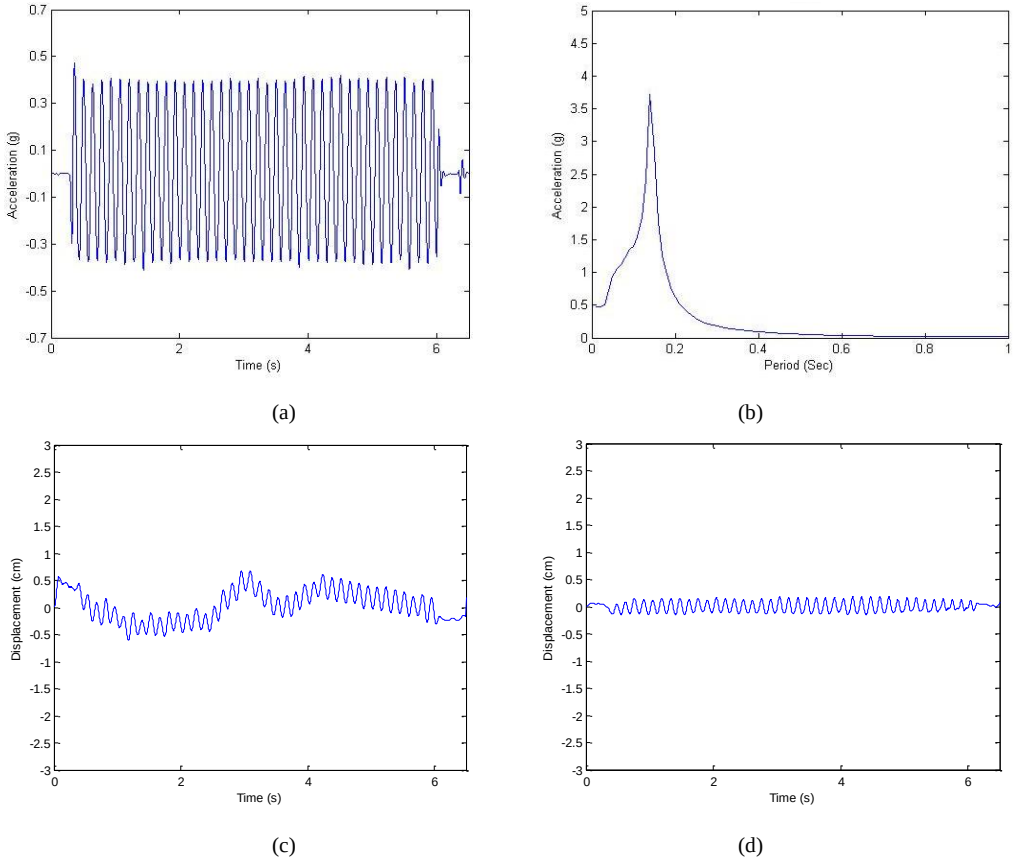

Figure 7.44. Test results for 0.3g with 7Hz of motion. a) Acc.-Time History of A9, b) Response Spec. of A9, c) Disp.-Time History of D2, d) Disp.-Time History of D3.

7.5.3.5. Test Results under 0.3g Acceleration with 14Hz of Frequency. Figure 7.45, represents the test results of the unreinforced embankment model subjected to 0.3g with 14Hz of motion for the selected measurements of A9, D2 and D3.

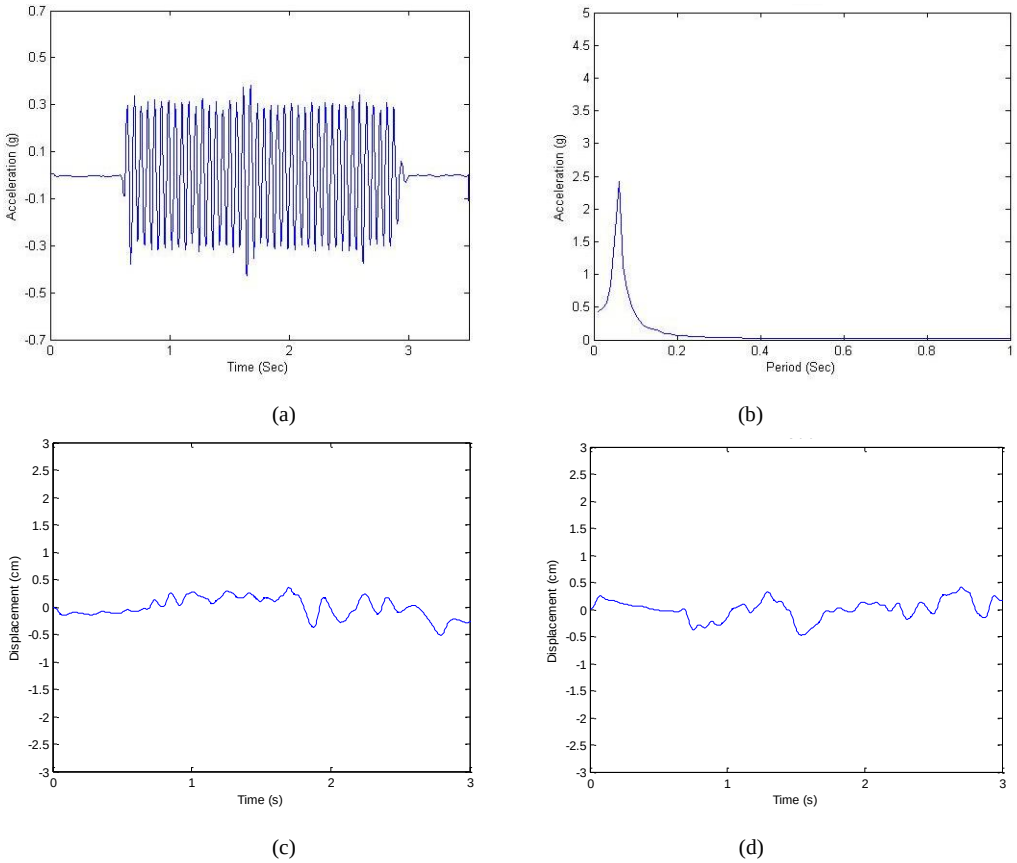

Figure 7.45. Test results for 0.3g with 14Hz of motion. a) Acc.-Time History of A9, b) Response Spec. of A9, c) Disp.-Time History of D2, d) Disp.-Time History of D3.

7.5.3.6. Test Results under 0.5g Acceleration with 2Hz of Frequency. Figure 7.46, represents the test results of the unreinforced embankment model subjected to 0.5g with 2Hz of motion for the selected measurements of A9, D2 and D3.

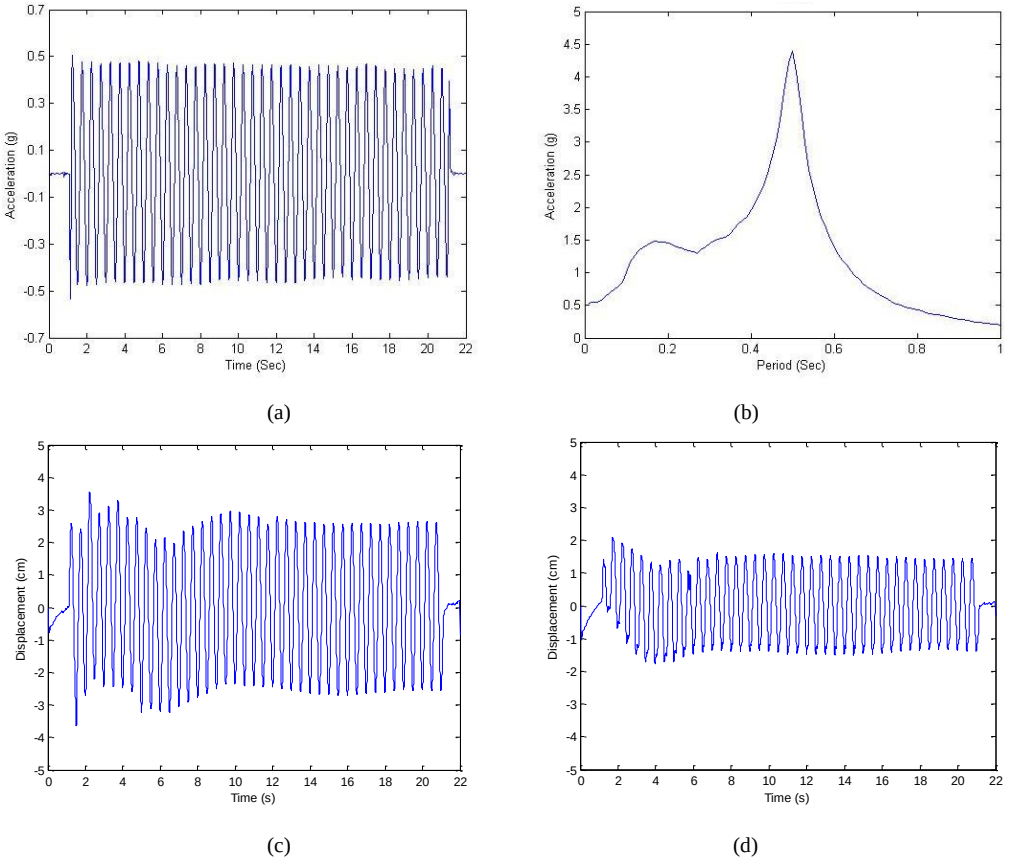

Figure 7.46. Test results for 0.5g with 2Hz of motion. a) Acc.-Time History of A9, b) Response Spec. of A9, c) Disp.-Time History of D2, d) Disp.-Time History of D3.

7.5.3.7. Test Results under 0.5g Acceleration with 5Hz of Frequency. Figure 7.47, represents the test results of the unreinforced embankment model subjected to 0.5g with 5Hz of motion for the selected measurements of A9, D2 and D3.

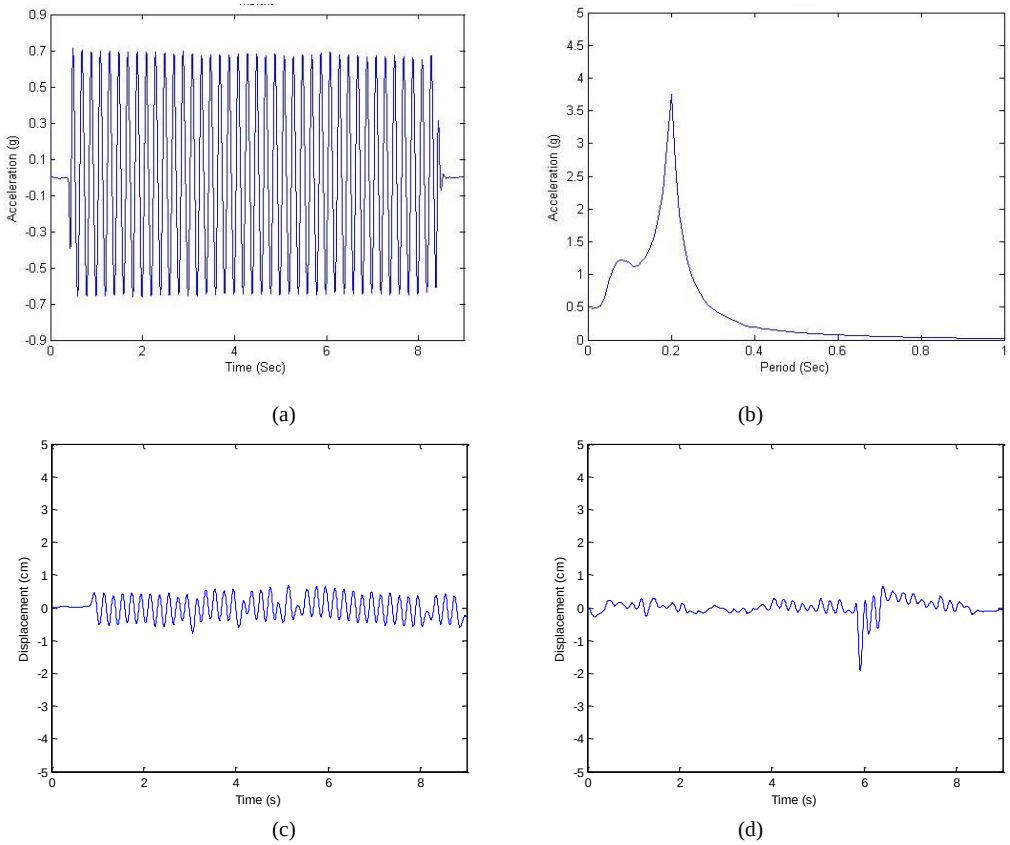

Figure 7.47. Test results for 0.5g with 5Hz of motion. a) Acc.-Time History of A9, b) Response Spec. of A9, c) Disp.-Time History of D2, d) Disp.-Time History of D3.

7.5.3.8. Test Results under 0.5g Acceleration with 7Hz of Frequency. Figure 7.48, represents the test results of the unreinforced embankment model subjected to 0.5g with 7Hz of motion for the selected measurements of A9, D2 and D3.

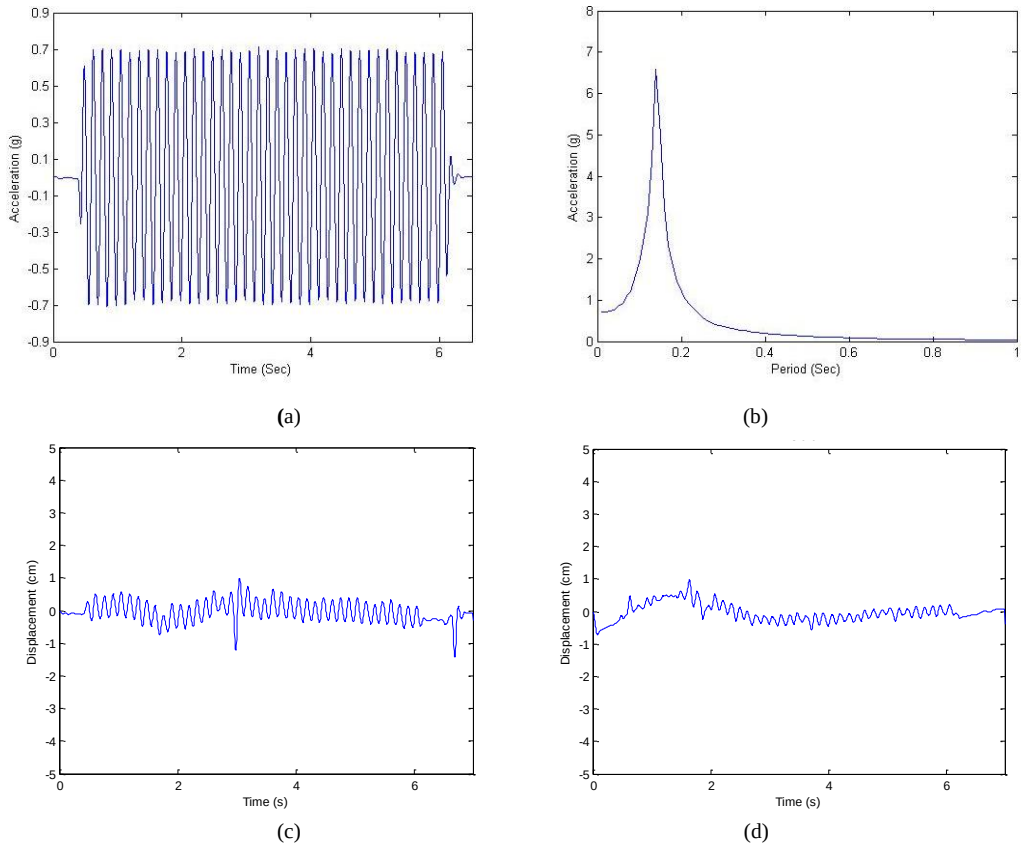

Figure 7.48. Test results for 0.5g with 7Hz of motion. a) Acc.-Time History of A9, b) Response Spec. of A9, c) Disp.-Time History of D2, d) Disp.-Time History of D3.

7.5.3.9. Test Results under 0.5g Acceleration with 14Hz of Frequency. Figure 7.49, represents the test results of the unreinforced embankment model subjected to 0.5g with 14Hz of motion for the selected measurements of A9, D2 and D3.

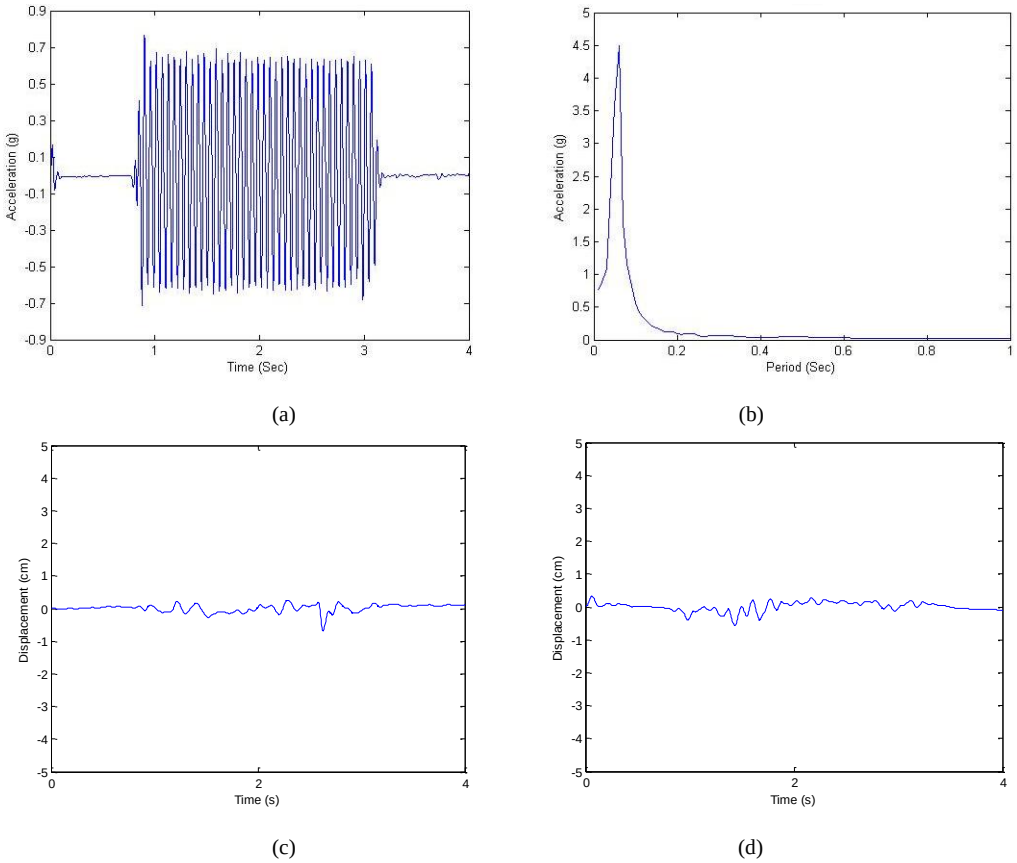

Figure 7.49. Test results for 0.5g with 14Hz of motion. a) Acc.-Time History of A9, b) Response Spec. of A9, c) Disp.-Time History of D2, d) Disp.-Time History of D3.

7.5.4. Test Results for Reinforced Embankment Model of 30° Inclination

Test results of the reinforced embankment model with the slope inclination of 30° are represented in Figures from 7.50 to 7.58.

7.5.4.1. Test Results for Düzce Earthquake Motions. Figure 7.50, represents the test results of the reinforced embankment model subjected to time scaled Düzce Earthquake excitations. Real earthquake record is time scaled due to the scaling laws of Iai (1989) and with respect to the scaling ratio of the model. Selected measurements of A9, D2 and D3 are used.

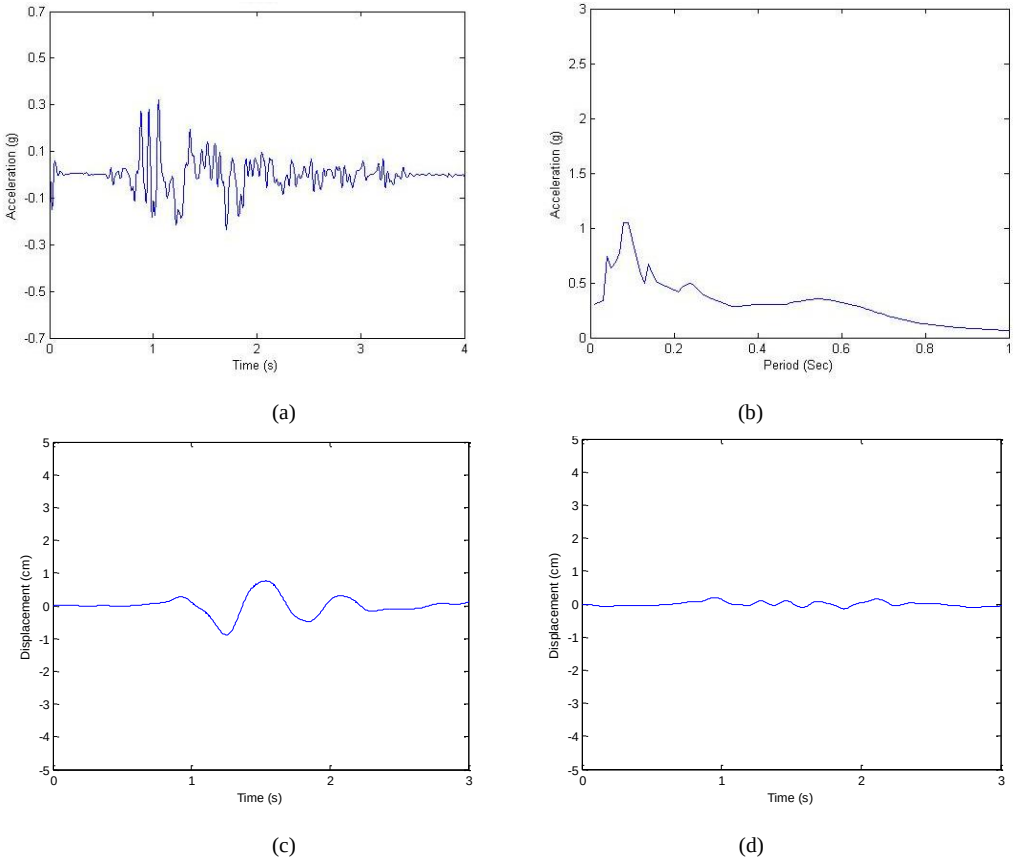

Figure 7.50. Test results for Düzce Eqe. a) Acc.-Time History of A9, b) Response Spec. of A9, c) Disp.-Time History of D2, d) Disp.-Time History of D3.

7.5.4.2. Test Results under 0.3g Acceleration with 2Hz of Frequency. Figure 7.51, represents the test results of the reinforced embankment model subjected to 0.3g with 2Hz of motion for the selected measurements of A9, D2 and D3.

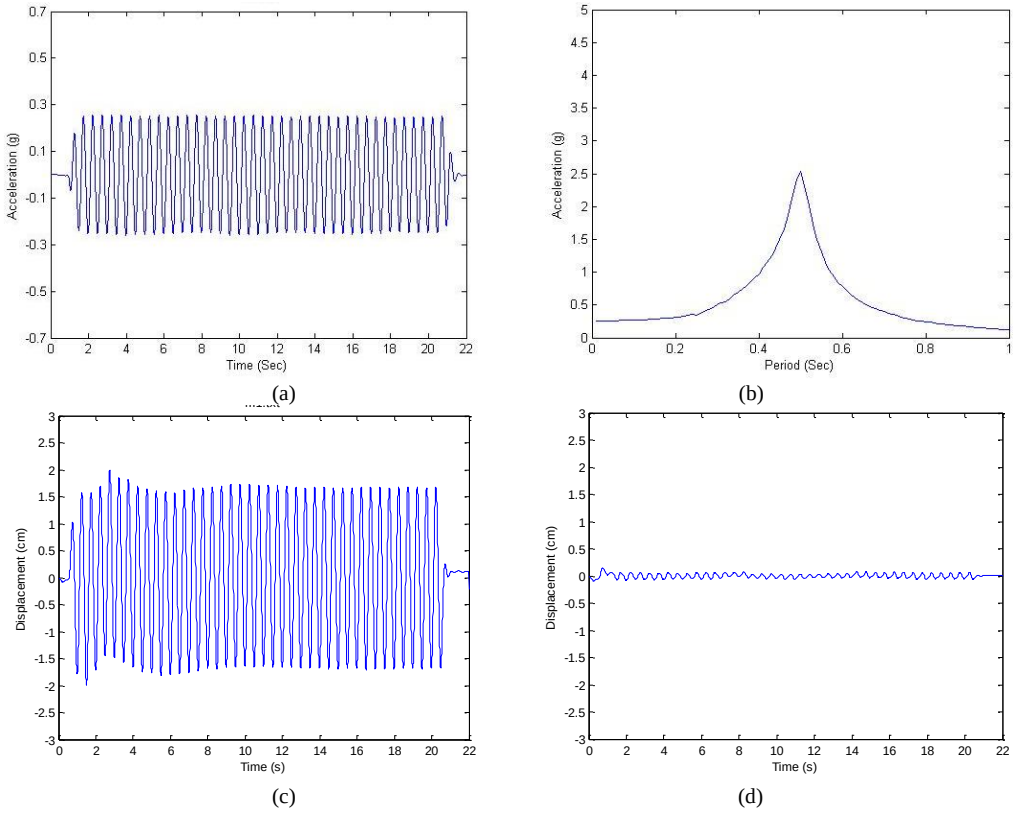

Figure 7.51. Test results for 0.3g with 2Hz of motion. a) Acc.-Time History of A9, b) Response Spec. of A9, c) Disp.-Time History of D2, d) Disp.-Time History of D3.

7.5.4.3. Test Results under 0.3g Acceleration with 5Hz of Frequency. Figure 7.52, represents the test results of the reinforced embankment model subjected to 0.3g with 5Hz of motion for the selected measurements of A9, D2 and D3.

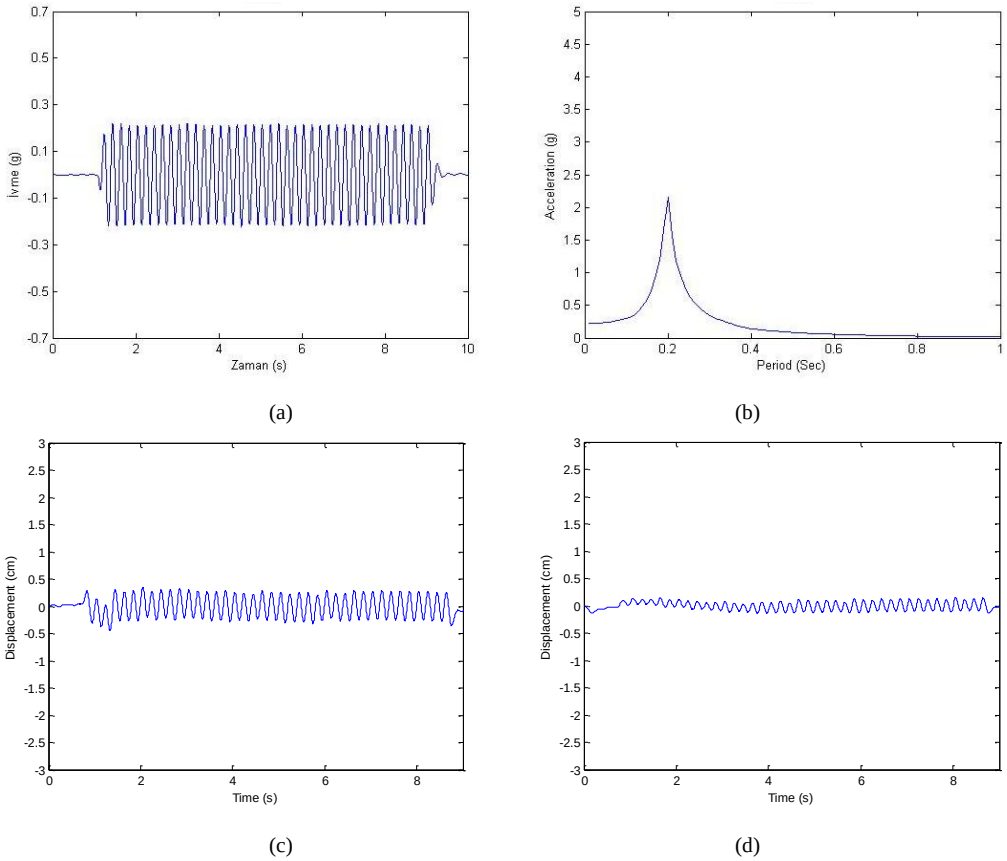

Figure 7.52. Test results for 0.3g with 5Hz of motion. a) Acc.-Time History of A9, b) Response Spec. of A9, c) Disp.-Time History of D2, d) Disp.-Time History of D3.

7.5.4.4. Test Results under 0.3g Acceleration with 7Hz of Frequency. Figure 7.53, represents the test results of the reinforced embankment model subjected to 0.3g 7Hz of motion for the selected measurements of A9, D2 and D3.

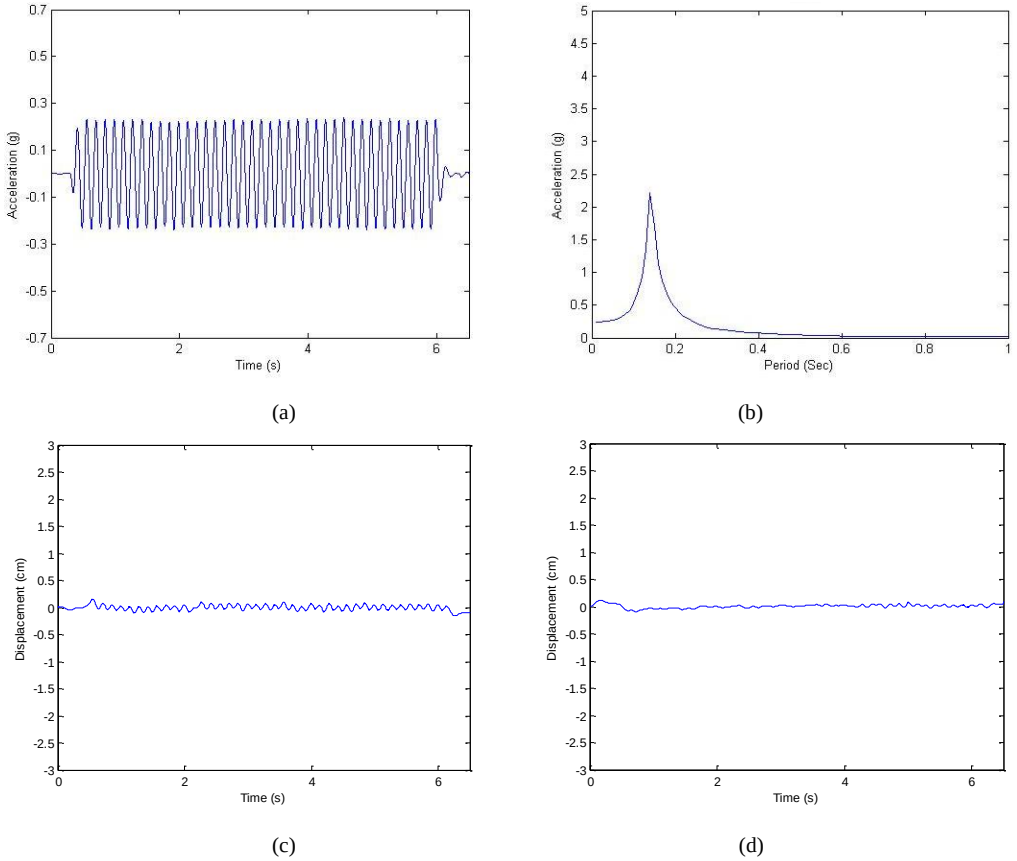

Figure 7.53. Test results for 0.3g with 7Hz of motion. a) Acc.-Time History of A9, b) Response Spec. of A9, c) Disp.-Time History of D2, d) Disp.-Time History of D3.

7.5.4.5. Test Results under 0.3g Acceleration with 14Hz of Frequency. Figure 7.54, represents the test results of the reinforced embankment model subjected to 0.3g with 14Hz of motion for the selected measurements of A9, D2 and D3.

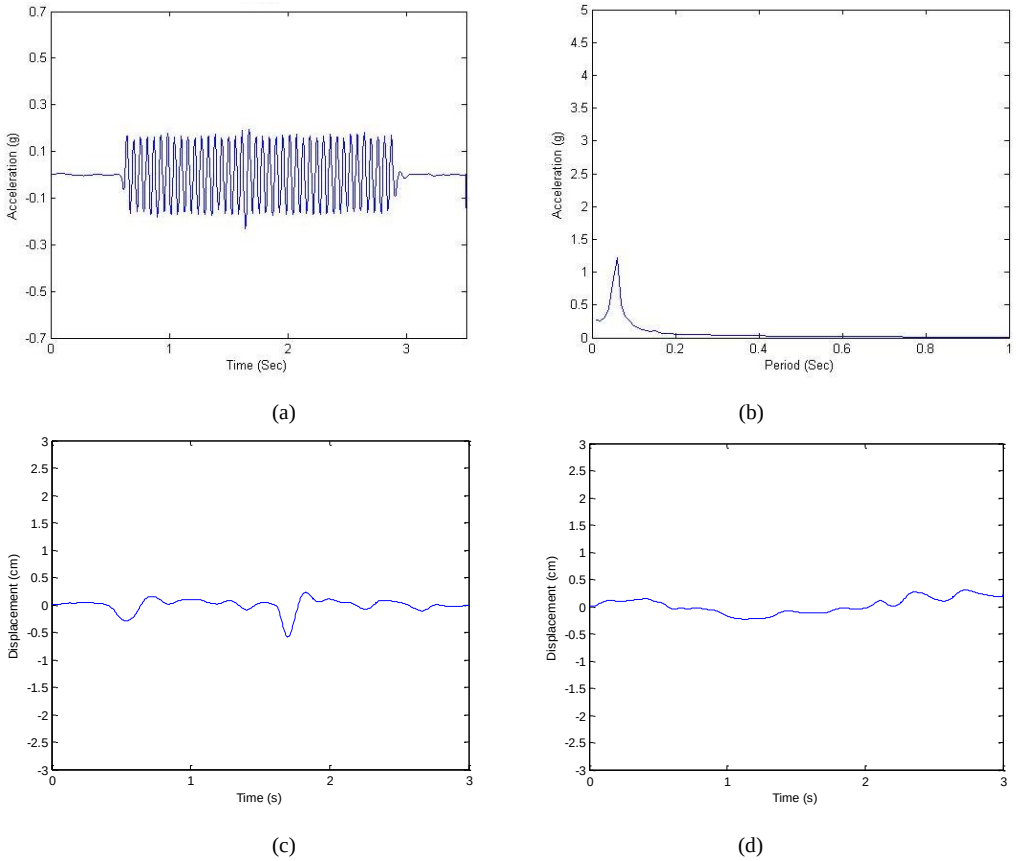

Figure 7.54. Test results for 0.3g with 14Hz of motion. a) Acc.-Time History of A9, b) Response Spec. of A9, c) Disp.-Time History of D2, d) Disp.-Time History of D3.

7.5.4.6. Test Results under 0.5g Acceleration with 2Hz of Frequency. Figure 7.55, represents the test results of the reinforced embankment model subjected to 0.5g with 2Hz of motion for the selected measurements of A9, D2 and D3.

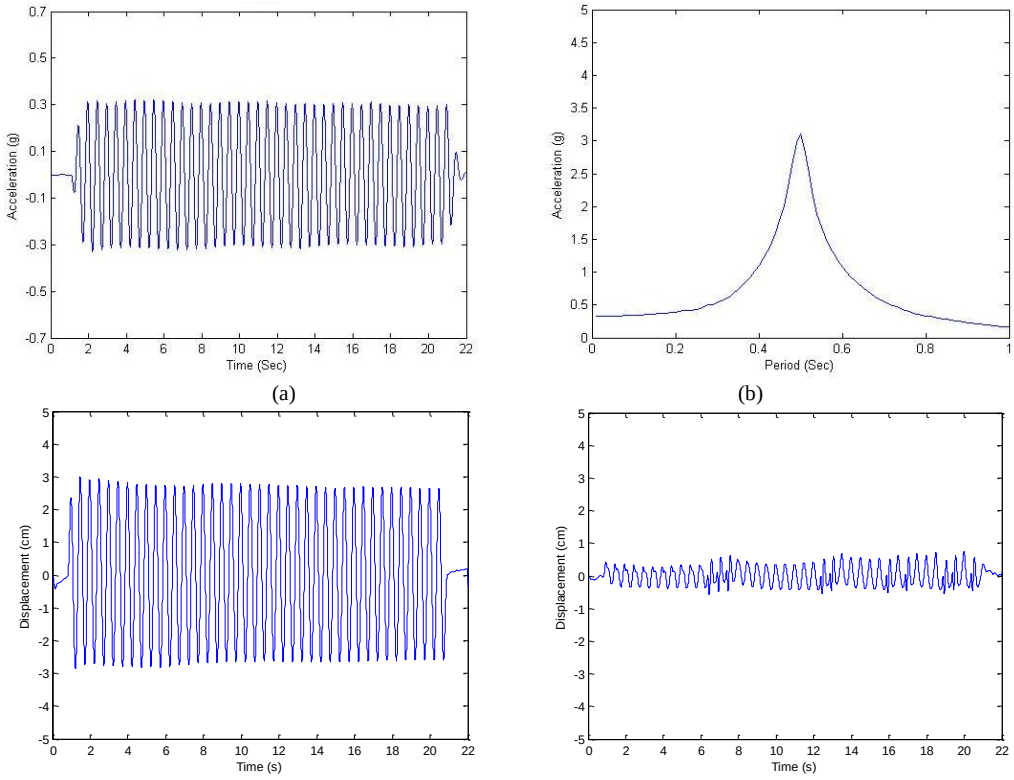

Figure 7.55. Test results for 0.5g with 2Hz of motion. a) Acc.-Time History of A9, b) Response Spec. of A9, c) Disp.-Time History of D2, d) Disp.-Time History of D3.

7.5.4.7. Test Results under 0.5g Acceleration with 5Hz of Frequency. Figure 7.56, represents the test results of the reinforced embankment model subjected to 0.5g with 5Hz of motion for the selected measurements of A9, D2 and D3.

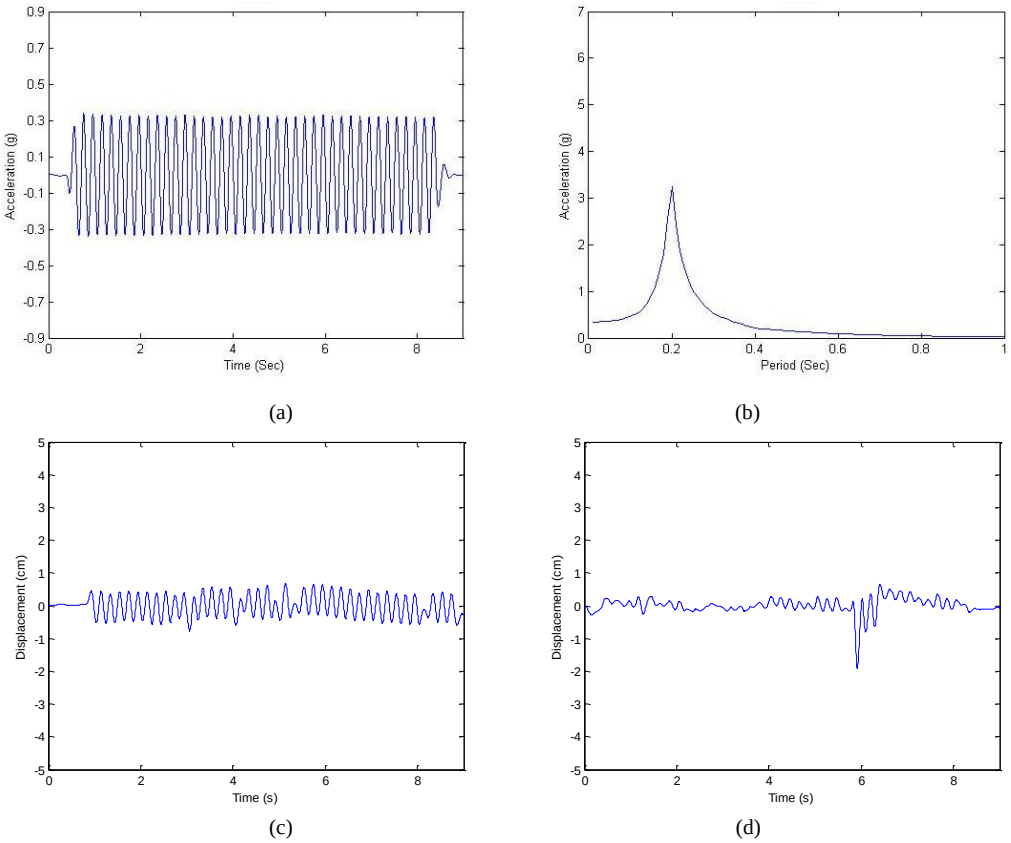

Figure 7.56. Test results for 0.5g with 5Hz of motion. a) Acc.-Time History of A9, b) Response Spec. of A9, c) Disp.-Time History of D2, d) Disp.-Time History of D3.

7.5.4.8. Test Results under 0.5g Acceleration with 7Hz of Frequency. Figure 7.57, represents the test results of the reinforced embankment model subjected to 0.5g with 7Hz of motion for the selected measurements of A9, D2 and D3.

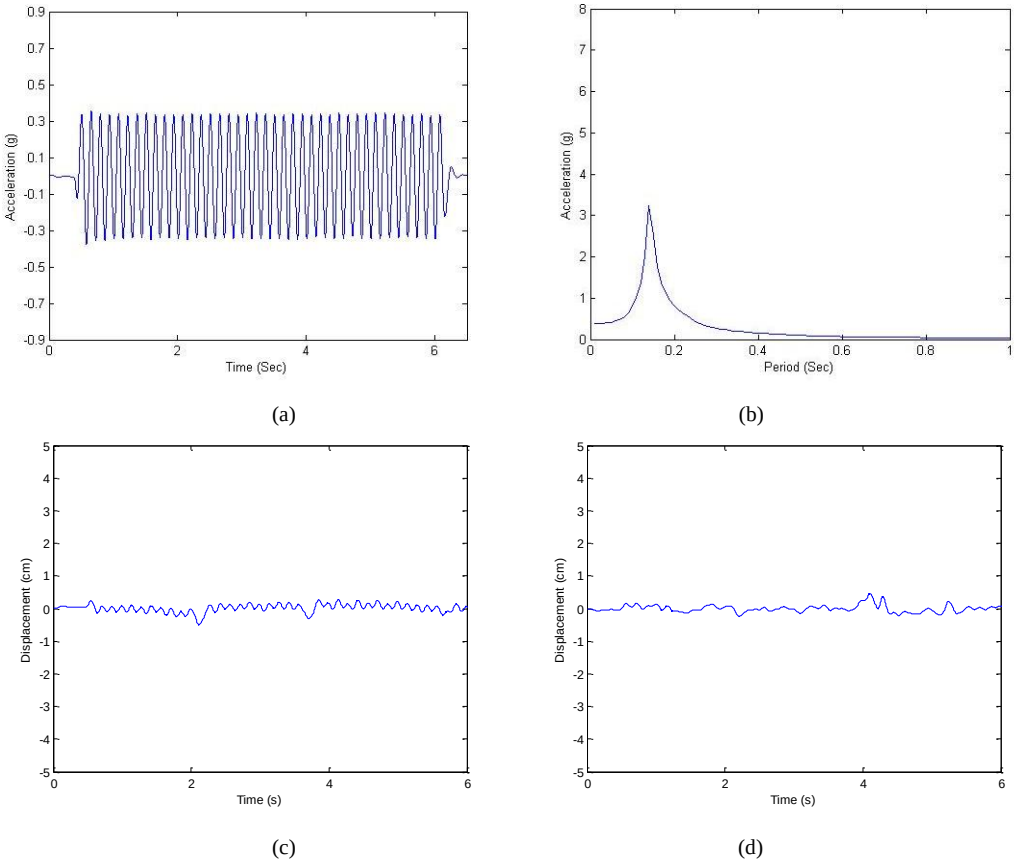

Figure 7.57. Test results for 0.5g with 7Hz of motion. a) Acc.-Time History of A9, b) Response Spec. of A9, c) Disp.-Time History of D2, d) Disp.-Time History of D3.

7.5.4.9. Test Results under 0.5g Acceleration with 14Hz of Frequency. Figure 7.58, represents the test results of the reinforced embankment model subjected to 0.5g with 14Hz of motion for the selected measurements of A9, D2 and D3.

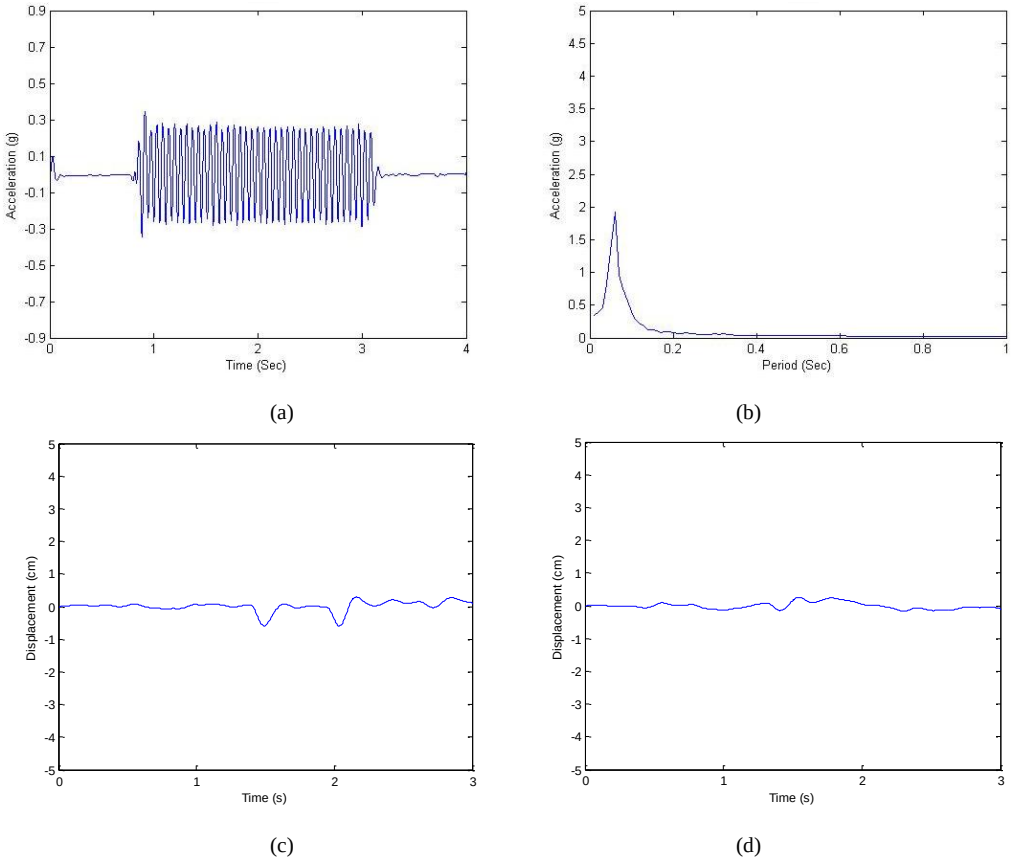

Figure 7.58. Test results for 0.5g with 14Hz of motion. a) Acc.-Time History of A9, b) Response Spec. of A9, c) Disp.-Time History of D2, d) Disp.-Time History of D3.

7.6. Evaluation of the Experimental Results

For a better evaluation and comparison of the performed experimental results, acceleration and displacement measurements for both models with two different slope inclinations are represented in Tables between 7.2 and 7.31.

7.6.1. Evaluation of the Acceleration-Time Histories Test Results

Evaluations of the results are given according to the following tabulated acceleration values. Table 7.2 represents the measured acceleration values of the embankment model with 45° inclination under Düzce Earthquake.

Table 7.2. Acceleration values under Düzce Earthquake excitations.

Scaled Düzce Eqe. (g)	Unreinforced	Reinforced
A1	0.35	0.35
A2	0.31	0.30
A3	0.24	0.24
A4	0.31	0.30
A5	0.30	0.30
A6	0.31	0.30
A7	0.34	0.32
A8	0.35	0.31
A9	0.39	0.34

As can be seen on Table 7.2, under the scaled Düzce Earthquake ground motion, the reinforcement effect is limited. The decrement of the transmitted accelerations is limited to 13% and was seen at A9. The measurements of A2-A6 are almost identical to the input. A7 measured 0.34g and 0.32g similarly, A8 measured 0.35g and 0.31g in the unreinforced and reinforced embankment models, respectively. Amplification Factor (AF) decreases from 1.11 to 0.97 at the crest of the model after reinforcement. It shows that inclusion of the geotextile reinfocement deamplificated the transmitted accelerations.

Table 7.3 shows the acceleration values of the unreinforced embankment model with 45° inclination under 0.3g of excitation and Table 7.4 shows the acceleration values of the reinforced embankment model with 45° inclination under 0.3g of excitation.

Table 7.3. Acceleration values of unreinforced embankment under 0.3g of excitation.

PGA (0.3g)	2Hz	5Hz	7Hz	14Hz
A1	0.30	0.30	0.30	0.30
A2	0.28	0.28	0.29	0.20
A3	0.27	0.25	0.27	0.23
A4	0.28	0.28	0.29	0.28
A5	0.28	0.29	0.29	0.28
A6	0.30	0.41	0.40	0.31
A7	0.35	0.45	0.42	0.38
A8	0.32	0.47	0.47	0.43
A9	0.33	0.54	0.57	0.47

Table 7.4. Acceleration values of reinforced embankment under 0.3g of excitation.

PGA (0.3g)	2Hz	5Hz	7Hz	14Hz
A1	0.30	0.30	0.30	0.30
A2	0.30	0.28	0.29	0.32
A3	0.25	0.21	0.26	0.23
A4	0.31	0.27	0.29	0.29
A5	0.32	0.27	0.30	0.28
A6	0.31	0.27	0.30	0.28
A7	0.31	0.28	0.32	0.26
A8	0.26	0.22	0.24	0.22
A9	0.27	0.24	0.26	0.25

Tables 7.3 and 7.4 represent the PGA values of the unreinforced and reinforced embankment models under 0.3g of motion with different frequency levels. Under 0.3g acceleration with 2Hz of frequency, the effect of reinforcement is very limited for the measurements of A2, A3, A4 and A5. The acceleration value is 0.30g for the unreinforced model and 0.28g for scaled geotextile reinforced model at A2. The difference between measurements of A3 for unreinforced and reinforced models is minor. A4 measured 0.31g of acceleration in the unreinforced model and 0.28g in the reinforced model. The measured acceleration value at A5 is 0.28g in the reinforced model which is 12.5% less than the unreinforced case. The effect of reinforcement remains minor at A6 with only 0.01g of difference between measurements. Measurements of A7 decreased with the effect of the reinforcement layers. A7 measured 0.35g in the unreinforced model and 0.31g in the reinforced model which makes a decrease of almost 12%. The effect of the reinforcement is noticable at the measurements of A8. In the unreinforced model, the acc. value is 0.32g while it was measured as 0.26g for the reinforced case. The reduction of the transmitted acc. roughly equals to 20%. Similarly the measurements of A9 is 20% less in the reinforced embankment model with 0.27g. It is determined that AF values decreased from 1.1 to 0.9 at the top of the reinforced embankment model.

Under 0.3g acceleration with 5Hz of frequency, there are minor differences between the PGA measurements of unreinforced and reinforced embankment models at A2-A5. The acceleration values are almost identical to each other between reinforced and unreinforced cases. The measurement of A6 decreases from 0.41g to 0.27g in the

reinforced model. This means that the reinforcement effect is reduced the acc. values 34%. A7 measured 0.45g and 0.28g and A8 measured 0.47g and 0.22g in the unreinforced and reinforced models respectively. The acc. values are reduced more than 50% with the reinforcement effect. Similarly A9 measurements reduced by 56% with the 0.24g of measurement in the reinforced model. In addition, AF value of 1.8 in the unreinforced model decreased to 0.8 in the reinforced model.

Under 0.3g acceleration with 5Hz of frequency, the similar dynamic behaviour trend is seen. Reinforcement effect is not clear at the locations of accelerometers A2-A5. The effect of reinforcement is noticable at A6. 0.40g of acc. value in the unreinforced model decreases to 0.30g in the reinforced model. A7 measured 0.42g and 0.32g and A8 measured 0.47g and 0.24g in the unreinforced and reinforced cases, respectively. The measurements of A9, which is located at the highest location in the system, gives the best results. Reinforcement effect decreased the transmitted acc. values by 54%, from 0.57g to 0.26g. Moreover AF values at the crest decreased from 1.9 to 0.87 in the reinforced embankment model.

Under the dynamic motions of 0.3g acceleration with 14Hz of frequency, A2-A5 measured acc. values similar to the base excitation and around 0.30g. 0.31g of acc. value in the unreinforced embankment model measured by A6, reduced to 0.28g in the reinforced model. A7 measured 0.38g and 0.26g in the unreinforced and reinforced cases, respectively. The reinforcement effect is even more clear at A8 and A9. The measurement of A8 was reduced by 49% in the reinforced model. A9 measured 0.47g in the unreinforced case however the same value is only 0.25g in the reinforced case which equals to a reduction in acc. values of 47%. Similarly, AF values are obtained as 1.57 to 0.83 for unreinforced and reinforced embankments, respectively. It shows a siginificant demamplification at the crest.

Table 7.5 and Table 7.6 represents the transmitted acceleration values of the unreinforced and reinforced embankment model with 45° inclination under 0.5g of excitation.

Table 7.5. Acceleration values of unreinforced embankment under 0.5g of excitation.

PGA (0.5g)	2Hz	5Hz	7Hz	14Hz
A1	0.50	0.50	0.50	0.50
A2	0.40	0.49	0.48	0.49
A3	0.46	0.49	0.45	0.37
A4	0.47	0.50	0.51	0.45
A5	0.47	0.50	0.51	0.45
A6	0.51	0.64	0.63	0.54
A7	0.53	0.66	0.67	0.61
A8	0.53	0.71	0.71	0.77
A9	0.57	0.79	0.76	0.81

Table 7.6. Acceleration values of reinforced embankment under 0.5g of excitation.

PGA (0.5g)	2Hz	5Hz	7Hz	14Hz
A1	0.50	0.50	0.50	0.50
A2	0.51	0.49	0.49	0.46
A3	0.40	0.45	0.46	0.34
A4	0.51	0.50	0.50	0.44
A5	0.51	0.50	0.51	0.45
A6	0.50	0.49	0.49	0.45
A7	0.50	0.50	0.50	0.51
A8	0.33	0.34	0.38	0.35
A9	0.34	0.36	0.39	0.39

As can be inferred from tables, under 0.5g of excitation with 2Hz of frequency, the acc. values are around and very close to 0.50g at A2-A6. A7 measured 0.53g in the unreinforced model and 0.50g in the reinforced model. The measurement of A8 in the reinforced model is 38% less than the unreinforced model. A8 measured 0.53g in the unreinforced case however the same measurement is only 0.33g. A9 measured 0.57g and 0.34g respectively in the unreinforced and reinforced embankment models. This time the reduction of acc. values is 40%. AF values at the crest decreased from 1.14 to 0.68 in the reinforced model under current dynamic motion.

Under 0.5g of excitation with 5Hz of frequency, A2-A5 follows the same trend where the effect of reinforcement is not present. A6 measured 0.64g and 0.49g in the unreinforced and reinforced models, respectively. The acc. measurements of A7 in the reinforced model is 25% less than the unreinforced model with 0.50g. The effect of reinforcement is significant at A8 and A9. 0.71g of acc. value at A8 decreased to 0.34g

in the reinforced model and similarly 0.79g of acc. value reduced by 55% with the reinforcement effect at A9. Similarly AF values decreased from 1.58 to 0.72.

Under dynamic motions of 0.5g with 7Hz of frequency, A2-A5 measurements are similar to the input excitation. A6 measured 0.63g and 0.49g for the unreinforced and reinforced cases, respectively. The reinforcement effect becomes more clear at the upper part of the embankment model. The measurement of A7 was 0.67g in the unreinforced embankment model while it was reduced to 0.50g due to the effect of reinforcement layers inside the embankment. A8 measured 0.71g and 0.38g in the unreinforced and reinforced models, respectively. The amount of reduction in the acc. value is 46% at A8 and 49% at A9 with 0.39g of transmitted acc. value. Also, AF value of 1.52 in the unreinforced model decreased to 0.78 in the reinforced model.

Under 0.5g of excitation with 14Hz of frequency, the measurements of A2-A5 are similar to each other and to the input motion. The effect of reinforcement is notable for the accelerometers A6-A9. The measurement of A6 in the unreinforced case is 0.54g and with the reinforcement effect, the same value reduced by 17%. A7 measured 0.61g and 0.51g in the unreinforced and reinforced cases, respectively. The measured transmitted acc. value of A8 reduced by 55% in the reinforced model with 0.35g. The acc. values of A9 decreased from 0.81g to 0.39g due to the reinforcement which equals to a reduction of 52%. AF value at the top of the embankment model decreased from 1.62 to 0.78.

Table 7.7 represents the measured acceleration values of the embankment model with 30° inclination under the Düzce Earthquake ground motion.

Table 7.7. Acceleration values under Düzce Earthquake excitations.

Scaled Düzce Eqe. (g)	Unreinforced	Reinforced
A1	0.35	0.35
A2	0.31	0.30
A3	0.30	0.31
A4	0.31	0.30
A5	0.30	0.30
A6	0.31	0.30
A7	0.34	0.31
A8	0.35	0.32
A9	0.37	0.34

PGA values of the unreinforced and reinforced embankment models with 30° of inclination under time scaled Düzce Earthquake is given in Table 7.7. Under scaled Düzce Earthquake ground motions, the reinforcement effect is limited. The decrement of the transmitted accelerations is around 10% and was seen at A8 and A9. The measurements of A2-A6 are almost identical to the input. A7 measured 0.34g and 0.31g similarly A8 measured 0.35g and 0.32g in the unreinforced and reinforced embankment models, respectively. AF values at the crest of the embankment slightly decreases from 1.23 to 1.13 in the reinforced case.

Table 7.8 shows the acceleration values of the unreinforced embankment model with 30° inclination under 0.3g of excitation and Table 7.9 shows the acceleration values of the reinforced embankment model with 30° inclination under 0.3g of excitation.

Table 7.8. Acceleration values of unreinforced model under 0.3g of excitation.

PGA (0.3g)	2Hz	5Hz	7Hz	14Hz
A1	0.30	0.30	0.30	0.30
A2	0.28	0.28	0.29	0.29
A3	0.27	0.27	0.27	0.27
A4	0.28	0.28	0.29	0.27
A5	0.28	0.29	0.29	0.28
A6	0.30	0.40	0.40	0.30
A7	0.31	0.45	0.43	0.35
A8	0.32	0.47	0.47	0.42
A9	0.32	0.48	0.49	0.43

Table 7.9. Acceleration values of reinforced model under 0.3g of excitation.

PGA (0.3g)	2Hz	5Hz	7Hz	14Hz
A1	0.30	0.30	0.30	0.30
A2	0.30	0.28	0.29	0.30
A3	0.26	0.28	0.28	0.28
A4	0.30	0.28	0.29	0.29
A5	0.32	0.27	0.30	0.29
A6	0.31	0.27	0.30	0.28
A7	0.30	0.25	0.31	0.26
A8	0.24	0.21	0.23	0.22
A9	0.26	0.22	0.24	0.25

As shown in Tables 7.8 and 7.9, under 0.3g acceleration with 2Hz of frequency, the effect of reinforcement is limited for the measurements of A2, A3, A4 and A5. The acceleration value is 0.28g for the unreinforced model and 0.30g for scaled geotextile reinforced model at A2. The difference between measurements of A3 for unreinforced and reinforced models is minor. A4 measurements are the same as A3 values. The effect of reinforcement remains minor at A6 with only 0.01g of difference between measurements. Measurements of A6 remains the same as the input ground acceleration for both cases. A7 measured 0.31g in the unreinforced model and 0.30g in the reinforced model. The effect of the reinforcement is noticable at the measurements of A8. In the unreinforced model, the acc. value is 0.32g while it was measured as 0.24g for the reinforced case. The reduction of the transmitted acc. equals to 25%. Similarly the measurements of A9 is 19% less in the reinforced embankment model with 0.26g. Also, AF values decreased from 1.07 to 0.87 in the reinforced model.

Under 0.3g acceleration with 5Hz of frequency, there are minor differences between the PGA measurements of unreinforced and reinforced embankment models at A2-A5. The acceleration values are almost identical to each other between reinforced and unreinforced cases. The measurement of A6 decreases from 0.40g to 0.27g in the reinforced model. This means that the reinforcement effect is reduced the acc. values 33%. A7 measured 0.45g and 0.25g and A8 measured 0.47g and 0.21g in the unreinforced and reinforced models respectively. The acc. values are reduced more than 50% with the reinforcement effect. Similarly A9 measurements reduced by almost 55% with the 0.22g of measurement in the reinforced model. AF value at the top of the model significantly decreased from 1.60 to 0.73.

Under 0.3g acceleration with 7Hz of frequency, the similar dynamic behaviour trend is seen. Reinforcement effect is not clear at the locations of accelerometers A2-A5. The effect of reinforcement is noticable at A6. 0.40g of acc. value in the unreinforced model decreases to 0.30g in the reinforced model. A7 measured 0.43g and 0.31g and A8 measured 0.47g and 0.23g in the unreinforced and reinforced cases, respectively. The measurements of A9, which is located at the highest location in the system, gives the best results. Reinforcement effect decreased the transmitted acc. values by 51%, from 0.49g to 0.24g. In addition, AF value of 1.63 in the unreinforced case decreased to 0.80.

Under the dynamic motions of 0.3g acceleration with 14Hz of frequency, A2-A5 measured acc. values similar to the base excitation and around 0.30g. 0.30g of acc. value in the unreinforced embankment model measured by A6, reduced to 0.28g in the reinforced model. A7 measured 0.35g and 0.26g in the unreinforced and reinforced cases, respectively. The reinforcement effect is even more clear at A8 and A9. The measurement of A8 was decreased from 0.42g to 0.22g that is a reduction of 48% in the acceleration values. A9 measured 0.43g in the unreinforced case however the same value is only 0.25g in the reinforced case which equals to a reduction in acc. values of 42%. At the top of the embankment model, AF values decreased from 1.43 to 0.83.

Table 7.10 and Table 7.11 represents the acceleration values of the unreinforced and reinforced embankment model with 30° inclination under 0.5g of excitation.

Table 7.10. Acceleration values of unreinforced model under 0.5g of excitation.

PGA (0.5g)	**2Hz**	**5Hz**	**7Hz**	**14Hz**
A1	0.50	0.50	0.50	0.50
A2	0.45	0.50	0.49	0.49
A3	0.46	0.49	0.45	0.46
A4	0.46	0.50	0.50	0.45
A5	0.47	0.51	0.51	0.46
A6	0.50	0.64	0.62	0.52
A7	0.51	0.66	0.65	0.60
A8	0.51	0.68	0.66	0.71
A9	0.52	0.70	0.70	0.75

Table 7.11. Acceleration values of reinforced model under 0.5g of excitation.

PGA (0.5g)	2Hz	5Hz	7Hz	14Hz
A1	0.50	0.50	0.50	0.50
A2	0.51	0.49	0.49	0.47
A3	0.49	0.48	0.48	0.45
A4	0.50	0.50	0.51	0.46
A5	0.51	0.51	0.51	0.47
A6	0.50	0.49	0.49	0.47
A7	0.47	0.48	0.50	0.52
A8	0.31	0.32	0.35	0.35
A9	0.32	0.35	0.38	0.36

PGA values of the unreinforced and reinforced embankment models with 30° of inclination under 0.5g of motion with different frequencies are represented in Tables 7.9 and 7.10. Under 0.5g of excitation with 2Hz of frequency, the acc. values are around and very close to 0.50g at A2-A6. A7 measured 0.51g in the unreinforced model and 0.47g in the reinforced model. The measurement of A8 in the reinforced model is almost 40% less than the unreinforced model. A8 measured 0.51g in the unreinforced case however the same measurement is only 0.31g. A9 measured 0.52g and 0.32g respectively in the unreinforced and reinforced embankment models. This time the reduction of acc. values is 39%. In the reinforced embankment model, AF value at the crest decreased from 1.04 to 0.64.

Under 0.5g of excitation with 5Hz of frequency, A2-A5 follows the same trend where the effect of reinforcement is not present. A6 measured 0.64g and 0.49g in the unreinforced and reinforced models, respectively. The acc. measurements of A7 in the reinforced model is 27% less than the unreinforced model with 0.48g. The effect of reinforcement is significant at A8 and A9. 0.68g of acc. value at A8 decreased to 0.32g in the reinforced model, which is a reduction of 53% and similarly 0.70g of acc. value reduced by 50% with the reinforcement effect at A9. Also, AF values decreased from 1.40 to 0.70 which equals to a reduction of 50%.

Under dynamic motions of 0.5g with 7Hz of frequency, A2-A5 measurements are similar to the input excitation. A6 measured 0.62g and 0.49g for the unreinforced and reinforced cases, respectively. The reinforcement effect becomes more clear at the

upper part of the embankment model. The measurement of A7 was 0.65g in the unreinforced embankment model while it was reduced to 0.50g due to the effect of reinforcement layers inside the embankment. A8 measured 0.66g and 0.35g in the unreinforced and reinforced models, respectively. The amount of reduction in the acc. value is 47% at A8 and 46% at A9 with 0.38g of transmitted acc. value. Moreover, AF values decreased from 1.40 to 0.76.

Under 0.5g of excitation with 14Hz of frequency, the measurements of A2-A5 are similar to each other and to the input motion. The effect of reinforcement is notable for the accelerometers A6-A9. The measurement of A6 in the unreinforced case is 0.52g and with the reinforcement effect, the same value reduced by 10%. A7 measured 0.60g and 0.52g in the unreinforced and reinforced cases, respectively. The measured transmitted acc. value of A8 reduced by 51% in the reinforced model with 0.35g. The acc. values of A9 decreased from 0.75g to 0.36g due to the reinforcement which equals to a reduction of 52%. Under current motion, AF values at the crest decreased from 1.50 to 0.72.

7.6.2. Evaluation of the Spectral Acceleration Measurement Test Results

The following tables represent the spectral acceleration and corresponding period values of the embankment models under input ground motions. Table 7.12 gives the shake table results under Düzce Earthquake for 45° inclination.

Table 7.12. SA and T values of embankment models under Düzce Earthquake.

	Unreinforced		Reinforced	
	SA (g)	T (s)	SA (g)	T (s)
A1	1.08	0.08	1.08	0.09
A2	1.08	0.08	1.07	0.09
A3	1.05	0.08	1.05	0.09
A4	1.06	0.08	1.06	0.09
A5	1.07	0.08	1.06	0.09
A6	1.05	0.08	1.05	0.09
A7	1.12	0.08	1.12	0.09
A8	1.13	0.04	1.05	0.09
A9	1.24	0.04	1.14	0.09

Tabulated spectral acceleration (SA) values reveal that the effect of scaled geotextile is present at A8 and A9 under Düzce Earthquake. As can be seen in Table 7.12, for both cases of reinforced and unreinforced embankment models (1:1), SA measurements of A2-A6 are very similar to A1, which measures the base excitation and there are only minor and ignorable differences in the measurements. A8 measured 1,13g of SA in the unreinforced case and 1,05g in the reinforced case. Also, A9 measured 1,24g and 1,14g in the unreinforced and reinforced cases respectively and the reinforcement reduced the SA values by 8%. On the other hand, the measured period values slightly increases due to the reinforcement. The period value measurements at A8 and A9 is 0.04 seconds in the unreinforced model but the same measurement increases to 0.09 seconds after the reinforcement.

Table 7.13 shows the test results of unreinforced model under 0.3g of excitation and Table 7.14 gives the test results under the same dynamic load for the reinforced case.

Table 7.13. SA and T values of unreinforced embankment.

0.3G	2Hz		5Hz		7Hz		14Hz	
	SA (g)	T (s)	SA (g)	T (s)	SA (g)	T (s)	SA (g)	T (s)
A1	2.83	0.5	2.73	0.2	2.69	0.14	1.94	0.06
A2	2.83	0.5	2.69	0.2	2.87	0.14	1.85	0.06
A3	2.81	0.5	2.64	0.2	2.86	0.14	1.83	0.06
A4	2.82	0.5	2.66	0.2	2.85	0.14	1.82	0.06
A5	2.83	0.5	2.66	0.2	2.87	0.14	1.84	0.06
A6	2.81	0.5	3.75	0.2	3.61	0.14	1.86	0.06
A7	2.85	0.5	3.84	0.2	3.72	0.14	2.15	0.06
A8	2.71	0.5	3.74	0.2	3.73	0.14	2.42	0.06
A9	2.83	0.5	4.04	0.2	4.09	0.14	2.49	0.06

Table 7.14. SA and T values of reinforced embankment.

0.3G	2Hz		5Hz		7Hz		14Hz	
	SA (g)	T (s)	SA (g)	T (s)	SA (g)	T (s)	SA (g)	T (s)
A1	2.81	0.5	2.73	0.2	2.68	0.14	1.94	0.06
A2	2.82	0.5	2.68	0.2	2.87	0.14	1.86	0.06
A3	2.80	0.5	2.64	0.2	2.85	0.14	1.84	0.06
A4	2.82	0.5	2.66	0.2	2.85	0.14	1.85	0.06
A5	2.82	0.5	2.65	0.2	2.88	0.14	1.84	0.06
A6	2.81	0.5	2.65	0.2	2.83	0.14	1.85	0.06
A7	2.85	0.5	2.71	0.2	2.92	0.14	1.42	0.06
A8	2.53	0.5	2.15	0.2	2.21	0.14	0.53	0.06
A9	2.65	0.5	2.32	0.2	2.41	0.14	0.98	0.06

Given in Tables 7.13 and 7.14, under 0.3g and 2Hz of dominant frequency, measurements of sensors A1-A6 are quite similar for both cases. A7 measured 2.85g of SA in the reinforced and unreinforced cases. The effect of reinforcement is apparent in the measurements of A8 and A9. A8 measured 2.71g and 2.53g of SA while A9 measured 2.83g and 2.65g of SA in the unreinforced and reinforced embankment models (1:1), respectively. SA values decreased up to 7% and this reduction is concentrated at the upper parts of the model.

Under 0.3g and 5Hz of frequency, similar behavior trend is observed in the measurements of A1-A5. SA measurement of A6 is 3.75g in the unreinforced model and 2.65g in the reinforced model. Similarly A7 measured 3.84g and 2.71g in the unreinforced and reinforced cases, respectively. The effect of reinforcement becomes more clear near the top of the model. A8 measured 3.74g and 2.15g and A9 measured 4.04g and 2.32g in the unreinforced and reinforced models, respectively. Under current dynamic loads, SA values decreased up to 43%.

Under 0.3g and 7Hz of frequency, SA measurements of A1-A5 are similar. The effect of reinforcement is present for the rest of the acceleration sensors located inside the embankment model around the reinforcement layers. SA measurement of A6 in the reinforced model reduced by 22% from 3.61g to 2.83g and the similar situation applies to the measurements of A7 too. A8 measurements decreased from 3.73g to 2.21g and A9 measurements also decreased from 4.09g to 2.41g. Under current excitations, observed reduction in SA values is up to 41%.

While A1-A6 measurements follow the same trend as previous cases, the effect of the reinforcement can be seen at A7, A8 and A9 in the model (1:1) under 0.3g and 14Hz of frequency. SA values decreased from 2.15g to 1.42g at A7, from 2.42g to 0.53g at A8 and 2.49g to 0.98g at A9. The ratio of decrement in SA values is between 34% and up to 78% at A8 under current dynamic load.

Table 7.15 and Table 7.16 represents the test results of the model with 45° inclination under 0.5g of excitation for the unreinforced and reinforced cases, respectively.

Table 7.15. SA and T values of unreinforced embankment.

0.5G	2Hz		5Hz		7Hz		14Hz	
	SA (g)	T (s)	SA (g)	T (s)	SA (sn)	T (s)	SA (g)	T (sn)
A1	4.54	0.5	4.70	0.2	4.43	0.14	2.75	0.06
A2	4.57	0.5	4.71	0.2	4.46	0.14	2.99	0.06
A3	4.52	0.5	4.71	0.2	4.45	0.14	2.95	0.06
A4	4.59	0.5	4.70	0.2	4.49	0.14	2.92	0.06
A5	4.58	0.5	4.70	0.2	4.50	0.14	2.97	0.06
A6	4.56	0.5	6.13	0.2	5.94	0.14	3.43	0.06
A7	4.61	0.5	6.32	0.2	6.24	0.14	3.85	0.06
A8	4.40	0.5	6.41	0.2	6.59	0.14	4.50	0.06
A9	4.65	0.5	6.83	0.2	7.09	0.14	4.76	0.06

Table 7.16. SA and T values of reinforced embankment.

0.5G	2Hz		5Hz		7Hz		14Hz	
	SA (g)	T (s)	SA (g)	T (s)	SA (g)	T (s)	SA (g)	T (s)
A1	4.53	0.5	4.71	0.2	4.42	0.14	2.76	0.06
A2	4.57	0.5	4.70	0.2	4.45	0.14	2.99	0.06
A3	4.52	0.5	4.72	0.2	4.44	0.14	2.97	0.06
A4	4.59	0.5	4.71	0.2	4.47	0.14	2.95	0.06
A5	4.57	0.5	4.70	0.2	4.51	0.14	2.98	0.06
A6	4.56	0.5	4.68	0.2	4.45	0.14	2.95	0.06
A7	4.61	0.5	4.83	0.2	4.67	0.14	3.32	0.06
A8	3.10	0.5	3.24	0.2	3.24	0.14	1.92	0.06
A9	3.29	0.5	3.45	0.2	3.48	0.14	2.02	0.06

Under 0.5g and 2Hz of frequency, the effect of reinforcement in the measured SA values is visible at the upper portions of the reinforced embankment model with 1:1

inclination. Sensors of A2-A6, that are placed inside the foundation soil, measures similar SA values to the input motion. As can be seen in Tables 7.14 and 7.15, A7 measured 4.61g of SA for both models. A8 measured 4.40g and 3.10g and A9 measured 4.65g and 3.29g in the unreinforced and reinforced cases, respectively. Under current motions, SA values decreased up to 30%.

When shaking table tests performed under 5Hz of frequency, results of the sensors inside the foundation soil indicates minor differences. A6 measured 6.13g of SA in the unreinforced case however the same measurement is 4.68g. Similarly 6.41g of SA value by A8 went down to 3.24g due to the reinforcement application. And finally A9 measured 6.83g and 3.83g in the unreinforced and reinforced models, respectively. The SA measurements are decreased between 24%-50% due to the reinforcement.

Under 0.5g and 7Hz of frequency, the effect of reinforcement on the measured SA values is apparent at the upper portions of the embankment model. SA measurements inside the foundation soil is very close to the SA value of the base excitation. A7 measured 6.24g of SA in the unreinforced case and 4.67g in the reinforced case. Similarly A8 measured 6.59g of SA and 3.24g of SA in the unreinforced and reinforced cases, respectively. The reduction in the SA measurement of A8 is around 51%. The SA measurement of A9 is 7.09g and with the reinforcement effect, the same value reduced by almost 51% and went down to 3.48g.

When 14Hz of dynamic load is applied to the embankment models, SA measurements reveal that A8 and A9 presents the effectiveness of the reinforcement. A7 measurements went down from 3.85g to 3.32g. A8 measured 4.50g of SA before reinforcement and 1.92g after reinforcement, in other words SA measurement of A8 reduced by 57% after reinforcement. Also the measurement of A9 went down from 4.76g to 2.02g. This time the ratio of the reduction is 58%.

Following tables represent the SA and T values of the embankment models for the 30° inclination. Table 7.17 gives the test results under time scaled Düzce Earthquake motions.

Table 7.17. SA and T values of embankment models under Düzce Earthquake.

	Unreinforced		Reinforced	
	SA (g)	T (s)	SA (g)	T (s)
A1	1.08	0.08	1.08	0.09
A2	1.08	0.08	1.07	0.09
A3	1.06	0.08	1.05	0.09
A4	1.07	0.08	1.06	0.09
A5	1.06	0.08	1.05	0.09
A6	1.05	0.08	1.05	0.09
A7	1.06	0.08	1.05	0.09
A8	1.10	0.08	1.07	0.09
A9	1.17	0.08	1.10	0.09

SA values in the given Table 7.17 reveal that the effect of scaled geotextile is present at A8 and A9 under Düzce Earthquake. For both cases of reinforced and unreinforced embankment models (30°) , SA measurements of A2-A6 are very similar to A1, which measures the base excitation and there are only minor and ignorable differences in the measurements. A8 measured 1.10g of SA in the unreinforced case and 1.07g in the reinforced case. Also, A9 measured 1.17g and 1.10g in the unreinforced and reinforced cases respectively and the reinforcement reduced the SA values by 6%. On the other hand, the measured period values slightly increases due to the reinforcement. The period value measurements are determined as 0.08 seconds in the unreinforced case and 0.09 seconds in the reinforced case.

Table 7.18 shows the test results of unreinforced model under 0.3g of excitation and Table 7.19 gives the test results under the same dynamic load for the reinforced highway embakment model with 30° inclination.

Table 7.18. SA and T values of unreinforced embankment.

0.3G	2Hz		5Hz		7Hz		14Hz	
	SA (g)	T (s)	SA (g)	T (s)	SA (g)	T (s)	SA (g)	T (s)
A1	2.83	0.5	2.73	0.2	2.69	0.14	1.94	0.06
A2	2.82	0.5	2.70	0.2	2.85	0.14	1.86	0.06
A3	2.82	0.5	2.65	0.2	2.84	0.14	1.84	0.06
A4	2.83	0.5	2.65	0.2	2.85	0.14	1.85	0.06
A5	2.80	0.5	2.66	0.2	2.86	0.14	1.85	0.06
A6	2.81	0.5	3.70	0.2	3.69	0.14	1.86	0.06
A7	2.81	0.5	3.81	0.2	3.78	0.14	2.21	0.06
A8	2.83	0.5	3.84	0.2	3.83	0.14	2.40	0.06
A9	2.84	0.5	3.85	0.2	3.85	0.14	2.44	0.06

Table 7.19. SA and T values of reinforced embankment.

0.3G	2Hz		5Hz		7Hz		14Hz	
	SA (g)	T (s)	SA (g)	T (s)	SA (g)	T (s)	SA (g)	T (s)
A1	2.81	0.5	2.73	0.2	2.68	0.14	1.94	0.06
A2	2.82	0.5	2.68	0.2	2.84	0.14	1.86	0.06
A3	2.81	0.5	2.65	0.2	2.85	0.14	1.85	0.06
A4	2.81	0.5	2.64	0.2	2.86	0.14	1.84	0.06
A5	2.82	0.5	2.65	0.2	2.88	0.14	1.84	0.06
A6	2.81	0.5	2.65	0.2	2.85	0.14	1.86	0.06
A7	2.83	0.5	2.66	0.2	2.91	0.14	1.42	0.06
A8	2.50	0.5	2.15	0.2	2.21	0.14	0.61	0.06
A9	2.63	0.5	2.31	0.2	2.40	0.14	1.00	0.06

Table 7.18 and 7.19 show the SA values of the embankment models with 30° inclination under 0.3g of dynamic load with varying frequencies for the unreinforced and reinforced cases, respectively. Under 0.3g and 2Hz of dominant frequency, measurements of sensors A1-A7 are quite similar for both cases. The effect of reinforcement is apparent in the measurements of A8 and A9. A8 measured 2.83g and 2.50g of SA while A9 measured 2.84g and 2.63g of SA in the unreinforced and reinforced embankment models (30°), respectively. SA values decreased up to 12% and this reduction is concentrated at the upper parts of the model.

Under 0.3g and 5Hz of frequency, similar behavior trend is observed in the measurements of A1-A5. SA measurement of A6 is 3.70g in the unreinforced model and 2.65g in the reinforced model. Similarly A7 measured 3.81g and 2.66g in the

unreinforced and reinforced cases, respectively. The effect of reinforcement becomes more clear near the top of the model. A8 measured 3.84g and 2.15g and A9 measured 3.85g and 2.31g in the unreinforced and reinforced models, respectively. Under current dynamic loads, SA values decreased up to 44%.

Under 0.3g and 7Hz of frequency, SA measurements of A1-A5 are similar. The effect of reinforcement is present for the rest of the acceleration sensors located inside the embankment model around the reinforcement layers. SA measurement of A6 in the reinforced model reduced by 23% from 3.69g to 2.85g and the similar situation applies to the measurements of A7 too. A8 measurements decreased from 3.83g to 2.21g and A9 measurements also decreased from 3.85g to 2.40g. Under current excitations, observed reduction in SA values is up to 42%.

While A1-A6 measurements follow the same trend as previous cases, the effect of the reinforcement can be seen at A7, A8 and A9 in the model (30°) under 0.3g and 14Hz of frequency. SA values decreased from 2.21g to 1.42g at A7, from 2.40g to 0.61g at A8 and 2.44g to 1.00g at A9. The ratio of decrement in SA values is between 36% and up to 75% at A8 under current dynamic load.

Table 7.20 and Table 7.21 represents the test results of the model with 30° inclination under 0.5g of excitation for the unreinforced and reinforced cases, respectively.

Table 7.20. SA and T values of unreinforced embankment.

0.5G	2Hz		5Hz		7Hz		14Hz	
	SA (g)	T (s)	SA (g)	T (s)	SA (g)	T (s)	SA (g)	T (s)
A1	4.54	0.5	4.70	0.2	4.43	0.14	2.75	0.06
A2	4.52	0.5	4.70	0.2	4.42	0.14	2.94	0.06
A3	4.52	0.5	4.71	0.2	4.43	0.14	2.92	0.06
A4	4.53	0.5	4.71	0.2	4.46	0.14	2.91	0.06
A5	4.54	0.5	4.71	0.2	4.49	0.14	2.93	0.06
A6	4.54	0.5	6.14	0.2	5.84	0.14	3.38	0.06
A7	4.56	0.5	6.31	0.2	6.18	0.14	3.85	0.06
A8	4.57	0.5	6.38	0.2	6.49	0.14	4.44	0.06
A9	4.59	0.5	6.45	0.2	6.62	0.14	4.52	0.06

Table 7.21. SA and T values of reinforced embankment.

0.5G	2Hz		5Hz		7Hz		14Hz	
	SA (g)	T (s)	SA (g)	T (s)	SA (g)	T (s)	SA (g)	T (s)
A1	4.53	0.5	4.71	0.2	4.42	0.14	2.76	0.06
A2	4.56	0.5	4.70	0.2	4.43	0.14	2.92	0.06
A3	4.52	0.5	4.71	0.2	4.45	0.14	2.91	0.06
A4	4.58	0.5	4.71	0.2	4.48	0.14	2.91	0.06
A5	4.56	0.5	4.72	0.2	4.50	0.14	2.93	0.06
A6	4.57	0.5	4.69	0.2	4.46	0.14	2.94	0.06
A7	4.60	0.5	4.82	0.2	4.51	0.14	3.32	0.06
A8	3.09	0.5	3.23	0.2	3.20	0.14	1.91	0.06
A9	3.27	0.5	3.42	0.2	3.45	0.14	2.00	0.06

Given in Tables 7.20 and 7.21, under 0.5g with 2Hz of base excitation, for both cases, SA measurements inside the foundation soil is are similar and the differences in the values are neglectable. A7 measurements are close to each other for both cases with 4.56g and 4.60g. A8 measured 4.57g in the unreinforced case however in the reinforced case the SA measurement is 3.09g. And after the reinforcement, the SA values decreased from 4.59g to 3.27g. Under current dynamic load, the SA values are reduced up to 32% at A8.

Under 0.5g and 5Hz of base excitation, similar behavior trend is observed in the SA measurements of foundation soil. The reduction in SA values is concentrated near the top of the embankment model (30°). A7 measured 6.31g of SA in the unreinforced case and 4.82g in the reinforced case. Similarly A8 measured 6.38g of SA and 3.23g of SA in the unreinforced and reinforced cases, respectively. The SA measurements reduced by almost 50% at A8. And the measurements of A9 decreased from 6.45g to 3.42g due to the reinforcement. This time the reduction ratio is 47%.

Under 7Hz of motion, differences in measurements inside the foundation soil is neglectable. Due to the reinforcement effect, SA measurements of A7 went down from 6.18g to 4.51g, A8 measurements decreased from 6.49g to 3.20g and the measurement of A9 went down to 3.45g with a reduction of 48%.

Like the rest of the dynamic motions, under 14Hz of excitation, SA measurements inside the foundation soil is similar to the SA value of the base excitation

and the minor differences are neglectable. Reinforcement application reduced the measured SA values especially at A8 and A9. The measurements of A8 in the unreinforced case is 4.44g however due to the reinforcement, it is measured as 1.91g and the reduction ratio here is 57%. Also A9 measured 4.52g and 2.00g in the unreinforced and reinforced cases, respectively. This time the reduction ratio is 56%.

7.6.3. Evaluation of the Displacement-Time Histories Test Results

Following tables represent the measured displacement values of embankment model with 45° inclination. Table 7.22 shows the measured displacement values under Düzce Earthquake motions.

Table 7.22. Displacement values under scaled Düzce earthquke.

Displacement (cm)	Unreinforced	Reinforced
D1	0.98	0.98
D2	0.75	0.88
D3	0.97	0.90
D4	0.49	0.20

As can be seen in Table 7.22 above, Under scaled Düzce Earthquake record, the scaled geotextile reinforcement application was capable of mitigating the amount of measured displacement values except the toe of the embankment. The measurement of D2 increased slightly in the reinforced case. The measurement of D3 decreased from 0.97cm to 0.90cm and the settlement values decreased from 0.49cm to 0.20cm, which equals to a reduction of 59%. Table 7.23. gives the displacement values of unreinforced embankment model under 0.3g of excitation and Table 7.24. represents the displacement values of reinforced embankment model under 0.3g of excitation.

Table 7.23. Displacement values of unreinforced embankment under 0.3g of acceleration.

Displacement (cm)	2 Hz	5Hz	7 Hz	14 Hz
D1	3.50	0.70	0.38	0.05
D2	2.99	0.76	0.50	0.59
D3	2.63	0.71	0.45	0.26
D4	0.73	1.91	0.46	0.37

Table 7.24. Displacement Values of Reinforced Embankment under 0.3g of acceleration.

Displacement (cm)	2 Hz	5Hz	7 Hz	14 Hz
D1	3.30	0.67	0.34	0.04
D2	1.99	0.44	0.16	0.58
D3	1.72	1.23	0.38	0.85
D4	0.15	0.15	0.12	0.30

Displacement values of the unreinforced and reinforced model under 0.3g of motion are given in Tables 7.23 and 7.24. Under the ground motions of 0.3g of acceleration with 2Hz of frequency, D2 measured a displacement value of 2.99cm at the lower part of the unreinforced embankment model. The amount of displacement was measured as 1.99cm in the reinforced case. The reinforcement application could reduce the amount of displacement around 33%. Measurements of D3 represents the displacement values at the upper part of the embankments. In the unreinforced case, D3 measured 2.63cm of displacement. However, geotextile reinforcement significantly decreases the amount of displacement to 1.72cm which equals to a reduction of almost 35%. Settlement values of the embankment models are determined by the measurements of the displacement sensor of D4. Results reveal that geotextile reinforcement used in this experiment, mitigates the amount of settlement measured at the top of the embankment models. In the unreinforced case, D4 measured 0.73cm of displacement and with the effect of the scaled reinforcement, the same value was measured as 0.15cm with a reduction of almost 80%.

D2 measured 0.76cm of displacement at the toe of the unreinforced embankment under ground motions of 0.3g of acceleration with 5Hz of frequency. Measurement of D2 in the scaled geotextile reinforced embankment is 0.44cm. Displacement values reduced by 42% with reinforcement layers. The measurements of D3 in the unreinforced and scaled geotextile reinforced models are different than the general behaviour trend. Using the geotextile reinforcement, the displacement value is measured as 1.23cm however the same measurement is 0.71 cm in the unreinforced model. Settlement measurements by D4 are quite significant for the evaluation of the reinforcement effect. Under current ground excitations, 1.91cm of settlement value in the unreinforced case reduced by 92% to 0.15cm in the scaled geotextile case.

D2 measured 0.50cm of displacement in the unreinforced case however it was only 0.16cm in the scaled reinforcement. Geotextile reinforcement is very efficient because the amount of displacement was reduced by 68%. Under current ground motions, the displacement value of 0.45cm measured by D3 in the unreinforced embankment model went down to 0.38cm in the scaled geotextile model. D4 measured 0.46cm of settlement at the top of the unreinforced embankment while the same value is 0.12cm in the geotextile reinforced case. Geotextile reinforcement is very useful for settlement mitigation in this study. Settlements at the top of the embankment was reduced by 74%.

Under current dynamic loads, the effect of reinforcement is very limited on displacement values. D2 measured 0.59cm of displacement in the unreinforced case and 0.58cm in the geotextile reinforced case. The measurements of D3 is also different than the general trend. In the unreinforced case, the amount of displacement is 0.26cm while in the scaled geotextile case the same measurement is 0.85cm. Reinforcement application is very effective to minimize the settlement values at the top of the embankment models regardless of the input ground motion. The amount of settlement measured by D4 in the scaled geotextile reinforcement is 0.30cm which is 19% less when compared with the unreinforced case.

Table 7.25 and Table 7.26 shows the displacement values under 0.5g of excitation for unreinforced and reinforced embankment models with 45° inclination, respectively.

Table 7.25. Displacement values of unreinforced embankment under 0.5g of acceleration.

Displacement (cm)	**2 Hz**	**5Hz**	**7 Hz**	**14 Hz**
D1	3.49	0.70	0.39	0.05
D2	3.64	1.18	1.42	0.69
D3	4.09	1.29	0.88	0.57
D4	2.10	0.83	0.99	1.60

Table 7.26. Displacement values of reinforced embankment under 0.5g of acceleration.

Displacement (cm)	2 Hz	5Hz	7 Hz	14 Hz
D1	3.50	0.70	0.38	0.05
D2	2.99	0.76	0.50	0.59
D3	2.63	0.71	0.45	0.26
D4	0.73	1.91	0.46	0.37

As represented in Tables 7.25 and 7.26, under 0.5g of acceleration with 2Hz of frequency, the displacement value at the toe of the embankment (D2) was measured as 3,64cm in the unreinforced embankment model. On the other hand, the same measurement was 2.99cm in the reinforced case. Under current dynamic loads, D3 measured 4.09cm and 2.63cm of displacement in the unreinforced and reinforced cases, respectively. The geotextile reinforcement mitigated the amount of displacement value at the top of the embankment around 36%. The settlement measurements by D4 reveal that the reinforcement application reduced the total settlement at the top of the embankment by 65%. The settlement values decreased from 2.10cm to 0.73cm.

Under 0.5g of acceleration with 5Hz of frequency, D2 measurements decreased from 1,18cm to 0.76cm in the reinforced embankment models. Similarly the measurements of D3 reduced by 45%, measured 0.71cm in the reinforced case. However, under current ground motions, the settlement values were a bit increased when the embankment model was reinforced.

Under 0.5g of acceleration with 7Hz of frequency, the displacement value at the toe of the embankment decreased significantly. In the unreinforced case, D2 measured 1,42cm of displacement and due to the reinforcement effect, the same measurement reduced by 65% to 0.50cm. Similarly the measurements of D3 decreased from 0.88cm to 0.45cm in the reinforced embankment model. Also the amount of total settlement measured by D4 at the top of the embankment was 54% less in the scaled geotextile reinforced embankment model.

Under 0.5g of acceleration with 14Hz of frequency, D2 measured 0.69cm and 0.59cm of displacement in the unreinforced and reinforced models, respectively. The effect of reinforcement is more expressive at the top of the embankment model. The

measurement of D3 reduced by 55% in the reinforced case. Moreover, the scaled geotextile reinforcement impressively mitigates the settlement values. D4 measures 1,60cm of displacement in the unreinforced model and only 0.37cm in the reinforced model. Under current dynamic loads, the total settlement values reduced by 77%. Tables below represent the measured displacement values of embankment model with 30° inclination. Table 7.27 shows the measured displacement values under Düzce Earthquake motions.

Table 7.27. Displacement values under scaled Düzce earthquke.

Displacement (cm)	**Unreinforced**	**Reinforced**
D1	0.98	0.98
D2	0.52	0.48
D3	0.60	0.57
D4	0.31	0.14

Under scaled Düzce Earthquake excitations, the reinforcement application mitigated the amount of measured displacement values less rather than the rest of the motions. As given in Table 7.26, the measurement of D2 slightly decreased in the reinforced case from 0.52cm to 0.48cm. Similarly the measurement of D3 decreased from 0.60cm to 0.57cm and the settlement values decreased from 0.31cm to 0.14cm, which equals to a reduction of 55%.

Table 7.28. gives the displacement values of unreinforced embankment model under 0.3g of excitation and Table 7.29. represents the displacement values of reinforced embankment model under 0.3g of excitation.

Table 7.28. Displacement values of unreinforced embankment under 0.3g of acceleration.

Displacement (cm)	**2 Hz**	**5Hz**	**7 Hz**	**14 Hz**
D1	3.50	0.70	0.38	0.05
D2	1.47	0.39	0.24	0.39
D3	1.85	0.31	0.39	0.15
D4	0.48	0.96	0.32	0.20

Table 7.29. Displacement values of reinforced embankment under 0.3g of acceleration.

Displacement (cm)	2 Hz	5Hz	7 Hz	14 Hz
D1	3.30	0.67	0.34	0.04
D2	1.20	0.28	0.10	0.31
D3	1.02	0.30	0.22	0.55
D4	0.10	0.09	0.08	0.12

Tables 7.28 and 7.29 give the displacement values of unreinforced and reinforced model for the 0.3g of acceleration value. Under the ground motions of 0.3g of acceleration with 2Hz of frequency, D2 measured a displacement value of 1,47cm at the lower part of the unreinforced embankment model. The amount of displacement was measured as 1,20cm in the reinforced case. The reinforcement application could reduce the amount of displacement around 19%. The measurements of D3 represents the displacement values at the upper part of the embankments. In the unreinforced case, D3 measured. 1,85cm of displacement. However, geotextile reinforcement significantly decreases the amount of displacement to 1,02cm which equals to a reduction of almost 45%. Settlement values of the embankment models are determined by the measurements of the displacement sensor of D4. Results reveal that geotextile reinforcement used in this experiment, mitigates the amount of settlement measured at the top of the embankment models. In the unreinforced case, D4 measured 0.48cm of displacement and with the effect of the scaled reinforcement, the same value was measured as 0.10cm with a reduction of almost 80%.

D2 measured 0.39cm of displacement at the toe of the unreinforced embankment under ground motions of 0.3g of acceleration with 5Hz of frequency. Measurement of D2 in the scaled geotextile reinforced embankment is 0.28cm. Displacement values reduced by 28% with reinforcement layers. The measurements of D3 in the unreinforced and scaled geotextile reinforced models are almost equal to each other. Using the geotextile reinforcement, the displacement value is measured as 0.30cm however the same measurement is 0.31 cm in the unreinforced model. Settlement measurements by D4 are quite significant for the evaluation of the reinforcement effect. Under current ground excitations, 0.96cm of settlement value in the unreinforced case reduced by 91% to 0.09cm in the scaled geotextile case.

D2 measured 0.24cm of displacement in the unreinforced case however it was only 0.10cm in the scaled reinforcement. Geotextile reinforcement is very efficient because the amount of displacement was reduced by 59%. Under current ground motions, the displacement value of 0.39cm measured by D3 in the unreinforced embankment model went down to 0.22cm in the scaled geotextile model. D4 measured 0.32cm of settlement at the top of the unreinforced embankment while the same value is 0.08cm in the geotextile reinforced case. Geotextile reinforcement is very useful for settlement mitigation in this study. Settlements at the top of the embankment was reduced by 75%.

Under current dynamic loads, with the effect of the reinforcement D2 measured 0.39cm of displacement in the unreinforced case and 0.31cm in the geotextile reinforced case. The measurements of D3 is also different than the general trend. In the unreinforced case, the amount of displacement is 0.15cm while in the scaled geotextile case the same measurement is 0.55cm. Reinforcement application is very effective to minimize the settlement values at the top of the embankment models regardless of the input ground motion. The amount of settlement measured by D4 in the scaled geotextile reinforcement is 0.12cm which is 40% less when compared with the unreinforced case.

Table 7.30 and Table 7.31 shows the displacement values under 0.5g of excitation for unreinforced and reinforced embankment models, respectively.

Table 7.30. Displacement values of unreinforced embankment under 0.5g of acceleration.

Displacement (cm)	**2 Hz**	**5Hz**	**7 Hz**	**14 Hz**
D1	3.49	0.70	0.39	0.05
D2	2.12	0.87	0.30	0.41
D3	2.89	0.85	0.61	0.46
D4	1.64	0.58	0.49	1.03

Table 7.31. Displacement values of reinforced embankment under 0.5g of acceleration.

Displacement (cm)	**2 Hz**	**5Hz**	**7 Hz**	**14 Hz**
D1	3.50	0.70	0.38	0.05
D2	1.56	0.54	0.12	0.30
D3	2.01	0.42	0.24	0.21
D4	0.58	0.23	0.11	0.29

As can be seen in Tables 7.30 and 7.31, under 0.5g of acceleration with 2Hz of frequency, the displacement value at the toe of the embankment (D2) was measured as 2,12cm in the unreinforced embankment model. On the other hand, the same measurement was 1,56cm in the reinforced case. Under current dynamic loads, D3 measured 2,89cm and 2,01cm of displacement in the unreinforced and reinforced cases, respectively. The geotextile reinforcement mitigated the amount of displacement value at the top of the embankment around 31%. The settlement measurements by D4 reveal that the reinforcement application reduced the total settlement at the top of the embankment by 65%. The settlement values decreased from 1,64cm to 0.58cm.

Under 0.5g of acceleration with 5Hz of frequency, D2 measurements decreased from 0.87cm to 0.54cm in the reinforced embankment models. Similarly the measurements of D3 reduced by 51%, measured 0.42cm in the reinforced case. In addition, under current ground motions, the settlement values were decreased from 0.58cm to 0.23cm in the reinforced model and the reduction ratio is 60%.

Under 0.5g of acceleration with 7Hz of frequency, the displacement value at the toe of the embankment decreased significantly. In the unreinforced case, D2 measured 0.30cm of displacement and due to the reinforcement effect, the same measurement reduced by 60% to 0.12cm. Similarly the measurements of D3 decreased from 0.61cm to 0.24cm in the reinforced embankment model with a reduction ratio of 61%. Also the amount of total settlement measured by D4 at the top of the embankment was 78% less in the scaled geotextile reinforced embankment model.

Under 0.5g of acceleration with 14Hz of frequency, D2 measured 0.41cm and 0.30cm of displacement in the unreinforced and reinforced models, respectively. The effect of reinforcement is more clear at the top of the embankment model. The measurement of D3 reduced by 54% in the reinforced case. Moreover, the scaled geotextile reinforcement impressively mitigates the settlement values. D4 measures 1,03cm of displacement in the unreinforced model and only 0.29cm in the reinforced model. Under current dynamic loads, the total settlement values reduced by 72%.

Table 7.32. Evaluation of this study comparing the similar studies in the literature.

Reference	Aim of the Study	Test Type	Box Type	Box Dimensions	Slope Model	Materials	Seismic Loading	Improvement	Comments
El-Emam and Bathurst (2004, 2005, 2007)	The influence of reinforcement design parameters on the dynamic response of soil retaining walls	Shaking table	-	-	H:1m wall Scale: 1/6	Synthetic sand	Sinusoidal (0.05g-0.7g)	Geogrid reinforcement T_{ult}:12.5kN/m and 144kN/m	With the increase of reinforcement length, stiffness and number of layers, lateral displacements decreased.
Yoon *et al*., 2005	Evaluation of the feasibility of using tire shred-sand mixtures as fill material in slopes	Static Loading (Traffic load)	Field scale	-	Size: 2.1x20x17m	50%Sand-50%Tire shreds by volume	-	Tire shreds	Small values of settlement was observed, no evidence of self-heating.
Lin and Wang, 2006	Studying seismic slope behavior	Shaking table	Rigid	4.4x1.3x1.2m	Size: 0.5x1.3m Angle: 30° Scale: 1/20	Uniform medium sand	Up to 0.6g	Unreinforced	Model behaves elastically under 0.4g of acceleration. Soil amplification is observed. Failure surface was found to be shalow and circular.
Hazarika *et al*., 2008	Mitigation of earthquake hazards using scrap tire derived waste	Underwater shaking table	Rigid	4x1.25x1.5m	Scale: 1/10 scaled quay wall	Sohma sand No:5	Hyogo-ken Nanbu Earthquake	Tire chips cushion	The application is low cost, environmental friendly and provides good seismic performance.
Anastasopoulos *et al*., 2010	Determination of the experimental and theoretical seismic response of bar-mat retaining wall.	Shaking table	Rigid	160x90x75cm	Size: H: 49.8cm Scale: 1/20	Longstone sand	Lefkada 1973-2003 Earthquakes, Kalamata Earthquake, cos sweep T:0.4s-0.8s	Bar-mat	Under medium intensity ground motion the response is quasti-elastic, for stronger motions the deformations are plastic with large displacements.

Yang *et al*., 2011	Calculating FOS of GRS structures	Centrifuge	Plexiglas	-	Size: H:228mm	Monterey No: 30 sand	36g and 50g	Nonwoven Interface Fabric T_{ult}: 0.124kN/m	FOS>1.3 provides a good criteria that ensures the serviceability of slopes.
Yang *et al*., 2013	Amplification and deamplification studies on GRS structures.	Centrifuge	Rigid	-	Size: 160x367mm Angle: 45° and 63,5°	Fine quartz sand	0.01-0.11g	Non-woven geotextile T_{ult}: 62.5kN/m and 112kN/m	Amplification characteristics are affected from input ground motion, location and frequency.
Srilatha *et al*., 2013	The effect of base shaking frequency on the dynamic response of slopes.	Shaking table	Laminar	50x100x80cm	Size: 85x60cm Angle: 45° and 60°	Clayey sand	0.3g (2Hz, 5Hz and 7Hz)	Unreinforced and geogrid reinforcement	Amplification of acceleration is higher near the top. Displacement response increases with frequency of shaking.
Rajabian *et al*., 2013	The effect of anchored geosynthetics on dynamic response of slope models under seepage flow	Centrifuge	PMMA	76x20x41cm	Size: 24x37cm Angle: 63°	Sand&Clay mixture (4:1)	50g	Non-woven geotextile, geogrid, geocomposite	Improved performance, deeper failure surface, decreased settlement.
Akay *et al*., 2013	Geofoam block use for slope remediation under seepage flow	Seepage flow	Plexiglas	200x20x60cm	Size: 100x55x20cm	SP sand	-	Geofoam blocks	Geofoam block configurations were unstable against seepage flow.
Aklik and Wu, 2013	Determination of Failure mechanisms and characteristics of GRS models.	Centrifuge	Rigid	440x400x155mm	Size: H: 270mm Angle: 65°, 75°, 85°	Uniform coarse sand	-	Geotextile	The slope failure emerges from lower parts of the structure.
Hartman *et al*., 2013	Seismic response of geosynthetic reinforced wall with lightweight TDA backfill.	Shaking table	Rigid	150x187x180cm	Size: 150x120cm MSE wall Scale: 1/3	Tire derived sand	Lima Prieta Earthquake (0.54g original record, 1.62g scaled)	Geogrid reinforcement	Good performance with no significant settlement.

This study	Improving the seismic performance of highway embankments using geosynthetics.	Shaking table	Plexiglas	90x40x50cm	Size: 20x20cm Scale: 1/50	Silivri sand	Düzce Earthquake (NS), Sinusoidal 0.3g (2Hz, 5Hz, 7Hz, 14Hz), 0.5g (2Hz, 5Hz, 7Hz, 14Hz) a total of 40 cycle	Geotextile	Geotextile reinforced highway embankments perform better and remain stable under dynamic loads with reduced transmitted accelerations and settlements.

8. NUMERICAL STUDY

Numerical studies of the reinforced and unreinforced highway embankments under harmonic motions with different predominant frequency levels are performed using the finite element modelling software PLAXIS 2D 2012. PLAXIS is a multi-purpose finite element modelling program which enables to model various types of real geotechnical applications. The program was developed by geotechnical professionals in the Technical University of Delft after years of continious research supported by the Dutch government.

8.1. Modelling of Embankments

Embankments are modelled using PLAXIS 2D V.2012-2. Plane strain model is used for the geometries instead of axisymmetric model (Figure 8.1). Displacements and strains are assumed as zero in Z-direction.

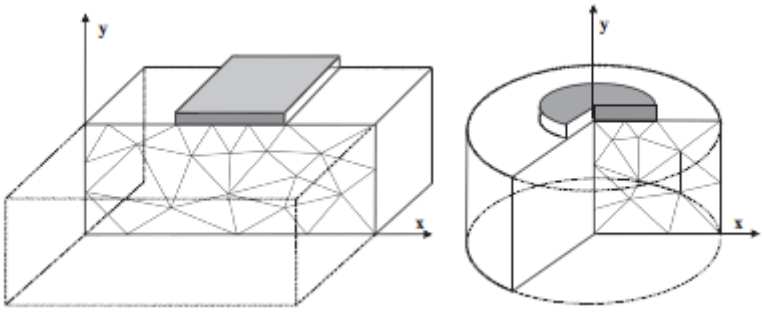

(a) (b)

Figure 8.1. (a) Plane strain model, (b) Axisymmetric model (Plaxis manual, 2012).

Finite element method is based on triangular shaped elements with nodes to solve engineering problems. PLAXIS program provides 6-node or 15-node triangular elements options. In this study 15-node triangle elements are selected as recommended in the manual. It provides very accurate and detailed stress results for complex problems. The comparison of the nodes and stress points of 6-node and 15-node models are represented below in Figure 8.2.

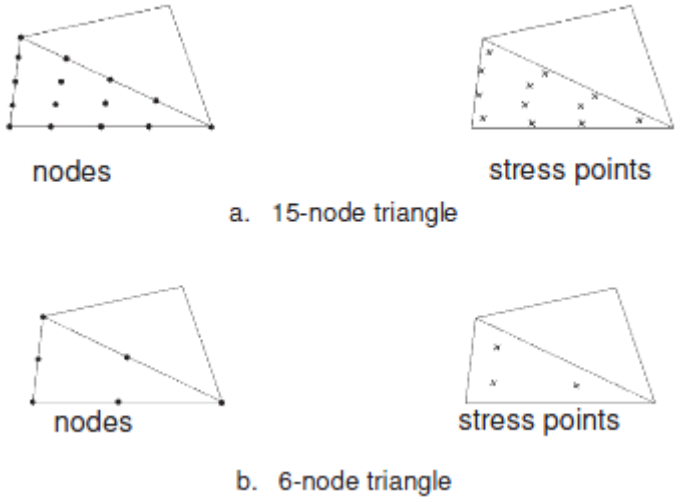

Figure 8.2. The comparison of 6-node and 15-node models.

The height of the embankment is H:5m and the width of the crest is L:20m. The inclination of 30° was chosen for the design. Since the embankment is symetric, only the right half of the structure is modelled.

8.2. Material Model and Material Details

Among a list of different material models, the hardening soil model was selected to define the material used for the model. The hardening soil model is an advanced model in order to simulate the behavior of different kinds of soils. PLAXIS Manual also suggests this material model for embankment related problems. The hardening soil model considers both shear hardening and compression hardening situations that is why it is also named as isotropic hardening. The material properties representing the highway embankment and the foundation soil are given in the following part.

8.2.1. Sand

Silivri Sand is used for modelling the embankment models. The material details are taken from previous studies with the same kind of sand. The foundation soil layer was modelled with a stiffer kind of sand material. Input parameters for Silivri Sand and the foundation soil are represented in Table 8.1, below.

Table 8.1. Input parameters of Silivri sand and foundation soil for hardening soil model.

Input Parameters	Embankment	Foundation Soil
γ_{unsat}	16.5kN/m^3	17kN/m^3
c'_{ref}	1.75kN/m^2	-
Ø	33°	33°
ψ	3°	3°
E_{50}^{ref}	20000kN/m^2	35000kN/m^2
E_{oed}^{ref}	20000kN/m^2	35000kN/m^2
E_{ur}^{ref}	60000kN/m^2	105000kN/m^2

8.2.2. Geotextile

Geotextile reinforcement is used for the numerical models. PLAXIS considers the axial stiffness (EA) instead of tensile strength for elastic behavior of geosynthetics. The rigidity parameter of EA:8750kN/m is used for the geotextile material in the experiments.

8.3. Modeling Details

As mentioned above, the analysed embankment has 5m of height and 20m of width and using the geometry line button on PLAXIS, right half of the embankment is drawn with the desired inclination. These are common steps for all model cases. The appearance and the dimensions of the embankment model is represented in Figure 8.3.

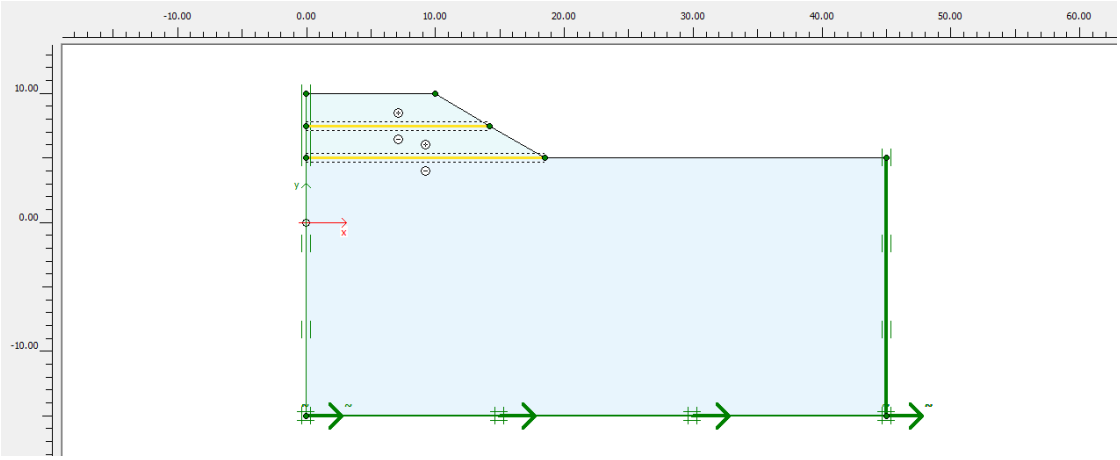

Figure 8.3. The appearance and the dimensions of the model.

8.3.1. Unreinforced Embankment

No geotextile reinforcement is used for this case. Results of the unreinforced embankment case will be used to evaluate the effectiveness of the reinforcement.

After the model layout is completed, “Standart Fixities” is selected on the program interface in order to impose general boundary conditions to the geometry model. After the previously defined material model is assigned to the clusters of the model, the finite element mesh must be generated for calculations. A composition of the triangular elements with nodes is called mesh in finite element analysis. The coarseness of the mesh is automatically defined by PLAXIS in version 2012. The generated mesh for unreinforced embankment model is represented in Figure 8.4.

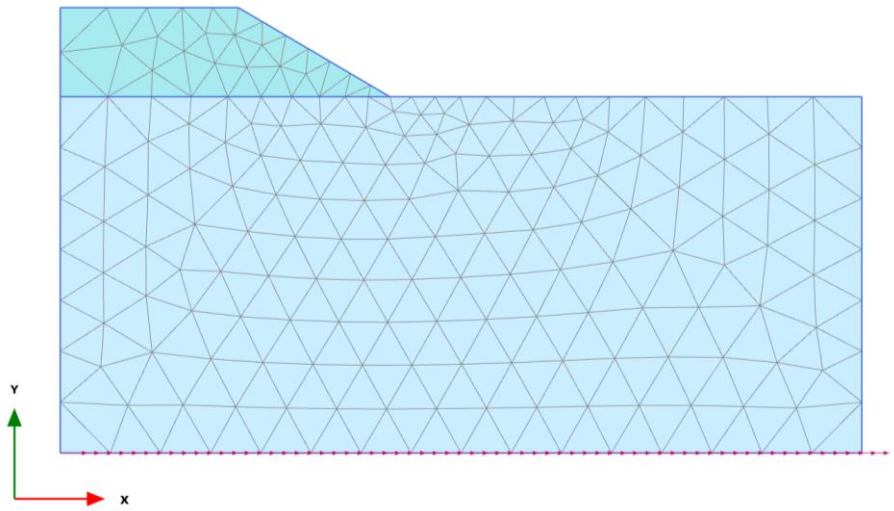

Figure 8.4. The generated mesh for unreinforced embankment.

8.3.2. Reinforced Embankment

Geosynthetic reinforcement is used in order to make the highway embankments more stable under static and dynamic forces. The same procedure which has been followed for unreinforced embankments is also followed for generating the reinforced embankment models. The only difference is the placement of the reinforcement layers at the bottom of the embankment over the foundation soil. Generated mesh for geotextile reinforced embankment can be seen in Figure 8.5, below.

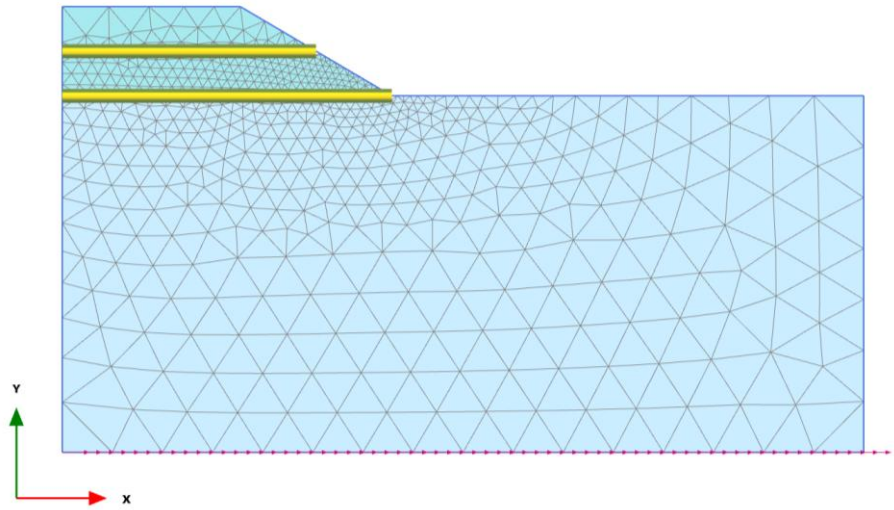

Figure 8.5. Generated mesh for geosynthetic reinforced embankment model.

8.4. Dynamic Analysis

Soils and structures are not only subjected to static loads but also dynamic loads such as earthquakes. And if the shaking of the ground is strong enough, the situation may cause severe damages. With the help of the PLAXIS dynamics module, it is possible to analyse the the effects of the dynamic loads in the soil and structures on it.

Modelling of boundaries is important in dynamics module. When a dynamic load is defined to the model, it is possible to observe spurious wave reflections at the boundaries of the models due to the reflection at the boundaries. To get rid of this situation, special considerations should be taken into account. First of all the boundaries of the model must be sufficiently far away from the region of interest and secondly absorbent boundaries must be defined to the edges of the finite element model except to the axis of symmetry line. In PLAXIS dynamic module, earthquakes are introduced to the model using prescribed displacements tool. In PLAXIS 2D 2012-2 version, using the standart earthquake boundaries tool, prescribed displacement is defined to the model automatically (PLAXIS Manual, 2012).

Selected dynamic loads which were previously defined in the experimental study are also used as an input in the finite element analysis. For the comparison of the experimental and numerical results, four different dynamic motions with the same

amplitude of 0.3g with different predominant frequencies of 2Hz, 5Hz, 7Hz and 14Hz was selected and used as input motions during the dynamic finite element analysis. The amplitude of the motions were selected intentionally considering that the majority of the strong earthquakes occured in Turkey and all around the world have a PGA value around 0.3g.

This section of the thesis includes the results of the dynamic finite element analysis of the embankment models with 30° inclination in the prototype scale. During the analysis vertical displacements and acceleration measurements of the selected important points corresponding to the locations of the accelerometers A6, A7, A8 and A9 in shaking table tests are determined in order to express the dynamic behaviour of the prototype embankment. In order to prevent any confusion, the location of the accelerometers A6, A7, A8, A9 in shaking table tests (Figure 7.10), which corresponds to the same locations in numerical analysis, are defined as P6, P7, P8 and P9.

8.4.1. Numerical Analysis of Embankment Models under 2Hz of Motion

For the analysis under 40 cycles of sinusoidal motion with 2Hz of predominant frequency, the time interval was set to 22s and additional steps and dynamic sub steps are defined by PLAXIS dynamic module.

Under current motion, P6 measurement is 0.27g in the unreinforced model and it is a bit lower than the PGA of the input motion which is 0.30g. P7, P8 and P9 measured 0.35g, 0.40g and 0.40g respectively. In the reinforced embankment models, these measurements decreases due to the applied geosynthetics at the bottom and inside the embankment model. The measurement of P6 with 0.28g is very similar to the measurement in the unreinforced case. P7 and P8 measured 0.27g of acceleration while A9 measured 0.26g. Also, vertical displacement values at the top of the model decreases from 32cm to 12.8cm in the reinforced model. Figure 8.6 shows the vertical displacement shadings of the unreinforced and reinforced embankment models under current dynamic motions.

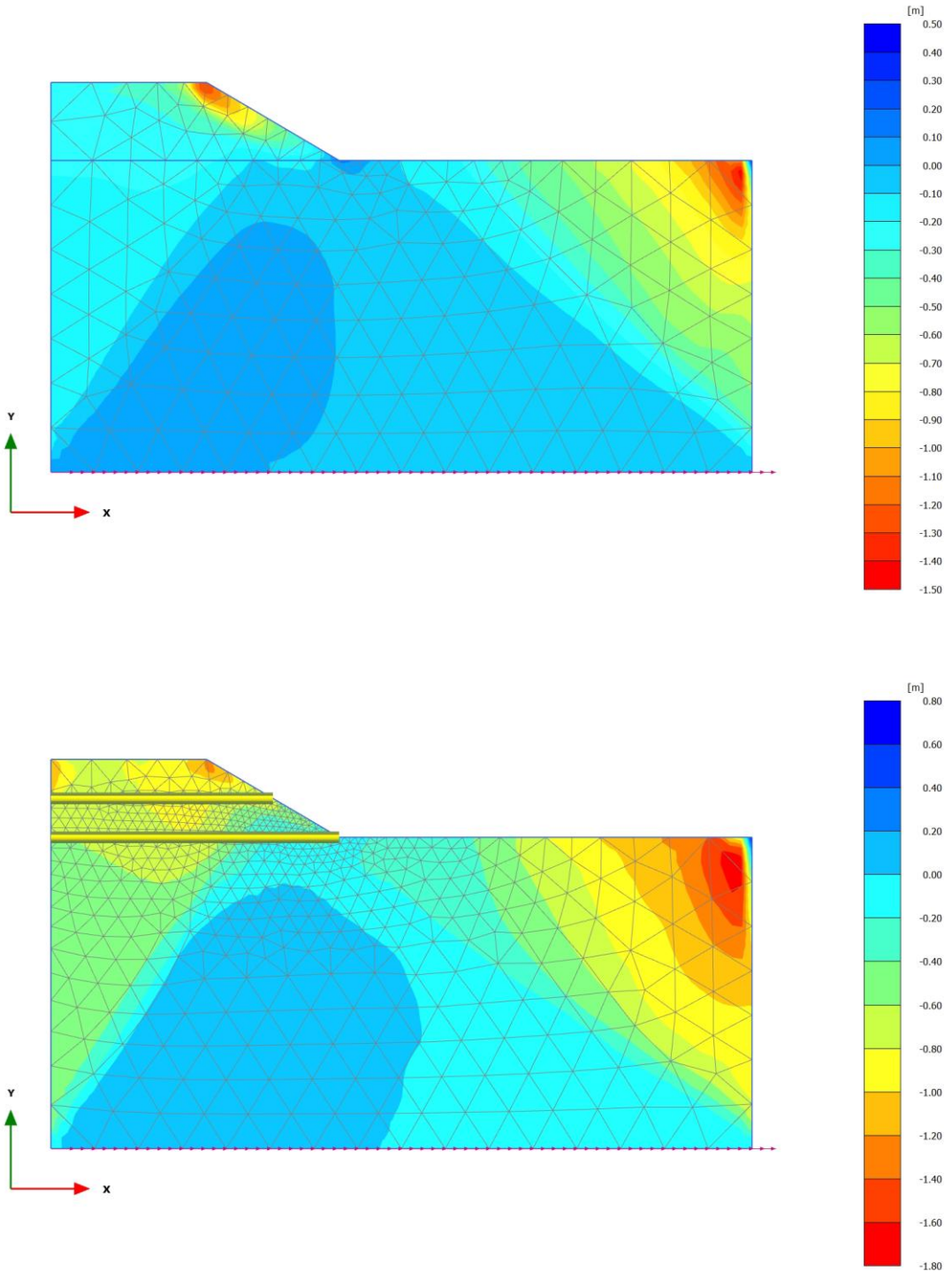

Figure 8.6. Vertical displacement shadings for unreinforced and reinforced models under 0.3g acceleration with 2Hz of frequency.

8.4.2. Numerical Analysis of Embankment Models under 5Hz of Motion

During the analysis with the given input, time interval of the analysis is set to 10s and additional steps and dynamic sub steps are defined by PLAXIS dynamic module. The total number of cycles is set to 40.

The measurements at P6 are generally stable and very close to the PGA of the input. Under current ground motions, 0.29g and 0.27g was measured at A6 in the unreinforced and reinforced models, respectively. The acceleration measurement at P7 was 0.41g in the unreinforced case, and due to the increasing height P8 and P9 give higher acceleration values with 0.43g and 0.50g. However due to the inclusion of reinforcement P7, P8 and P9 measured 0.27g, 0.23g and 0.22g, respectively. In addition, vertical displacement measurements at the top of the embankment model was decreased from 10.1cm to 5.8cm. Figure 8.7 shows the vertical displacement shadings of the unreinforced and reinforced embankment models under current dynamic motions.

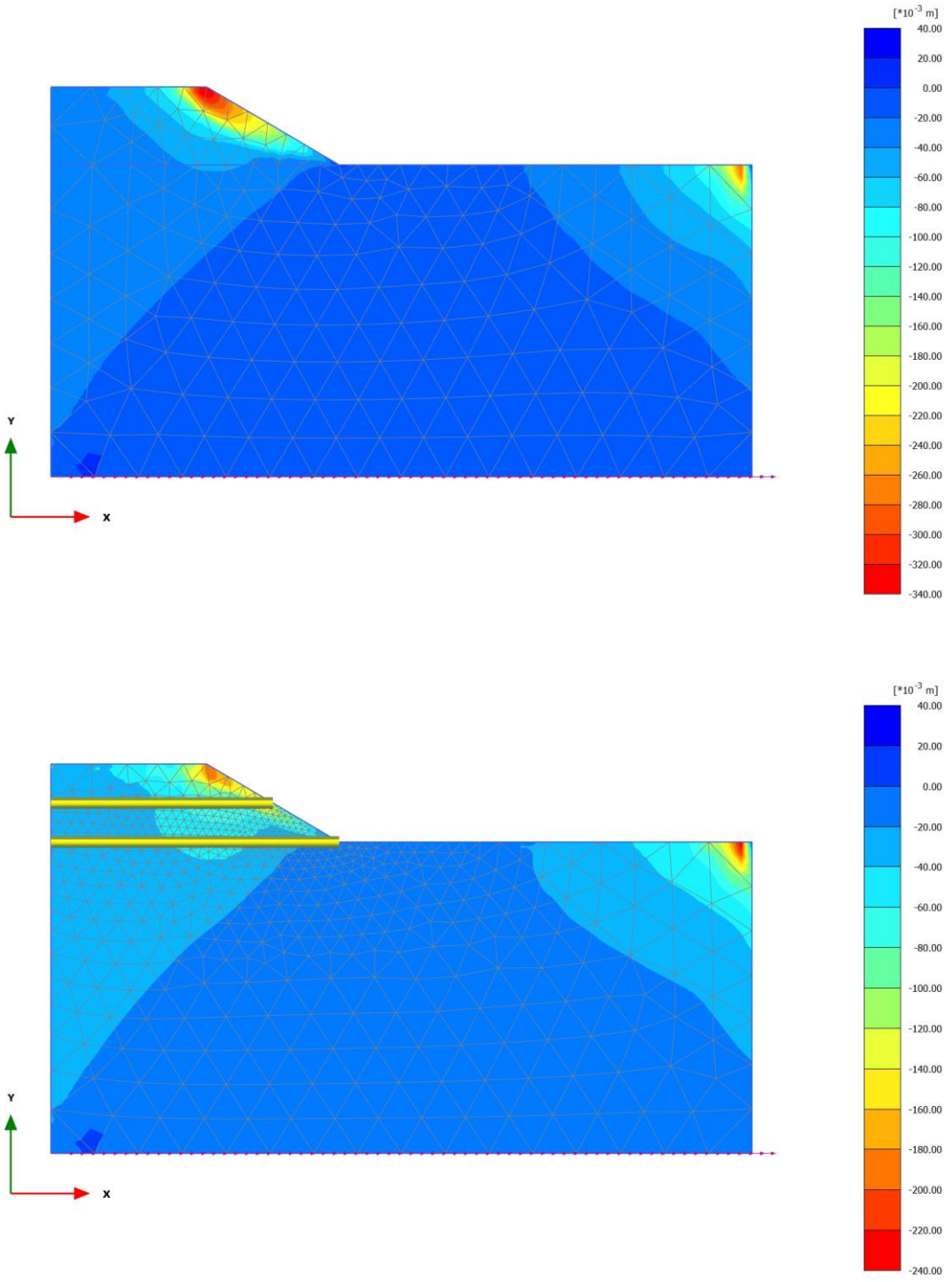

Figure 8.7. Vertical displacement shadings for unreinforced and reinforced models under 0.3g acceleration with 5Hz of frequency.

8.4.3. Numerical Analysis of Embankment Models under 7Hz of Motion

Under 7Hz of dynamic motion case, time interval of the analysis is set to 7s and additional steps and dynamic sub steps are auto-defined by PLAXIS dynamic module. The total number of cycles are fixed at 40.

Similar to recent cases, P6 provides similar measurements without reflecting the reinforcement effect. In the unreinforced embankment model, the acceleration measurement at P6 was 0.28g which is exactly the same value as it is in the reinforced case. P7 measurements decreased from 0.28g to 0.25g due to the reinforcement just like the acceleration measurements of P8 whose measurements decreased from 0.35g to 0.24g. P9 defines a point above the second reinforcement layer and it is seen that the acceleration measurements also decreases from 0.40g to 0.25g under current ground excitations. The vertical displacement measurement in the unreinforced model is 8.4cm. It is observed that, after two layers of geotextile layers are applied to the embankment model the vertical displacement measurements at the top of the embankment model was significantly decreased to 3.8cm. Figure 8.8 shows the vertical displacement shadings of the unreinforced and reinforced embankment models under current dynamic motions.

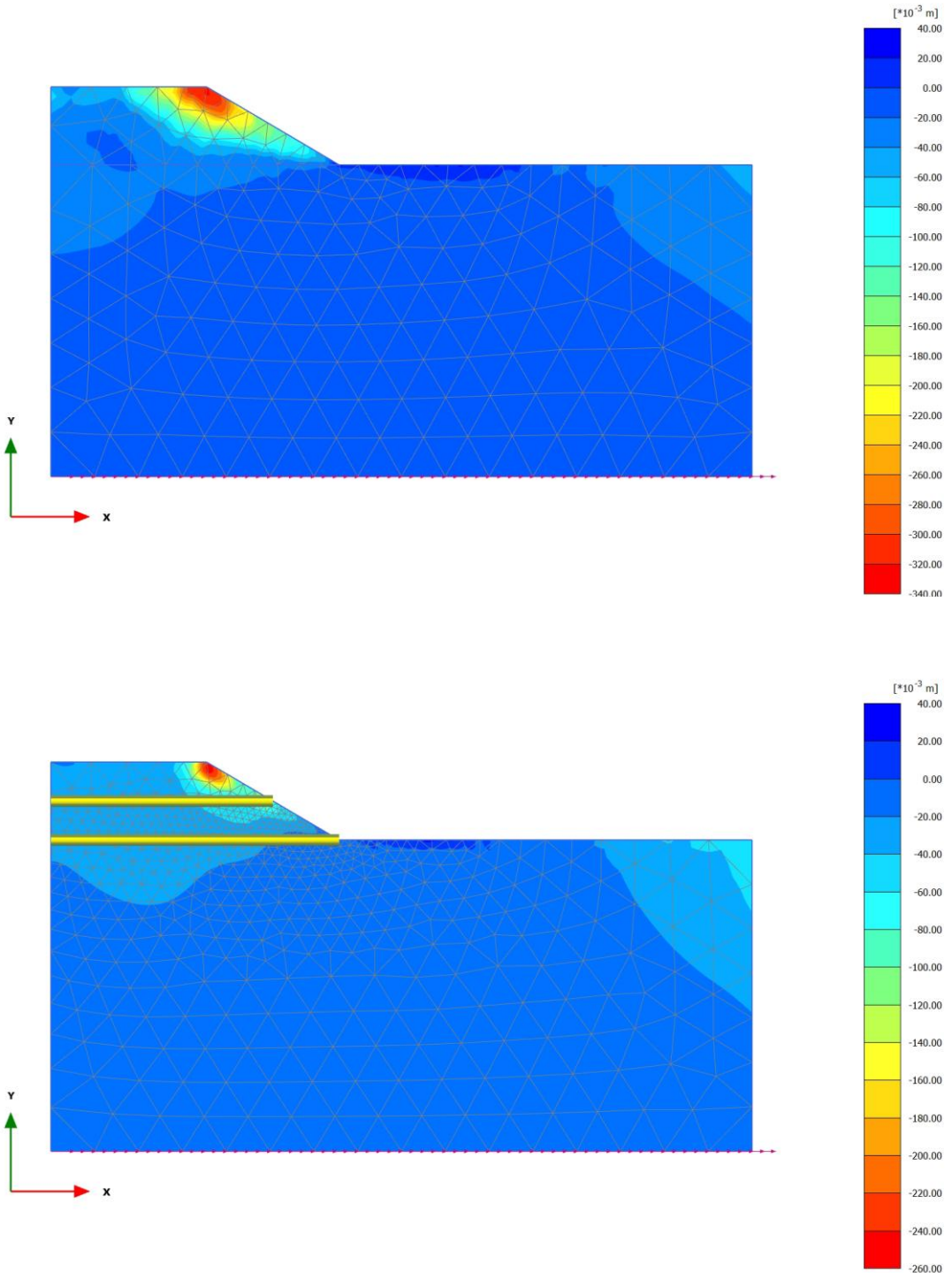

Figure 8.8. Vertical displacement shadings for unreinforced and reinforced models under 0.3g acceleration with 7Hz of frequency.

8.4.4. Numerical Analysis of Embankment Models under 14Hz of Motion

Before starting the calculation process, time interval of the analysis is set to 3.5s for the current motion and additional steps and dynamic sub steps are automatically defined by PLAXIS dynamic module. 40 cycle of motion was subjected to the embankment models.

P6 measured 0.30g and 0.28g in the unreinforced and reinforced cases, respectively. Beneath the first reinforcement layer, the measurements at P7 are decreased from 0.33g to 0.25g in the reinforced case. PGA measurement at P8 in the unreinforced model is 0.45g. However, in the reinforced model under the same excitation, the PGA measurement at P9 was impressively decreased from 0.46g to 0.24g. On the other hand, 2.1cm of settlement value at the top of the model in the unreinforced case was decreased to 1.8cm in the reinforced case. Figure 8.9 shows the vertical displacement shadings of the unreinforced and reinforced embankment models under current dynamic motions.

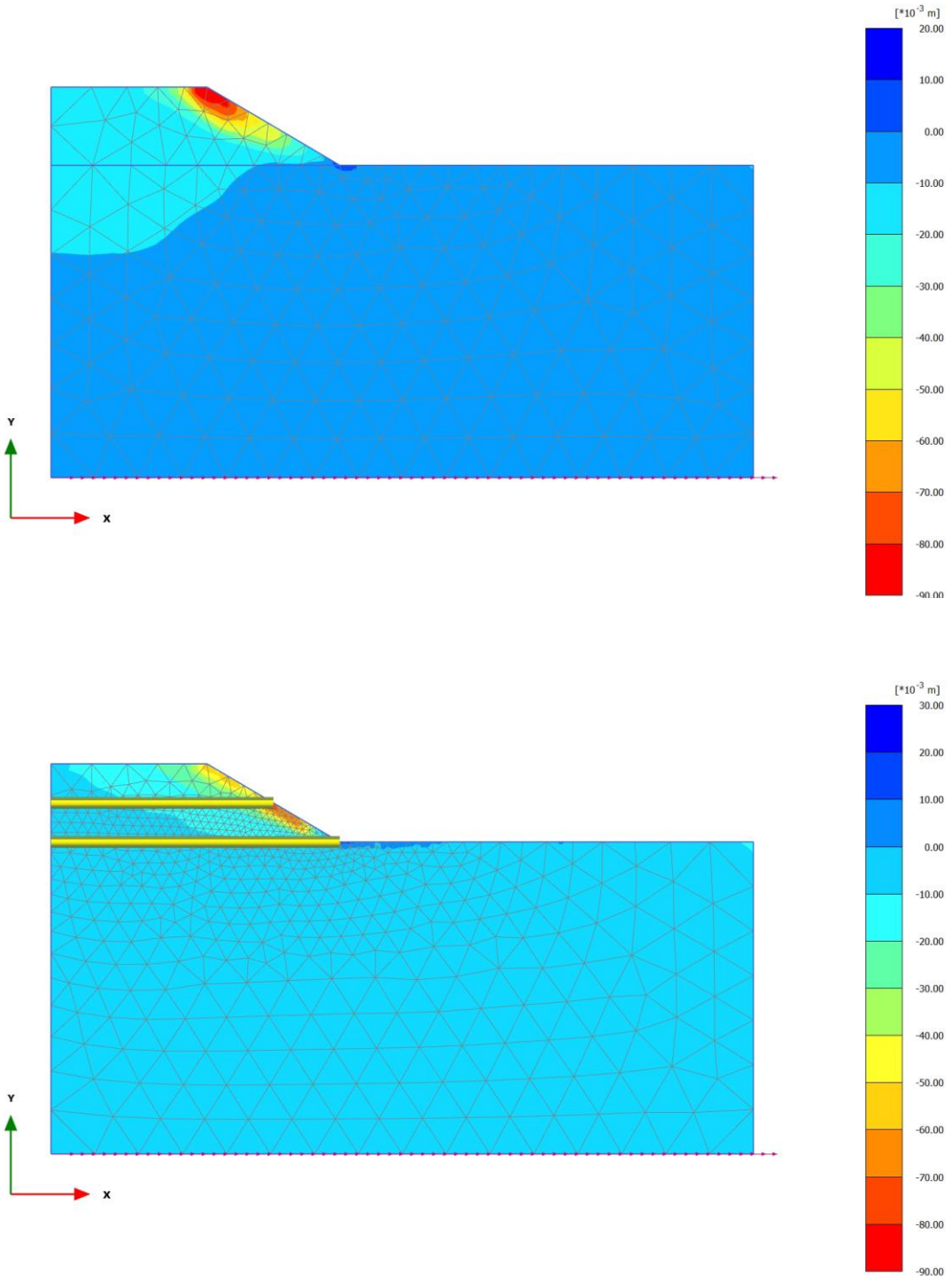

Figure 8.9. Vertical displacement shadings for unreinforced and reinforced models under 0.3g acceleration with 14Hz of frequency.

Results of the study are tabulated for a better and easy comparison and evaluation. Maximum value of the settlement values of the numerical study are represented in Table 8.2 and the acceleration measurements for the important locations are given in Table 8.3.

Table 8.2. Maximum value of the settlements.

Settlements (cm)		**Unreinforced Model**	**Reinforced Model**
0.3g	*2Hz*	32	12.8
	5Hz	10.1	5.8
	7Hz	8.4	3.8
	14Hz	2.1	1.8

Table 8.3. PGA measurements of P6 - P9.

Peak Ground Accelerations (g)		**Unreinforced Model**				**Reinforced Model**			
		P6	**P7**	**P8**	**P9**	**P6**	**P7**	**P8**	**P9**
0.3g	*2Hz*	0.27	0.35	0.40	0.40	0.28	0.27	0.27	0.26
	5Hz	0.29	0.41	0.43	0.50	0.27	0.27	0.23	0.22
	7Hz	0.28	0.28	0.35	0.40	0.28	0.25	0.24	0.25
	14Hz	0.30	0.33	0.45	0.46	0.28	0.25	0.23	0.24

8.5. Evaluation of the Results

The test results of the numerical analysis were evaluated in detail for all considered cases in this section of the thesis.

The measurements at P6, which corresponds to the location of A6 in experimental tests, are quite similar to each other under any ground excitation and regardless of the reinforcement. All acceleration measurements at P6 are around 0.3g, just as the PGA of the inputs. It is possible to say that P6 measurements don't express the effect of reinforcement in embankment models.

The measurements at P7 express the likely dynamic behavior of the model right under the first geotextile layer. It is obtained that P7 measurements are in the range of 0.28g to 0.41g in the unreinforced model however in the reinforced case, the range is only between 0.25g to 0.27g. It is seen that as a result of the reinforcement, acceleration measurements at P7 are reduced under all considered dynamic motions. As can be seen in Table 8.3, the reduction of the PGA values are concentrated under 2Hz and 5Hz of motions and the maximum reduction ratio in the reinforced case is determined as 34% under 5Hz of motion.

P8 is located between two geosynthetic layers. Increased height inside the embankment model results higher PGA measurements. In the unreinforced models, PGA measurements at P8 are between 0.35g to 0.45g under different frequency ranges. It can be seen that, reduction ratios in PGA measurements are increasing towards to the crest of the embankment. In other words, reduction ratios are much higher at the crest than the toe of the embankment. PGA measurements in the reinforced model are lower than the input PGA level and it is in the range of 0.23g to 0.27g. The maximum reduction ratio due to the geosynthetic reinforcement under current motion is 48.9%.

As can be seen in Table 8.3, the PGA measurements at P9 are observed to be in the range of 0.40g to 0.50g under four different motion in the unreinforced model. As P9 is located above the second reinforcement layer, which is the highest location for measurements, the range of the PGA values are higher than other points. Due to the

reinforcement, all PGA measurements are effectively decreased to a range of 0.22g to 0.26g. Again, the effectiveness of the geosynthetic reinforcement is at its best under 5Hz of motion. The maximum reduction ratio of PGA measurements is 56%. AF values are also calculated for P9 measurements. In the unreinforced embankement model, AF values are in the range of 1.33 (2Hz and 7Hz) and 1.67 (5Hz). Due to the inclusion of geosynthetic layers, AF values are reduced to be in the range of 0.73 (5Hz) and 0.87 (2Hz).

The evaluation of the vertical displacement measurements at the top of the embankment models reveal that higher frequency motions cause less settlement values. As can be seen in Table 8.2, settlement values under 2Hz of motion are at least ten times higher than the measurements under 14Hz of motion.

Under 2Hz of harmonic motion, 32cm of vertical displacement in the unreinforced case decreases to 12.8cm after geosynthetic application. Although the settlement values of both unreinforced and reinforced models decrease with the increased frequency ranges, reduction ratios of settlement measurements in reinforced models are higher in low frequency ranges. Under 2 Hz of motion the reduction ratio is 60%, however under 5Hz of motion, 10.1cm of vertical displacement measurement goes down to 5.8cm with a reduction ratio of 42.6%. Similarly 2.1cm of settlement decreases to 1.8cm under 14Hz of motion and the reduction ratio is only around 15%.

Another important point that should be noted is related with the distribution of the vertical displacements within the embankment model. Dynamic finite element analysis with different predominant frequencies reveal that vertical displacement distribution is concentrated near the crest under low predominant frequency of motions and the opposite situation applies to the toe of the embankments. As can be seen in Figure 8.6, displacement distribution is concentrated at the crest of the embankment under 2Hz of motion. However, Figure 8.9 reveals that the displacements due to the dynamic motions of 14Hz of frequency are around the toe.

9. CONCLUSIONS

Seismic behavior of 1/50 scaled unreinforced and reinforced highway embankment models were investigated using shaking table test facilities at Bogazici University. Experiments were performed in a designed plexiglas soil container under nine different dynamic motions including a time scaled real earthquake record and eight sinusoidal waves with two amplitudes and four predominant frequencies. Also finite element model was created for the prototype scale and the following conclusions are reached as follows:

1. The geosynthetic reinforcement application is capable of reducing the transmitted acceleration values up to 56% in the embankment model with 45° slope angle and up to 55% in the model with 30° slope angle in the shaking table tests. The reduction ratio is so much higher near the crest of the embankments.

2. The effect of reinforcement is better observed under 5Hz and 7Hz of frequencies.

3. For both slope inclinations, the reinforcement effect on the reduction of measured acceleration values are relatively low under time scaled Düzce Earthquake motions. Up to 13% and 10% reduction is observed in the models with 45° and 30° inclination, respectively.

4. Observed failure surfaces are shallow and likely to be circular both in the shaking table experiments and the finite element models.

5. The effect of slope inclination on the AF values are restricted. But it is possible to say that, AF values are slightly higher for the steeper embankment slope.

6. Response spectrums indicate that SA values are higher in the unreinforced model. Also, SA values tend to increase in higher frequency motions but this not always the case.

7. Observed SA values reveal that the reinforcement material is the most effective under 14Hz of frequency and when the current dynamic load is subjected to the models, SA values decrease up to 78%. The geosynthetic material is the least effective under scaled earthquake record and 2Hz of frequency.

8. Embankment models of both slope inclinations express no significant difference in dynamic behavior by means of SA.

9. Geotextile reinforcement application is quite effective to reduce earthquake induced settlement. Under 5Hz of frequency, vertical displacement values reduced by more than 90% for both embankment slope inclinations.

10. Displacement values occasionally decrease with the increasing frequency and slope angle. Also, the increasing frequency levels cause higher amounts of horizontal displacement at the toe and top of the embankment except 14Hz of motion case for both slope inclinations.

11. By means of amplitude in experimental tests, 0.5g presents lower AF values than 0.3g. In addition, AF value reduction is higher under 5Hz and 7Hz of motion for both amplitudes. In numerical simulation studies, it is also observed that the maximum AF reduction occurs under 5Hz of harmonic motion.

12. In the numerical study, the effect of reinforcement can be clearly seen under 2Hz of harmonic motion by means of vertical displacements. The maximum value of the vertical displacements were reduced by up to 60% under 2Hz of motion.

13. The effect of reinforcement is better observed around the crest of the embankment models. In numerical analysis, the maximum reduction ratio of the

transmitted PGA values is 56% at P9 (crest), however, the same reduction ratio is observed to be 34% at the toe of the embankment model.

14. It is observed that the effect of geosynthetic reinforcement is well observed under 5Hz of frequency with regards to numerical analysis.

15. It is found that experimental results and numerical results are comparable in some cases but generally similar to each other.

As a summary, experimental study and numerical simulations reveal that geosynthetics are preferable materials with good vibration absorbtion properties. Geosynthetics can successfully mitigate the earthquake hazards and earthquake induced damages. It is understood that geotextile reinforced highway embankments perform better and remain stable during dynamic loads. Highways are essential lifelines that should be in operation after disasterous events. For that reason, during and after earthquakes highways and highway embankments should be stable enough to provide required safety and emergency needs.

REFERENCES

Abramson, L. W., T. S. Lee, S. Sharma, G.M. Boyce, 2002, *Slope Stability and Stabilization Methods*, John Wiley&Sons, Inc, New York, USA.

Akay, O., A. T. Özer, G. A. Fox, S.F. Bartlett, D. Arellano, 2013, "Behavior of Sandy Slopes Remediated by EPS-Block Geofoam under Seepage Flow", *Geotextiles and Geomembranes,* Vol. 37, pp. 81-98.

Bathurst, R. J., M. El-Emam, M. M. Mashhour, 2002, "Shaking Table Model Study on the Dynamic Response of Reinforced Soil Walls", *Proceedings of the 7th International Geosynthetics Conference*, Nice, France, 22-27 September 2002. Balkema, Lisse, The Netherlands, Vol. 1, pp. 99-102.

Brinkgreve, R. B. J., E. Engin, Swolfs W. M., 2014, *User's Manual for PLAXIS* Delft, Netherlands.

Çağatay, A., 2008, *Investigation of the Effect of Tire Waste Inlusions on the Shear Strength Parameters of Sand*, M.Sc. Thesis, Boğaziçi University.

Day, R. W., 2002, *Geotechnical Earthquake Engineering Handbook*, McGRAW-HILL.

Duncan, J. M., S. G. Wright, 2005, *Soil Strenght and Soil Slope Stability*, John Wiley&Sons, Inc, New York, USA.

Edinçliler, A., 2007, "Using waste tire–soil mixtures for embankment construction", *International Workshop on Scrap Tire Derived Geomaterials ''Opportunities and Challenges"*. Kanto Branch of Japanese Geotechnical Society, pp. 319–328.

Edinçliler, A., G. Baykal and A. Saygılı, 2010, "Influence of different processing techniques on the mechanical properties of used tires in embankment construction", *Waste Management, Waste Management,* Vol. 30, pp.1073–1080.

El-Emam, M. E., R. J. Bathurst, 2004, "Experimental design, instrumentation and interpretation of reinforced soil wall response using a shaking table", *International Journal of Physical Modelling in Geotecnics*, Vol. 4, pp. 13-32.

El-Emam, M. E., R. J. Bathurst, 2007, "Influence of reinforcement parameters on the seismic response of reduced-scale reinforced soil retaining walls", *Geotextiles and Geomembranes,* Vol. 25, pp. 33-49.

Environmental Protection Agency (US), 2002, *Secondary Drinking Water Regulations: Guidance for Nuisance Chemicals*.

Federal Highway Administration (FHWA), 2009, *Design and Construction of Mechanically Stabilized Earth Walls and Reinforced Soil Slopes,* Publication No. FHWA-NHI-09-083.

Hartman, D., M. Ledezma, M. Xiao, M. Zoghi, 2013, "Shake Table Test of MSE Wall with Tire Derived Aggregerates (TDA) Backfill", *Geo-Congress*, pp. 1168-1177.

Hazarika, H., E. Kohama, and T. Sugano, 2008, "Shaking Table Tests on Waterfront Structures Protected with Tire chips Cushion", *Journal of Geotechnical and Environmental Engineering*, ASCE, pp.134-11.

Hazarika, H., S. Okuzono, Y. Matsuo, 2003, "Seismic stability enhancement of rigid nonyielding structures", *Proceedings of the 13th International Offshore and Polar Engineering Conference*, Honolulu, HI, USA, 25–30 May 2003, pp. 1244–1249.

Huang, C. C., J. C. Horng, W. J. Chang, J. S. Chiou, C. H. Chen, 2011, "Dynamic behaviour of reinforced walls - Horizontal displacement response", *Geotextiles and Geomembranes*, Vol. 29, pp. 257-267.

Humphrey, D. N., 1996, *Invertigation of Exothermic Reaction in Tire Shred Fill Located on SR 100 in Ilwaco, Washington*, Consulting Report to FHWA, US Department of Transportation.

Iai, S., 1989, "Similitude for shaking table tests on soil-structurefluid models in 1-g gravitational field", *Soils and Foundations*, Vol. 29, No.1, pp. 105-118.

Koerner, R. M., 2005, *Designing with Geosynthetics*, Pearson Education, Inc, Upper Saddle River, NJ, USA.

Lin, M. L., K. L. Wang, 2006, "Seismic behavior in a large-scale shaking table test", *Engineering Geology*, Vol. 86, pp. 118-133.

Ling, H. I., M. H. Wu, D. Leshchinsky, B. Leshchinsky, 2009, "Centrifuge Modelling of Slope Instability", *Journal of Geotechnical and Geoenvironmental Engineering*, Vol. 135, 758-767.

Lo Grasso, A. S., M. Maugeri, P. Recalcati, 2005, "Seismic Behavior of Geosynthetic Reinforced Slopes with Overload by Shaking Table Tests", *Slopes and Retaining Structures under Static and Seismic Conditions*, ASCE Geotechnical Special Publication No. 140, CDROM.

Perez, A., R. D. Holtz, 2004, "Seismic Response of Reinforced Steep Soil Slopes: Results of Shaking Table Study", *Geotechnical Engineering for Transportation Projects*, ASCE Geotechnical Special Publication No. 126, pp. 1664-1672.

Rajabian, A., H. Ghiassian, B. V. S. Viswanadham, 2013, "Centrifuge study of anchored geosynthetic slopes", *Geosynthetics International*, 20, No.3.

Srilatha, N., G. Madhavi Latha, C. G. Puttappa, 2013, "Effect of frequency on seismic response of reinforced soil slopes in shaking table tests", *Geotextiles and Geomembranes*, Vol. 36, pp. 27-32.

Tamate, S., N. Suemasa, T. Katada, 2012, "Simulation of Precipitation on Centrifuge Models of Slopes", *International Journal of Physical Modelling in Geotechnics*, Vol. 12, pp. 89-101.

Taylor, C. A., A. R. Dar, A. J. Crewe, 1996, "Shaking Table Modelling of Seismic Geotechnical Problems", *Earthquake Engineering Research Centre*, University of Bristol, UK.

Towhata, I., 2008, *Geotechnical Earthquake Engineering*, Springer, Verlag Berlin Hiedelberg, Germany.

Viswanadham, B. V. S., D. König, 2009, "Centrifuge Modelling of Geotextile Reinforced Slopes Subjected to Differential Settlements", *Geotextiles and Geomembranes*, Vol. 27, pp. 77-88.

Wartman, J., R. B. Seed, J. D. Bray, 2005, "Shaking Table Modelling of Seismically Induced Deformations in Slopes", *Journal of Geotechnical and Geoenvironmental Engineering*; Vol. 131, No. 5, pp. 610-622.

Yang, K. H., W. Y. Hung, E. Y. Kencana, 2013, "Acceleration-Amplified Responses of Geosynthetic-Reinforced Soil Structures with a Wide Range of Input Ground Accelerations", *Geo-Congress 2013*, ASCE 2013.

Yoon, S., M. Prezzi, N. Z. Siddiki, B. Kim, 2005, "Construction of a Test Embankment Using a Sand-Tire Shred Mixture as Fill Material", *Waste Management*, Vol. 26, pp. 1033-1044.